Design of an independent front wheel steering system with optimal driver feedback

M.H. te Morsche

Delft University of Technology

15 June 2014

Design of an independent front wheel steering system with optimal driver feedback

By

M.H. te Morsche

in partial fulfilment of the requirements for the degree of

Master of Science
Master of Science Mechanical Engineering, Precision and Microsystems Engineering, Automotive

at the Delft University of Technology,
to be defended publicly on Monday June 30, 2014 at 08:45 AM.

Supervisor:	Prof.dr.ir. E.G.M. Holweg
Thesis committee:	A. Kunnappillil Madhusudhanan, TU Delft
	B. Shyrokau, TU Delft
	P.M. van Leeuwen, TU Delft

This thesis is confidential and cannot be made public until June 29, 2014.

An electronic version of this thesis is available at http://repository.tudelft.nl/.

TU Delft Delft University of Technology

Abstract

In this thesis, Independent Front Wheel Steering (IFWS) is studied. To implement an IFWS system, it is important to understand how dynamics of the front wheel and steering motor work. Furthermore it can be challenging to provide haptic feedback to the driver, especially when an active safety system is constantly adjusting the angle of the front wheel and causing interference.

First a model of a front wheel steering system with a variable gear ratio between motor and front wheels is created. At low gear ratios, the simulations show an improvement of the response of the steering system to the tyre forces. A compromise should be made between a small motor and low gear ratio. A low gear ratio is desirable as it improves the accuracy of a direct current measurement (DCM), which is required for providing the driver with haptic feedback with road information.

Then a virtual model (VM) based on the bicycle model is created which can estimate the actual tyre forces within a 16 % accuracy. The error in the VM is caused by the approximation of nonlinear vehicle dynamics. The DCM and the VM are compared to their reference tyre forces in a modified double lane change and a steady state corner simulation.

A combiner of the DCM and VM (Combiner DCM and VM (CDV)) is proposed which can blend the two feedback sources. At low interference frequencies, the CDV shows good results. At high interference frequencies, presence of the inertia and damping of the steering system become more dominant compared to the tyre forces and causes a phase lead in the DCM. Towards the natural frequency of the steering system, the magnitude of the required motor current decreases. The result is a poor performance of the CDV at high interference frequencies.

One of the recommendation for improving the CDV is installing a motor with a high constant torque value. The motor is coupled to the front wheel with a low gear ratio and will lower the inertia and damping of the steering system. This increases the eigenfrequency of the steering system and improves the bandwidth of the DCM. However the space requirements of a bigger motor can cause problems for implementation.

Table of Contents

List of Figures

List of Tables

Chapter 1

Market Analysis

Since the 1920s fatal traffic collisions in the US remained almost constant. Meanwhile the amount of vehicles participating in the traffic has grown exponentially. Deaths per million vehicle miles have dropped from 17 to less than 2. Reason for this is the ongoing development in the automotive industry. There is a constant search for improving the performance of vehicles. Creating a better handling car enhances its safety, which can tip the balance in favor of a company and improve its sales.

An Independent Front Wheel Steering (IFWS) system is able to independently steer both front wheels. The system constantly adjusts each wheel's steering angle to maximize the vehicle's stability and performance. This market analysis focusses on IFWS systems and tries to answer the next four market research questions:

1 How can IFWS enhance the performance of a vehicle?

2 Which current systems are used to implement independent front wheel steering into a vehicle?

3 Which control systems are used to implement IFWS and maintain driver steering feeling?

4 What are the requirements to implement IFWS?

1.1 Introduction

In this section different terms are explained and a conclusion is made to answer the first market research question: How can IFWS enhance the performance of a vehicle?

1.1.1 Slip angle

The slip angle is the angular difference between the plane of rotation of the tyres and the actual path they are taking. A slip angle is possible due to deformations in the tyre's carcass and tread. The friction in the contact area between the tyre and the road will ensure that this area of the tyre is stationary in reference to the road. If there is a side slip angle, and thus a side slip velocity, the contact area of the tyre will be deformed, see Figure 1-1. This deformed contact patch lets the tyre move in the lateral direction.

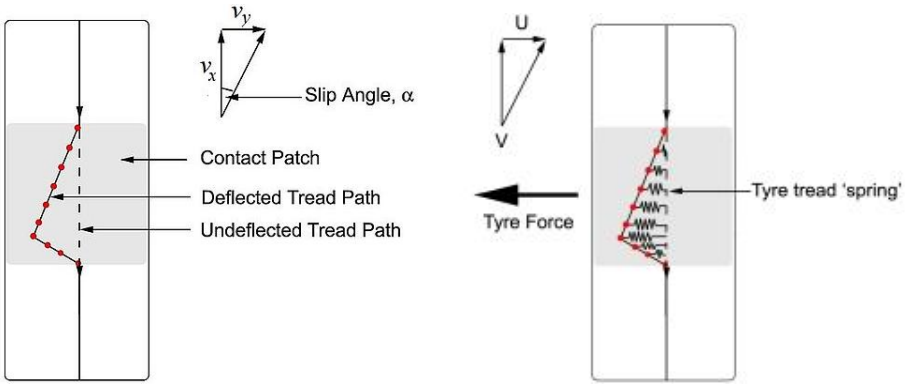

Figure 1-1: Slip angle

1.1.2 Lateral forces

The deformed contact path causes reaction forces in the tyre. These forces work perpendicular on the tyre's plane of rotation and are called lateral forces. At small slip angles the lateral force is proportional to the slip angle. At higher angles the lateral force becomes highly nonlinear. The Pacejka "Magic Formula" tyre model gives a good approximation of the relation between lateral forces and slip angle, see Figure 1-2. It clearly shows a maximum in lateral force, after which the lateral force declines. Ideally the lateral force should be held before saturation point, in the linear tyre region.

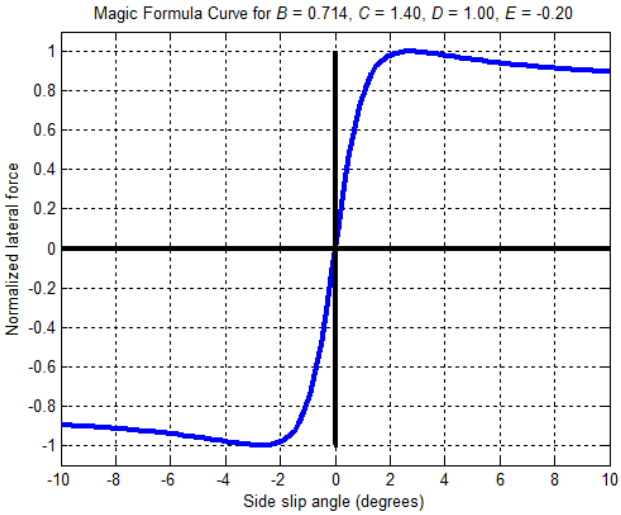

Figure 1-2: Pacejka "Magic Formula" tyre model [1]

1.1.3 Tyre utilization coefficient

A tyre utilization coefficient (TUC) shows how much a tyre is used compared to the maximum longitudinal and lateral forces. This is shown in Figure 1-3. The tyre utilization coefficient is defined as k in the equation below.

$$k = \frac{F_x^2}{F_{xmax}^2} + \frac{F_y^2}{F_{ymax}^2}, \; where \; 0 \leq k \leq 1 \qquad (1\text{-}1)$$

Both forces, F_x and F_y, are highly nonlinear functions of the slip ratio, side slip angle, camber and vertical load [2]. Cornering can create different TUC's among the tyres. If the center of gravity lies above the roll center of a vehicle, the vertical load on the outer tyres will be higher compared to the inner tyres. Due to this higher load, the outer tyres can handle higher longitudinal and lateral forces, which results in lower TUC's in the outer tyres. In high-speed corners this leads to saturation of the inner tyres while the outer tyres are not fully exploited.

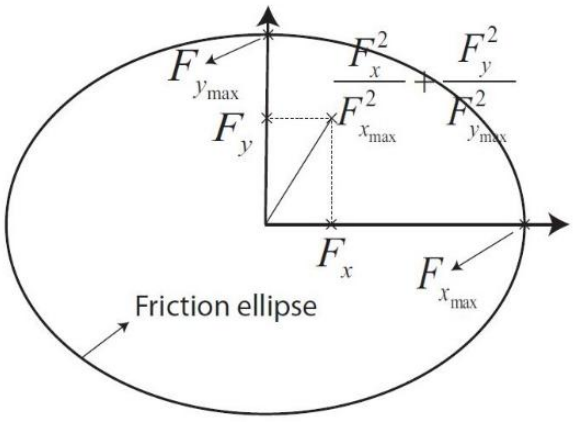

Figure 1-3; Friction ellipse [2]

1.1.4 Ackermann steering

For low speeds it is desirable to have an Ackermann steering geometry, shown in Figure 1-4. With Ackermann steering geometry the outer tyre will turn less than the inner tyre. This will minimalize the tyre scrub and also the related noise and wear of the tyres [3]. For high performance maneuvers an anti-Ackermann steering geometry is desirable [4]; the outer tyre has a larger steering angle than the inner tyre. Due to the earlier saturation of the inner tyre, an anti-Ackermann steering geometry transfers the lateral force more to the outer tyre, doing so by its increased angle. This allows a vehicle to handle higher lateral forces and enables it to handle high performance maneuvers, see Figure 1-4b.

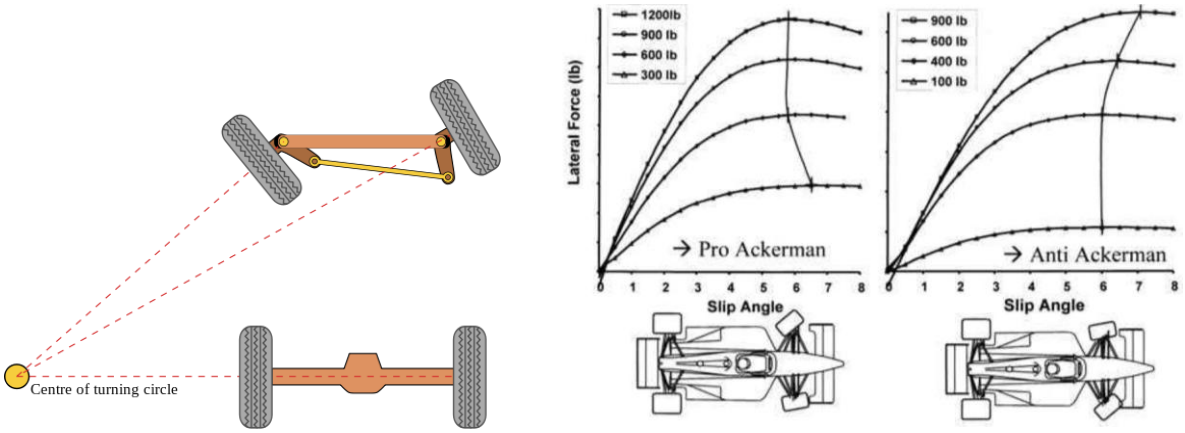

(a) Mechanism *(b) Lateral force vs. slip angle, Pro / Anti - Ackermann*

Figure 1-4: Ackermann steering

1.1.5 Tyre utilization coefficient control

In [2] a system to control the TUCs by utilizing an independent steering system is proposed as shown in Figure 1-5. With this control system, the Ackerman steering geometry can be maintained at low performance maneuvers. At high performance maneuvers the system transfers forces from the inner tyres, with a high or saturated TUC, to the outer tyres [5]. The steering angle of the inner tyres is thus reduced to lower their workload while the steering angle of the outer tyres is increased.

The paper shows that in a simulation it is possible for the left and right tyre from each *axil* to have equal TUCs ($k_{front\ left} = k_{front\ right}$ and $k_{rear\ left} = k_{rear\ right}$). By doing so, a vehicle with a TUC controller can maintain stability in an extreme sine with dwell maneuver, while a car without this system goes in over steer. The next step in this work is to design and develop an independent front wheel steering system.

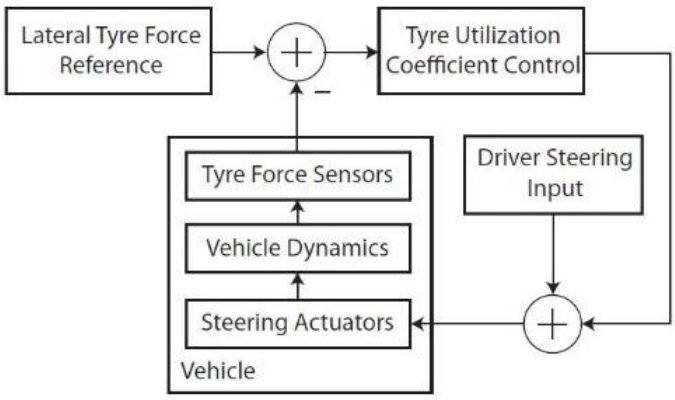

Figure 1-5: Control structure [2]

1.1.6 Summary

The utilization difference between the inner and outer tyre, in a corner, provides a possibility to improve the performance of a vehicle. By reducing the inner tyre's slip angle, saturation can be delayed. By simultaneously enlarging the outer tyre's slip angle, the inner tyre would operate in linear operation region as well as the outer tyre, which improves the vehicle's performance. To implement the TUC controller a system is required which can independently steer the both front wheels.

1.2 Historical developments

1.2.1 Four wheel steering

In the 80's it was discovered that steering the rear wheels could greatly enhance the performance of a vehicle [6]. By turning the rear wheels in the opposite direction of the front wheels, the maneuverability of a vehicle increases, which is especially useful at low speeds, shown in Figure 1-6. At higher speeds the rear wheels are steered in the same direction as the front wheels to increase stability. To steer the rear wheels mechanical, hydraulic or electro-mechanical systems are used.

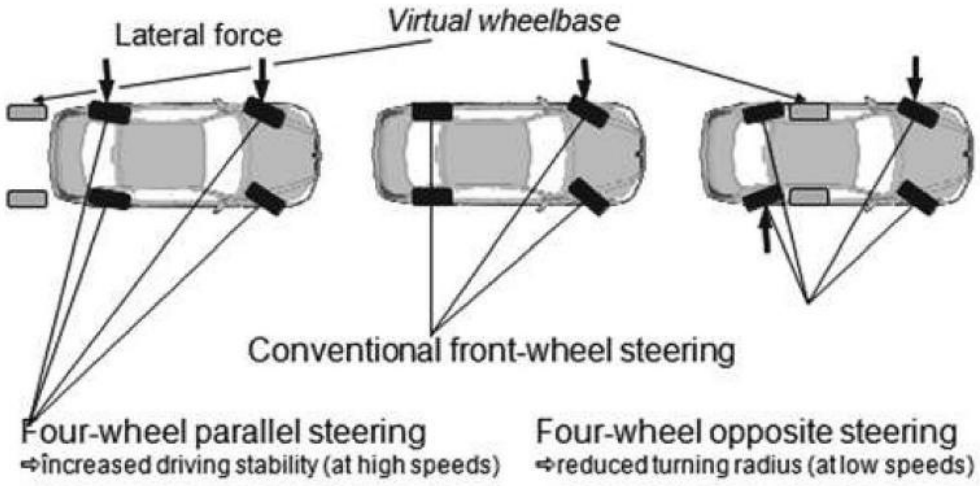

Figure 1-6: Parallel and opposite-direction rear-wheel steering systems [7]

1.2.2 Active front steering

In the 90's Active front steering was being developed. In 2003 ZF Friedrichshafen AG delivered active steering for the first passenger cars. The mechanical link between the steering wheel and front wheels is maintained. A planetary gear assembly is installed into the steering column shaft [6]. The steering wheel is connected to the sun gear while the planet gears are connected to the front wheels of the vehicle. An electric motor can turn the ring gear to create an adjustment to the steering angle of the front wheels, i.e. the system adds an active front steering (AFS) angle to the steering angle of the driver. The mechanism is shown in Figure 1-7a. With this extra input the system is able change the steering ratio. This adjustable steering ratio can enhance the response of the front wheels, which reduces the driver's effort at lower speeds, e.g. parking. At higher speeds the sensitivity is lowered to improve the directional stability of the vehicle, see Figure 1-7b. An alteration of the steering angle is also possible. In case of an over steer situation the system reduces the steering angle, which lowers the yaw rate of the vehicle and prevents it from spinning.

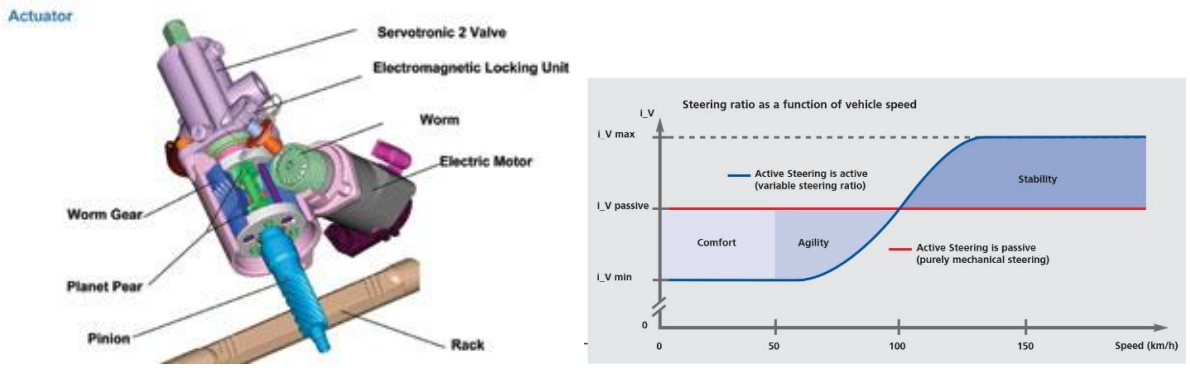

(a) Mechanism *(b) Agility / Stability region*

Figure 1-7: Active front steering

1.2.3 Conventional Steer-by-wire

A fairly new concept in the automotive industry is to control the front wheels of a vehicle by a steer-by-wire system (SBW). In the airplane industry this is already a very mature system for both controlling military and commercial airplanes [8]. In a steer-by-wire system the mechanical connection between the steering wheel and the actual steering system is removed, Figure 1-8. A sensor attached to the steering wheel measures the direction the driver wants to go. With this input angle and many other parameters of the vehicle the desired direction of the front wheel is computed. A motor, connected to the steering rack can move the wheels in the desired direction.

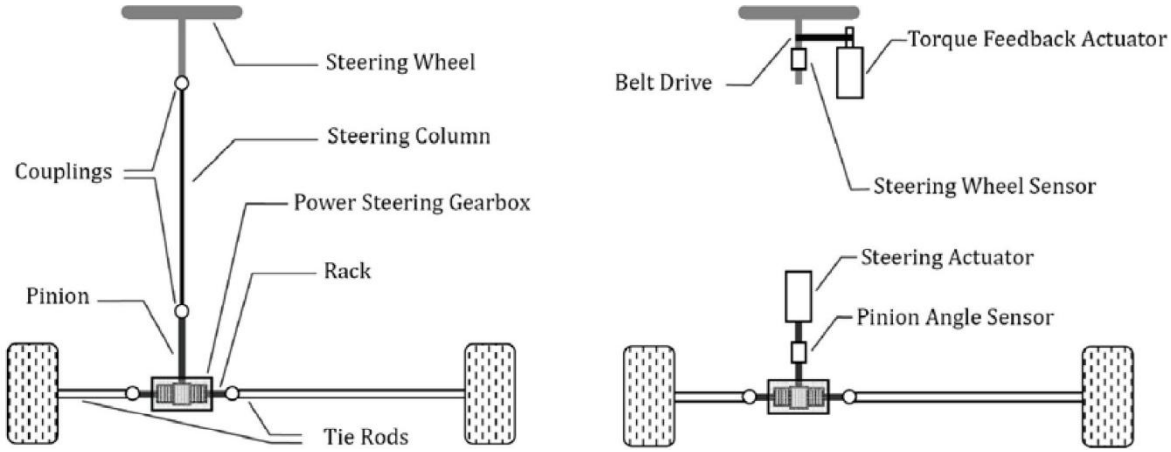

(a) Traditional *(b) Steer-by-wire*

Figure 1-8: Steering system [9]

The steer-by-wire system has many advantages:

- Active steering capabilities. An onboard computer can adjust the steering angle without disturbing the driver's steering feeling.
- No noise and vibrations are passed though the steering column to the driver
- The steering ratio and steering effort is adjustable, which can even be optimized for an individual driver.
- The absence of the steering column will improve the utilization of space in the engine compartment and may reduce the weight of the vehicle.
- Due to the loss of the mechanical connection the steering wheel can freely be placed in the interior of the car.

One of the main drawbacks of the steer-by-wire system is its safety concerns. The reliability of the system is extremely important. Therefore there has to be a backup system to avoid total loss of control. A mechanical backup or doubling of the electric system are the main solutions [10]. The redundancy of both systems creates extra costs.

After vision, haptic feedback is one of the highest rated input for a driver to control a vehicle [11]. Another major challenge of steer by wire designs is maintaining the haptic feedback in the steering wheel, while removing the mechanical link between the wheels and the steering wheel. In steer-by-wire systems an electric motor is connected to the steering wheel to provide the driver with the desired haptic feedback. Especially when the system adjusts the angle of the front wheels, determining the correct feedback for the driver is important and can create obstacles for implementing this system.

Safety concerns and haptic feedback are the main reasons why steer-by-wire systems are not widely implemented in commercial vehicles. There even are concepts that go a step further; Steer-by-wire systems combined with an independent actuation system. This makes it possible to fully exploit the active steering capabilities of this technique. This will be further discussed in section 1.3.2.

1.2.3.1 First production vehicle

In 2013 Nissan introduced the Infiniti Q50. See Figure 1-9. This vehicle uses a steer-by-wire system and is the first production vehicle with this technology. The direct link between steering wheel and front wheels is removed. Sensors in the steering wheel measure the desired direction and pass this to the controller that powers the actuators, connected to the front wheels. A clutch placed in the traditional mechanical connection serves as backup system and is engaged when a failure occurs to maintain the safety of a conventional vehicle.

(a) Infiniti Q50 *(b) Steer-by-wire system*

Figure 1-9: Nissan Infiniti Q50 Steer-by-wire system

1.3 Independent front wheel steering systems

This section categorizes independent front wheel steering in two different system types and answers the second market research question: Which current systems are used to implement independent front wheel steering into a vehicle?

Independent front wheel steering (IFWS) systems are able to steer both front wheel of the vehicle independently. An IFWS system is able to improve the vehicle's stability at higher speeds by transferring workload from the saturated inner tyre to the unexploited outer tyre, see section 1.1.5. There are two types of systems: independent differential steering and independent steer-by-wire, shown in Figure 1-10. In differential steering systems the mechanical link between the front wheels and the steering wheel is maintained, while this link is removed in the second type of systems.

Independent steer-by-wire systems are very similar to a conventional steer by wire systems, only with independent actuation of both wheels.

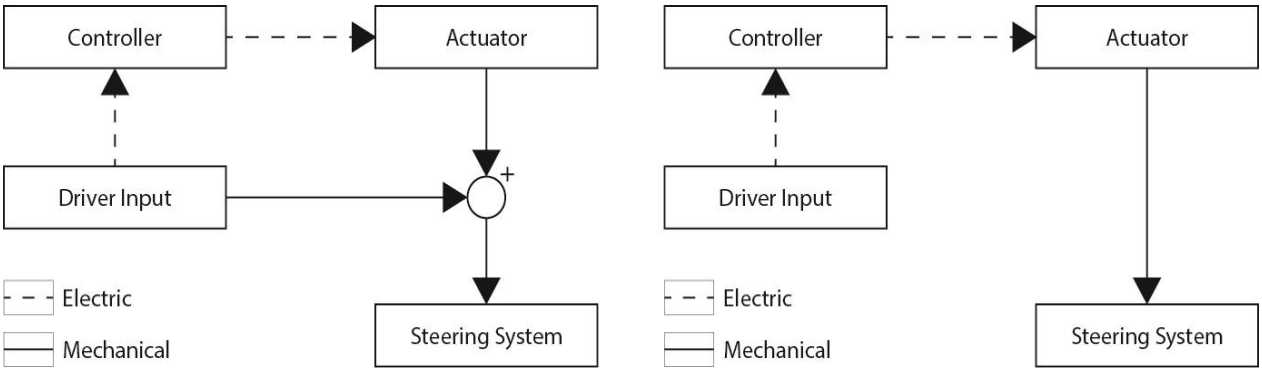

(a) Differential steering *(b) Steer-by-wire*

Figure 1-10: Steering systems (2)

1.3.1 Differential steering (Independent)

A differential steering system mechanically adds an AFS angle to the driver's steering angle. The mechanical linkage between the steering wheel and the front wheels is maintained, which has important advantages. In case of an electronic malfunction the mechanical system is intact and will behave like a conventional steering system, i.e. there will be no loss of control. Second, the mechanical connection gives haptic feedback to the driver, which has to be created if this connection is removed. Two different differential steering systems will be discussed further.

1.3.1.1 Double active front steering system

The system proposed in [12] uses a conventional steering column combined with two steering racks. The steering racks are each independently linked to the steering column by a planetary gear, shown in Figure 1-11. Each planetary gear is driven by an electric motor to add an AFS angle, independent for each front wheel. This is comparable to a double active steering system. It has the same advantages, if there is a malfunction the planetary gears assemblies lock and the conventional steering system is maintained. Further the haptic feedback for the driver is maintained. The drawbacks are the costs for doubling the entire AFS system and the space required for implementation. In 2012 this system was patented in the US [13].

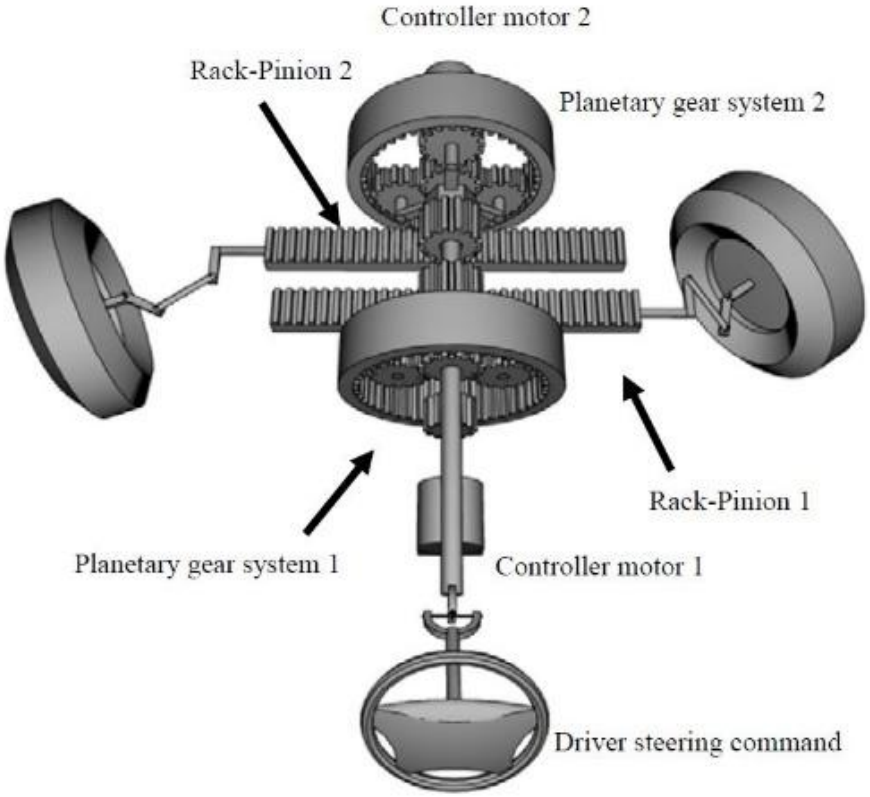

Figure 1-11: Double active front steering system mechanism, full view [12]

1.3.1.2 Active Geometry Suspension

A variable geometry suspension system continuously adjusts the suspension geometry to introduce an AFS angle to the steering angle. The goal is to improve the stability of the vehicle at higher speeds. Active geometry suspension is superior to other independent steering systems in terms of simple structure, low costs and low power consumption [14].

In [15] a variable-geometry suspension system is proposed to implement an AFS angle to the steering and camber angle. The suspension geometry is actuated at points A1 and A2, in lateral direction, shown in Figure 1-12. The steering rod connects the front wheel (point K) and the steering rack (point S). The paper showed that the height of point K determines how sensitive the steering angle is to a displacement of point A. A higher position for point K increases the sensitivity and creates the ability for the tyres to handle increased lateral forces. They concluded that their system is well suited to be used as a driver assistance system.

The drawback of active geometry suspension is the issue of adding a possible undesirable camber angle to the steering geometry. Especially in research projects altering other steering parameters can cause problems. It is difficult to link results of the research directly to the altered steering angle if other parameters are changing as well.

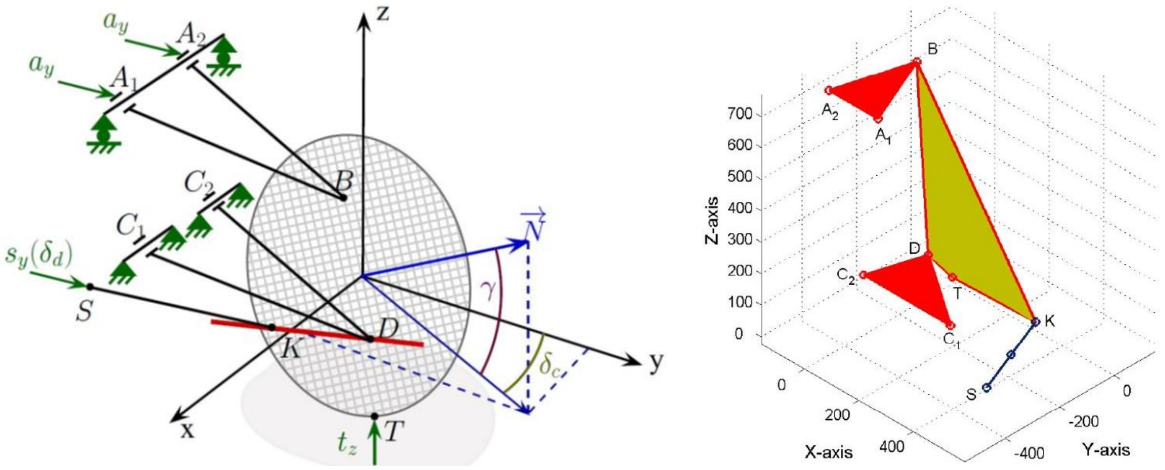

(a) Wheel position related to steering and camber angle (b) Mechanism of the suspension system

Figure 1-12: Active Geometry Suspension system [14]

1.3.1.3 Active Wheel

In the 2008 Paris motor show, Michelin introduced an active wheel. See Figure 1-13. This wheel can replace many traditional vehicle components, such as motor, gearbox and importantly the suspension [16]. It has a miniature propulsion engine and an electrical suspension system built into the wheel. This system can actively control the pitch and roll of the vehicle and thus greatly enhances the stability of the vehicle. This system does not directly change the steering angle but due to resemblance with the previous system it is worth mentioning.

Figure 1-13: Michelin active wheel [16]

1.3.2 Steer-by-wire (Independent)

A steer-by-wire system can be transformed to independent steer-by-wire system. A possibility is to remove the steering rack and actuate each wheel independently with a linear actuator, either electric or hydraulic. The drawbacks compared to a conventional steer-by-wire system are the safety concerns.

Having two actuators, left and right, doubles the chance of malfunction. Installing backup actuators requires two extra actuators and creates problems in terms of costs and space. There are concepts that minimalize the costs and space requirements while keeping in mind the safety aspect.

1.3.2.1 Independent steer-by-wire system

Figure 1-14 shows a steer-by-wire system. It uses two electric motors. The primary motor adjusts the steering rack from left to right, like a conventional steer-by-wire system. The secondary motor shortens or extents the length of the steering rack, by the use of a ball spline. The combination of the two motors creates an independent adjustable steering angle for each front wheel. In a malfunction of the secondary motor the system behaves like a conventional steer-by-wire system. If the primary motor fails, a spring system will upgrade the secondary motor to primary motor in order to maintain control [17].

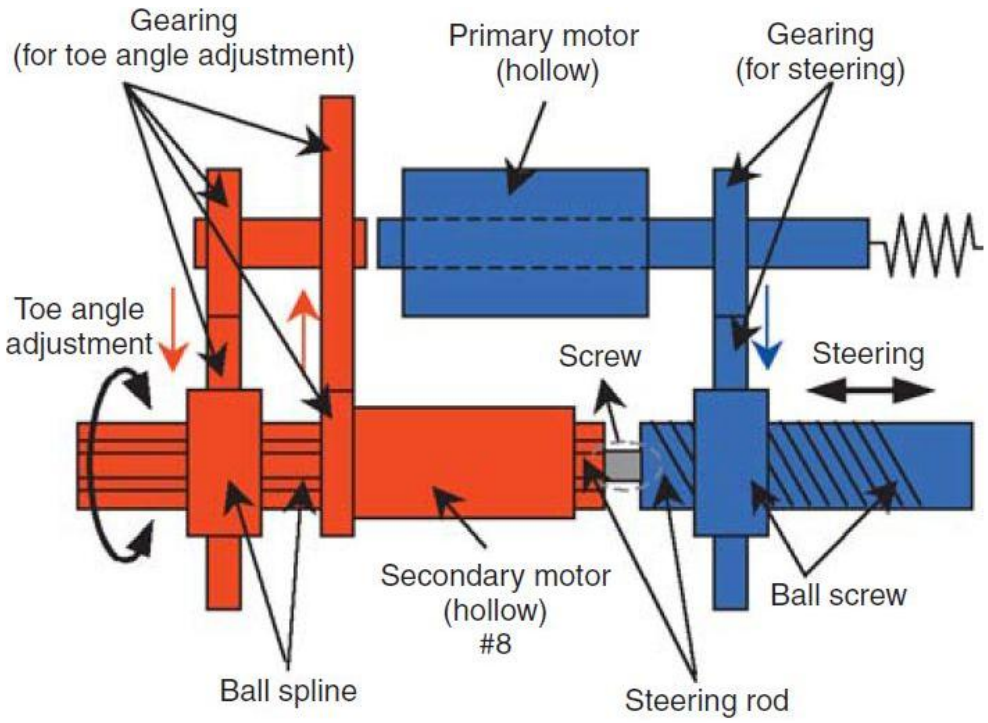

Figure 1-14: Steer-by-wire system [17]

1.3.2.2 Autonomous Corner Module

Zetterström designed an autonomous corner module for Volvo, see Figure 1-15. This product makes it possible to steer each wheel independently with a in-wheel electro motor. The idea was to create an universal module that could be installed in all kinds of vehicles. The system has the same advantages as an normal steer-by-wire system and due to it small size there are advantages in terms of complexity and space requirements [18]. The design was patented by Volvo in 2002.

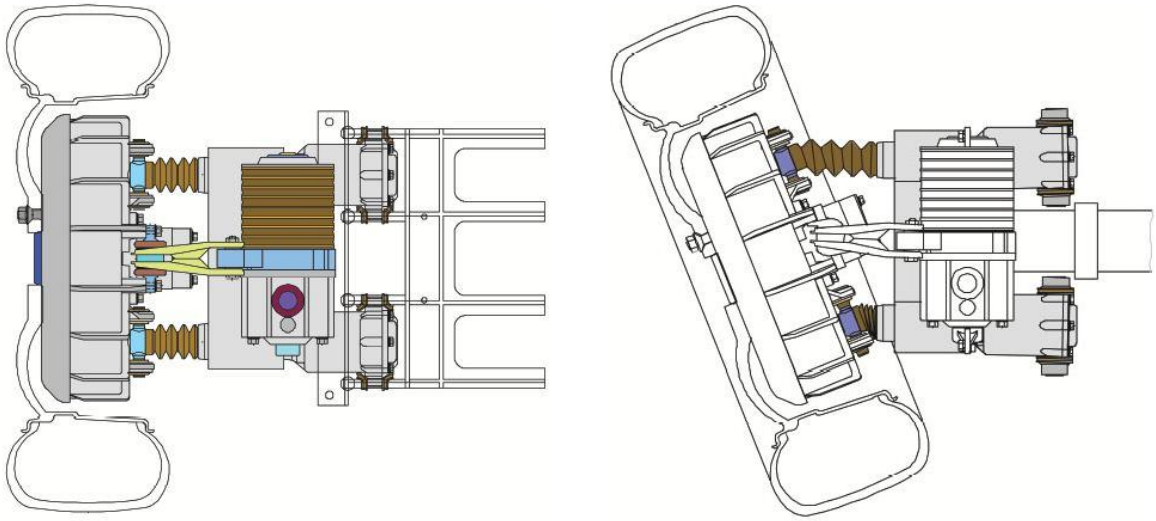

(a) Wheel, part of body structure and module *(b) Maximum steering angle; 22 deg*

Figure 1-15: Autonomous Corner Module [18]

1.3.3 Summary

Table 1-1 shows the two different independent steering systems: differential steering and steer-by-wire. Differential steering maintains the mechanical link between driver and steering system, while this connection is lost in steer-by-wire systems. Losing this connection provides flexibility in implementation, but creates problems in terms of safety and feedback. Active geometry suspension is relatively cheap and an easy system to implement, but unattractive for educational projects due to the disturbance of other steering parameters.

Table 1-1: Steering systems comparison

	Differential steering		**Steer-by-wire**
	Double active steering	**Active Geometry Suspension**	
Mechanical connection	Maintained		Removed
Feedback driver	Maintained		Feedback system
Safety	Maintained		Backup system
Disturbance	No	Camber angle	No

1.4 Control

For a driver, the feeling in the steering wheel is the most important feedback after vision [11]. Section 1.4 discusses the feedback control problem, especially when an active steering system adjust the angle of the front wheel. There are not many articles available on independent steering controllers. Nevertheless there are many concepts on conventional active steering and steer-by-wire system. This section handles the third market research question: Which control systems are used to implement IFWS and maintain driver steering feeling?

1.4.1 Differential steering

1.4.1.1 Steering feeling

In a conventional steering system the torque feedback is a combination of the steering system dynamics (moment inertia, damping and friction) and the external dynamics (tyre properties, road conditions, vehicle velocity). The mechanical link, in differential steering systems, between steering wheel and steering system is intact, which transfers these reaction forces directly to the driver.

1.4.1.2 *Active front steering*

Active front steering is the implementation of an AFS angle to the driver's input. The angle of the front wheels is changed by the AFS system to maximize stability and performance. This change of front wheel angle results in different road forces. When these road forces are transferred to the steering wheel it may feel unnatural for the driver. This unexpected feedback for the driver, due to the change in front wheel angle, is called steering interference.

In differential steering systems it is inevitable that an active steering system causes steering interference when the steering angle is significantly altered [19]. An experimental setup shows that two major problems occur when AFS system interferes, see Figure 1-16a. First, the steering wheel moves in the opposite direction of the front wheels. This gives the driver the wrong perception about the movement of the vehicle. The second problem is the decrease in feedback torque provided to the driver [19]. This can provoke a steering reaction and destabilize the vehicle.

In [19] a system that uses a power assist motor combined with an AFS system is proposed. When the AFS system add an AFS angle, a change in road reaction forces is generated. These forces would normally disrupt the stability of the vehicle. In an experimental setup the power assist motor is able to compensate for these reaction forces and maintain a natural steering feeling for the driver. Together with the reaction torque the steering wheel angle is also more constant, shown in Figure 1-16b.

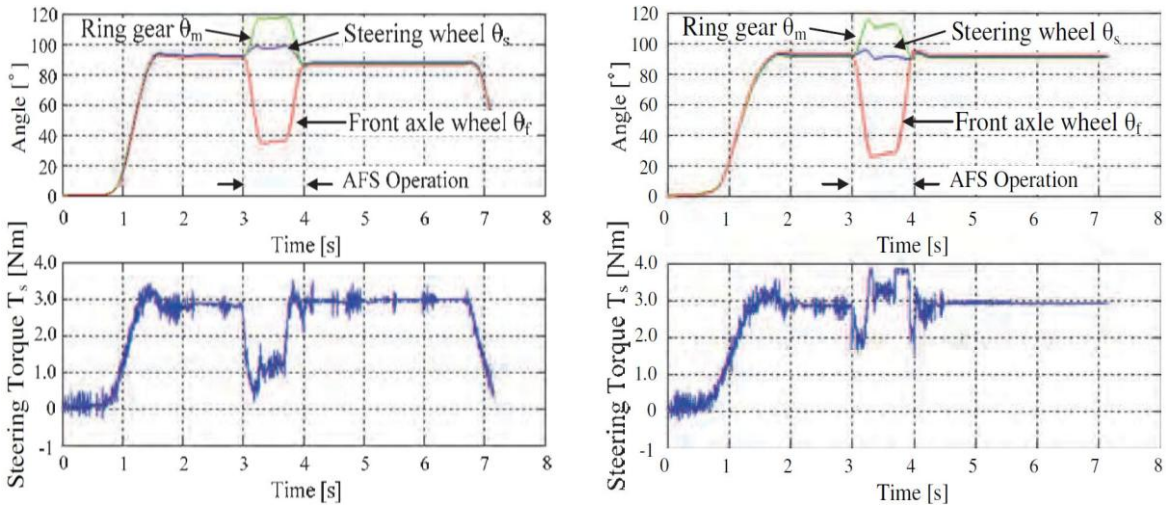

(a) AFS system control

(b) AFS system combined with variable assist ratio

Figure 1-16: Experimental result active steering (differential steering system) [19]

1.4.2 Steer-by-Wire

A challenge for controlling a steer by wire system is providing the driver with a realistic feeling of the steering system, without de-stabilizing the vehicle. To control the steering wheel motor different techniques can be used to determine the haptic feedback.

1.4.2.1 *Direct current measurement*

In 2009 Nguyen et al. proposed a system that measures the current of the motor that steers the front wheels, [20]. The current is proportional to the torque (or force) the motor delivers, and thus the road reaction forces and would be a good indication how much feedback is required. A diagram of the system is shown in Figure 1-17. Combining current, steering angle and vehicle velocity a feedback torque value can be constructed through a torque map. He concluded that this concept is a cheap and easy way to reproduce the driver's feeling.

1.4.2.2 Active steering

A steer-by-wire system combined with a system that adjusts the total steering angle creates a problem in the control system. The feedback of the driver cannot be based on the reaction torque of the road wheels; this value can be disturbed by the contribution of the AFS angle, created by the system. Providing this feedback to the driver can cause an unnatural feeling and provoke a reaction, which can destabilize the vehicle [9].

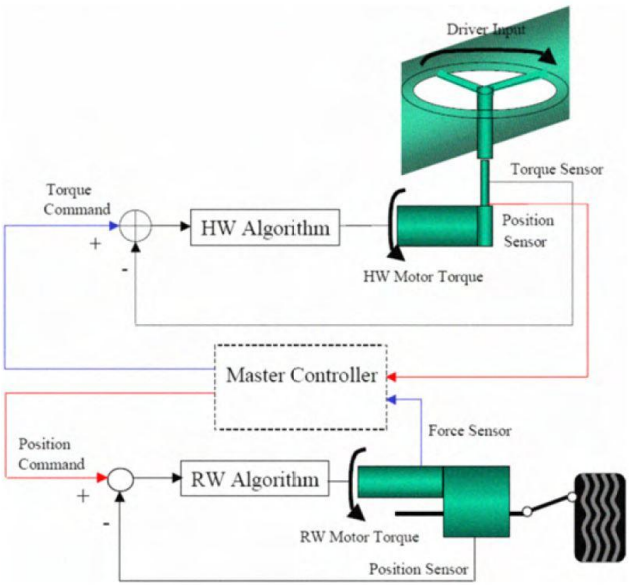

Figure 1-17: Position-force control scheme [20]

1.4.2.3 Virtual model

In [9] a system that decouples the steering wheel feedback and the vehicle tyre dynamics is proposed. A virtual vehicle model is used as a reference to determine the driver feedback, see Figure 1-18. The virtual modeled feedback does not estimate the real tyre forces, but it can provide the driver with the feeling of a conventional steering system. For the driver the AFS angle does not disrupt the steering feeling because this angle is excluded from the feedback controller algorithm. Compared to the direct current measurement method the performance of the AFS angle controller improves, because it behaves like no feedback system is present. A major drawback of this control scheme is the absence of road information for the driver. If the vehicle hits a bump or drives on gravel no extra steering wheel reaction torque is generated, not notifying the driver of a possible dangerous situation.

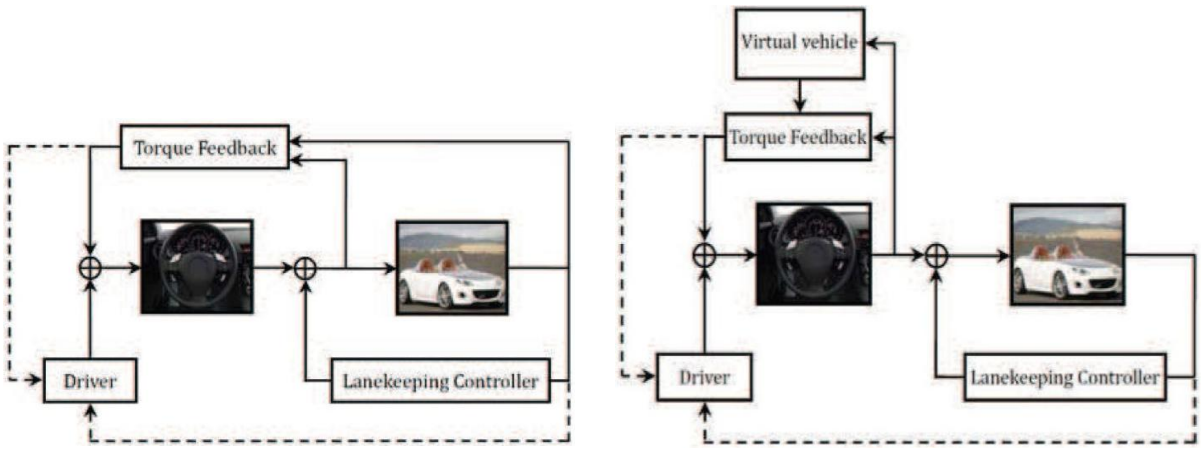

(a) Based on actual tyres reaction torque *(b) Based upon a virtual vehicle*

Figure 1-18: Haptic feedback system [9]

1.4.2.4 Reaction torque observer

Minaki et al. also realized that using a virtual model for providing feedback to the driver removes all the road information. They proposed a control system based on estimated reaction torque, shown in Figure 1-19.

The reaction forces T_{RTRS} from the road surface are unknown and should be estimated to provide the driver with road information. First the angle of the front wheel $\hat{\theta}_f$ is estimated by using reference torque T_f^* combined with a steering characteristics model P_n. This estimated angle is compared to the actual front wheel angle θ_f to create the AFS steering angle $\Delta\theta$. The road reaction forces $\hat{T}_{RTRS}$ can be computed by the AFS angle $\Delta\theta$ and the inverse model of the steering characteristics P_n^{-1}. If feedback would be transferred to the driver directly the same problem would occur as with conventional active steering, see Figure 1-16a. It is necessary to adjust the gain and frequency of $\hat{T}_{RTRS}$ by implementing a controllable low-pass filter Q [19].

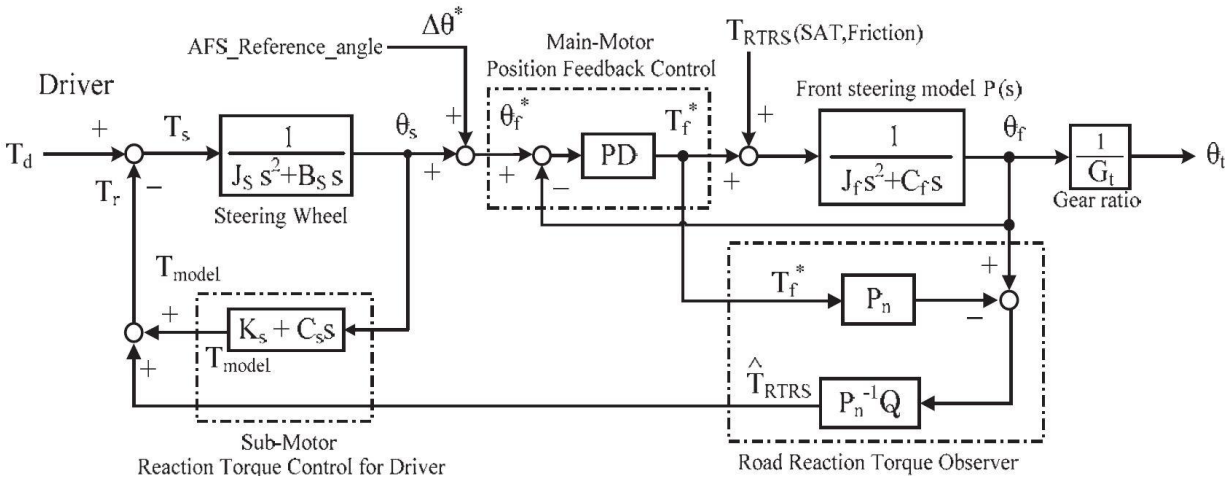

Figure 1-19: Reaction torque control based on estimated reaction torque [19]

1.4.3 Conclusion

The mechanical link between front wheels and steering wheel remains in differential steering systems, guaranteeing safety. The road reaction forces are directly transferred to the driver. Active steering systems can constantly adjust the steering angle, which create unexpected reaction forces. This steering interference makes safe driving difficult. A control system that cooperates the power steering and active steering system can disguise these disturbances.

One of the major problems for implementing steer-by-wire is maintaining a safe system. The feedback problem, although difficult to control, provides opportunities to fully control and exploit the driver feedback. Providing haptic feedback in steer-by-wire systems can be done by a direct current measurement of the front wheel actuators. For steer-by-wire systems, that use active steering, this is not a realistic possibility, because unexpected tyre forces cause steering interference. A system that decouples the steering system and uses a virtual model to compute the feedback for the driver is a very stable system, but all the road information is lost. Using a virtual model and combining this with a system that estimates the road reaction forces and controls the gain and frequencies of this feedback can result in a system without significant steering interference and loss of road information.

1.5 Requirements

Articles are consulted to get an indication of the required amount of power for implementing an independent steering system into a BMW 5 series e60. This vehicle is chosen since it was the primary vehicle available for a possible implementation of an IFWS system. Values for steering torque and

steering velocities are combined with the characteristics of a BMW 5 series e60, which are also obtained through literature and measurements. Secondly the steering angle response of the TUC controller, discussed in section 1.1.5, is implemented in a Simulink model to compute the power required to actuate the front wheel of the BMW. Finally measurements are done to visualize the amount of space available for implementing a system. This section answers the last market research question: What are the requirements to implement IFWS?

1.5.1 Power

1.5.1.1 Literature

The steering ratio for the BMW e60 5 series, lock-to-lock angle and actuation distance of the front wheels are shown in

Table 1-3.

Table 1-2: Parameters BMW 5 series e60 [21]

Symbol	Parameter	Value	Unit
SR	Steering ratio	13.8	-
LTL	Lock-to-lock angle	1009	deg
N_L	Actuation distance front wheel	0.12	m

Under normal driving circumstances a driver exerts a steering wheel torque between 0 to 2 Nm. When an emergency maneuver is preformed this can increase to up to 15 Nm [22], [23]. A published American opinion suggested in 1951 that the lock-to-lock time of a private vehicle is 4 seconds, which is equal to 0.7 rotations per second [24]. A paper [25] proposed a higher performance steer-by-wire design; a steering wheel rate of two rotations per second.

Combining the driver's steering inputs with the BMW characteristics, the required torque and angular velocity of the front wheels is calculated.

$$\delta_{sw} = \frac{\delta_{fw}}{SR} = \frac{x_{rack} \cdot N_L}{SR} \tag{1-2}$$

δ_{sw} = steering angle [rad]
δ_{sw} = front wheel angle [rad]
x_{rack} = position steering rack [m]

Table 1-3: Conventional steering system characteristics, both wheels combined, Literature

	Steering wheel (δ_{sw})		Front wheels (δ_{fw})		Steering rack (x_{rack})	
Torque / Force	15	Nm	207	Nm	1725	N
Velocity (angular)	12.56	rad/s	0.910	rad/s	0.109	m/s
Power	188	W	188	W	188	W

1.5.1.2 Steer-by-wire

The tyre utilization coefficient control proposed in Section 1.1.5 actuates each front wheel independently. Figure 1-20 shows the angle of the front left wheel in a timeframe of 6 seconds.

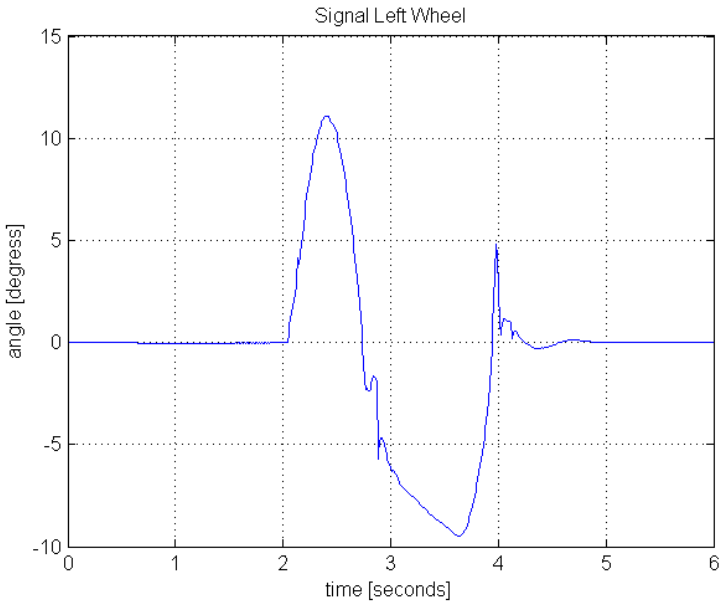

Figure 1-20: TUCC reference angle, left front wheel

A power spectral density shows clearly the dominant presence of the low frequencies, shown in Figure 1-21. These low frequencies are the main contributors to the power required for tracking the reference angle with the steering system dynamics.

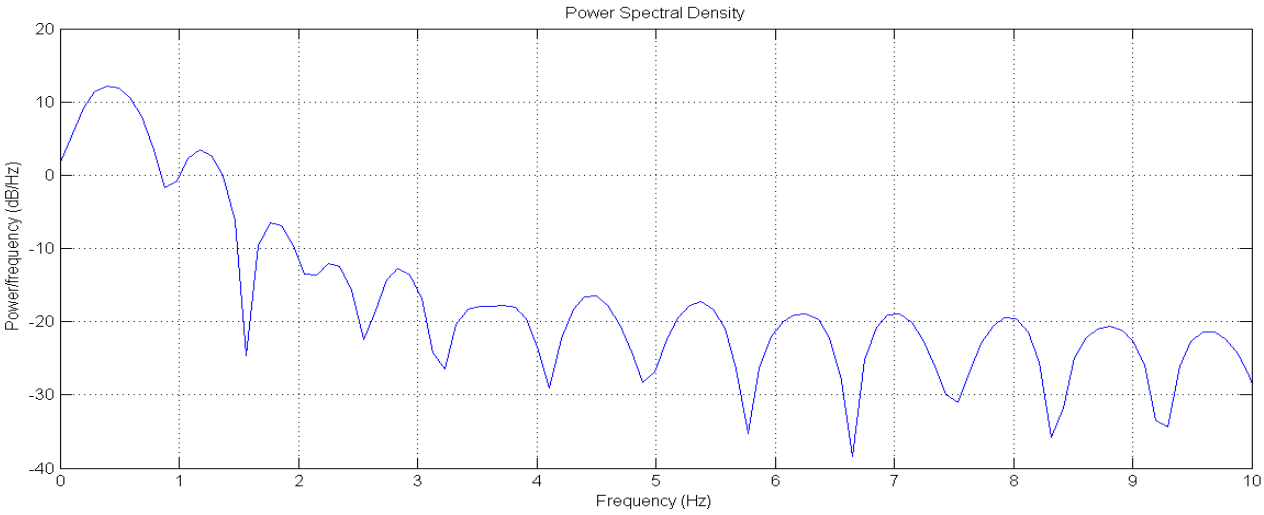

Figure 1-21: Power Spectral density, TUCC reference angle, left front wheel

The equation below shows the equilibrium equation of the front wheel steering dynamics. The setup is shown in Figure 1-22.

$$J_{fw}\ddot{\delta_{fw}} + B_{fw}\dot{\delta_{fw}} + \tau_{tyre} = F_m\, N_l \qquad (1\text{-}3)$$

J_{fw}	= moment of inertia about the z-axis	[kg m^2]
B_{fw}	= angular damping about the z-axis	[N·m·s/rad]
τ_{tyre}	= tyre torque	[N·m]
F_m	= force steering motor	[N]
N_L	= actuation distance	[m]

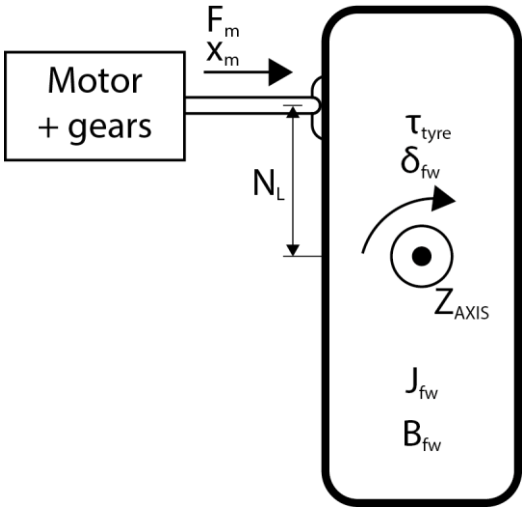

Figure 1-22: Front wheel, motor setup, top view

Inertia and damping

First the reference angle tracking is implemented in a simplified Simulink model to determine the requirements in terms of force and velocity of the actuator, see Figure 1-23. The simulation uses a PD controller to create a closed loop bandwidth of 10 Hz, see Figure 1-24. The front wheel is modeled as a moment of inertia combined with an angular damping, the tyre torque is excluded from this model for now. The moment of inertia is calculated by the weight and dimension of the front wheel and the connected brake disk. The value for the angular damping is found in the literature. The values are shown in Table 1-4.

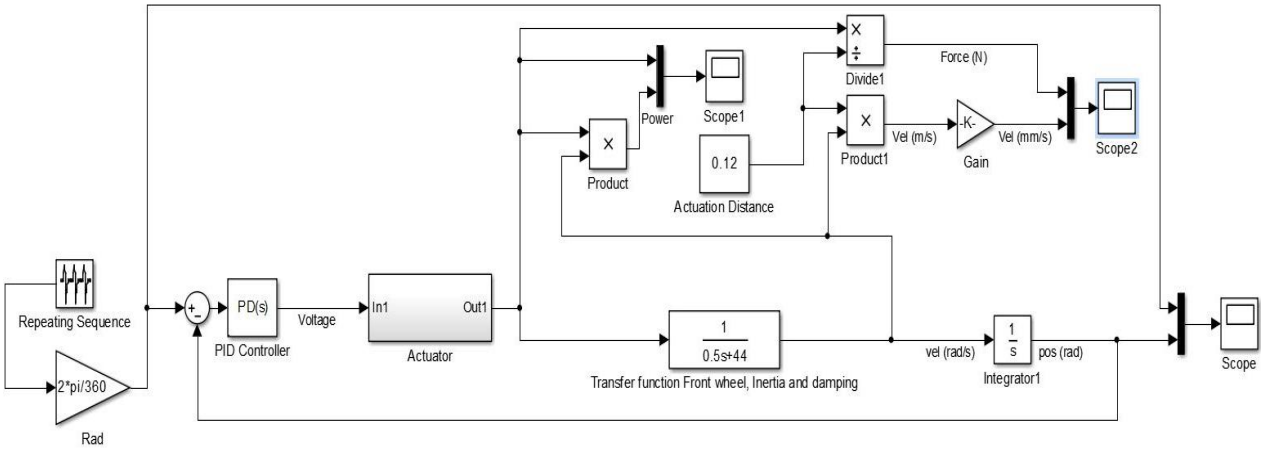

Figure 1-23: Simplified Simulink model, inertia and damping

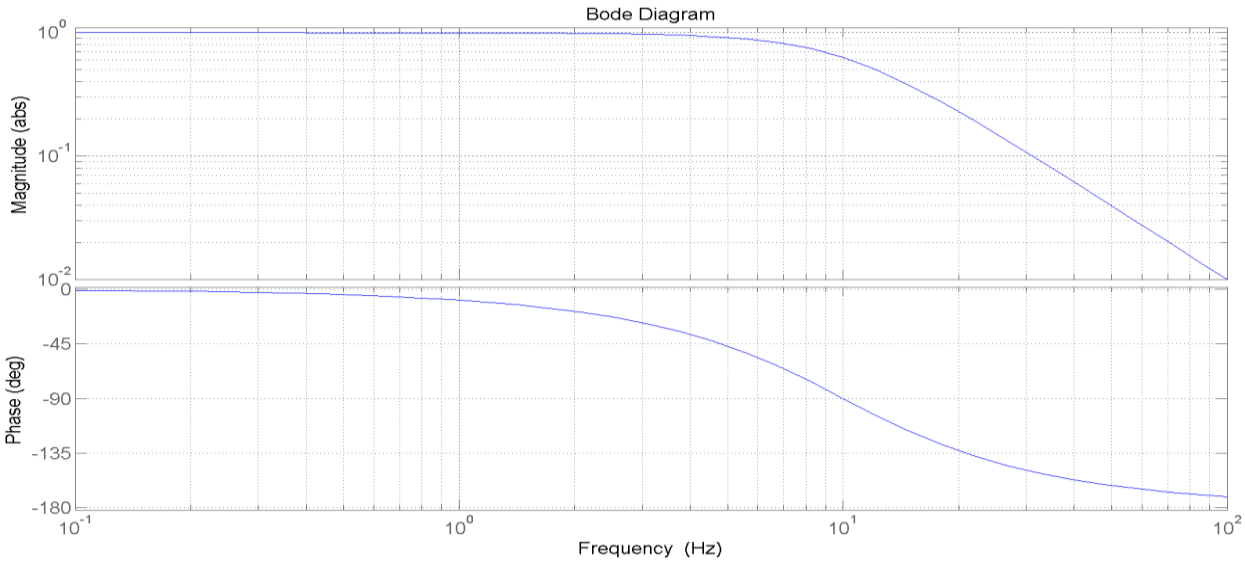

Figure 1-24: Bode plot simplified Simulink model, inertia and damping

Table 1-4; Parameters Simulink model

Symbol	Parameter	Value	Unit
N_l	Actuation distance front wheel	0.12	m
J_{fw}	Moment of inertia about the z-axis	0.5	Kg·m^2
B_{FW}	Angular damping about the z-axis [26]	44	N·m·s/rad

Figure 1-25 shows the force and velocity required to follow the reference signal in a 10 Hz closed loop system, 'scope2' of the Simulink model. A peak force (= $F_{m,IB}$) of approximately 1120 N is required at a velocity (= v_{SBW}) of 0.23 m/s. Figure 1-26 shows the angular response of the system.

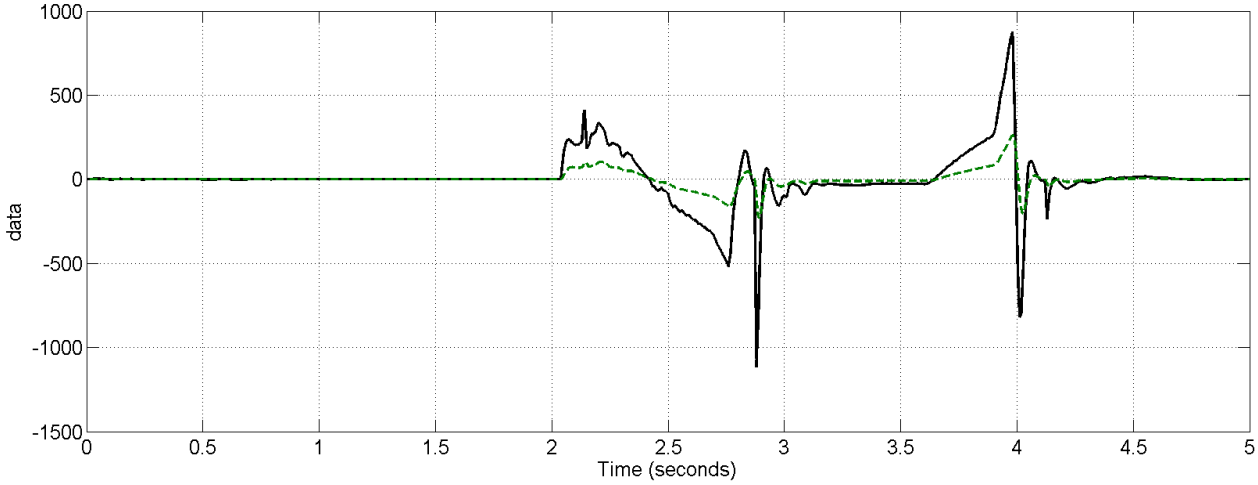

Figure 1-25: Force and velocity requirement for front wheel tracking, steer-by-wire
y-axis: line: force [N], dotted line: velocity [mm/s]

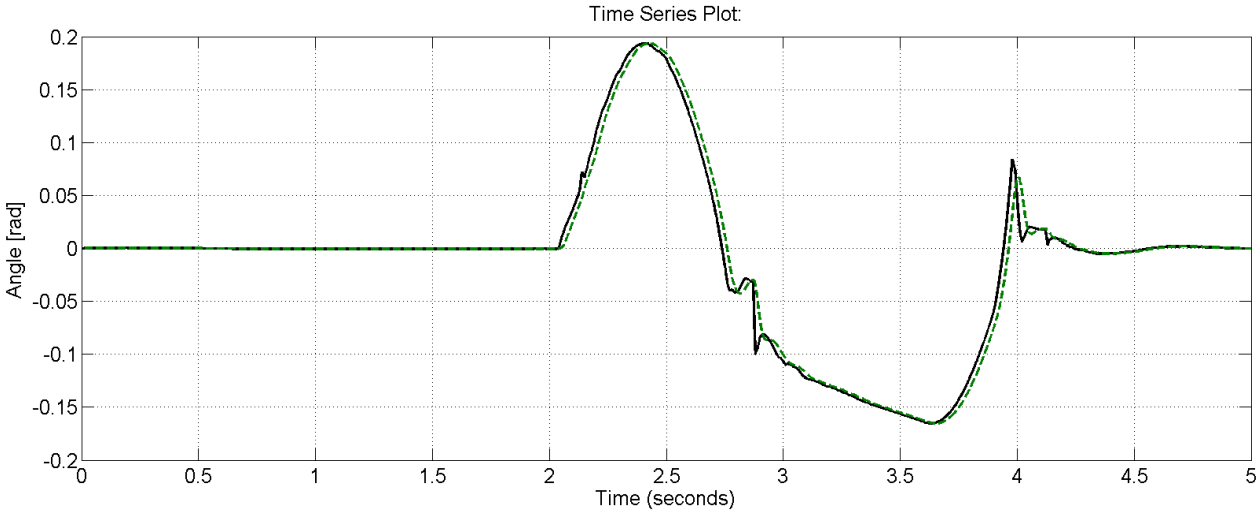

Figure 1-26: Front wheel angle
y-axis: line: reference signal, dotted line: system response

Tyre torque

The tyre torque is added to this model. The maximum tyre force of the front wheel is 5000 N. This force works at a distance (mechanical and pneumatic trail) to create the tyre torque, see Equation (2-3) and Figure 1-27. This tyre torque has to be compensated by the motor, by applying a force at an actuation distance. Values are shown in Table 1-5.

$$\tau_{tyre} = (t_p + t_m)F_{tyre} = F_{m,a}N_l \qquad (1\text{-}4)$$

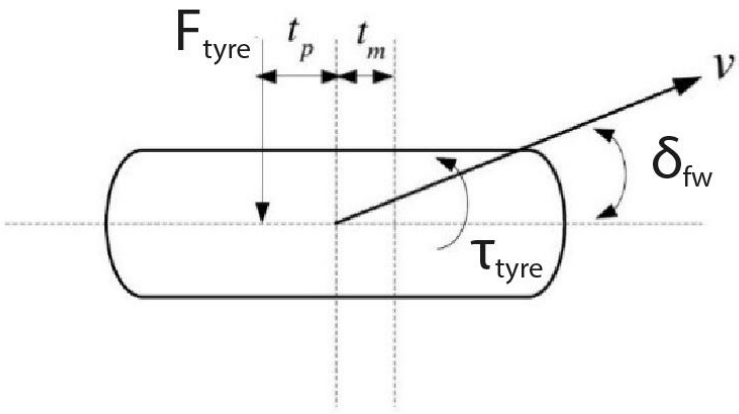

Figure 1-27: Tyre torque at a side-slip angle [27]

Table 1-5: Aligning torque, parameters and results

Symbol	Parameter	Value	Unit
F_{tyre}	Tyre force	5000	N
t_p	Pneumatic trail [27]	0.012	m
t_m	Mechanical trail [27]	0.010	m
τ_{tyre}	Tyre torque	110	Nm
N_L	Actuation distance front wheel	0.12	m
$F_{m,tyre}$	Force motor to compensate for tyre torque	917	N

Total requirements

The equation below shows amount of power the steering motor has to deliver.

$$P_{SBW} = \left(F_{m,IB} + F_{m,tyre}\right) v_{SBW} \qquad (1\text{-}5)$$

The total amount of power is 469 W, shown in Table 1-6. The moment of inertia, angular damping and aligning moment are taken into account. Excluded from this model is the dry friction, no value could be accurately estimated to model this component. Note that these numbers reflect the actuation of one front wheel.

Table 1-6: Results steer-by-wire, Simulink model and aligning torque

Symbol	Parameter	Value	Unit
v_{SBW}	Velocity motor, steer by wire system	0.23	m/s
$F_{m,IB}$	Force motor to compensate for inertia and damping	1120	N
$F_{m,a}$	Force motor to compensate for tyre torque	917	N
F_m	Force motor, ($F_{m,IB}$ + $F_{m,a}$)	2037	N
P_{SWB}	Power motor, steer by wire system	469	W

1.5.1.3 Differential steering

The difference in terms of actuation power between steer-by-wire and differential steering is the amount of displacement. The angle of the front wheels is a combination of the driver's steering angle and the AFS angle of the system. The actuator of a steer-by-wire system has to displace the total steering angle. A differential steering system only has to displace the AFS steering angle. The driver's angle is transferred by the steering wheel to the front wheels mechanically. A differential system has to generate forces that are the same as for a steer-by-wire system. The velocity at which these forces are generated are different.

Figure 1-28 shows the reference signal for the AFS angle of the left tyre. The amplitude is significantly smaller (2.75 deg), compared to the total steering angle (11.5 deg). Interesting is the velocity response in a same 10 Hz closed loop bandwidth system shown in Figure 1-29. It shows a maximum velocity of 0.19 m/s. A maximum motor power of 387 W is required, shown in Table 1-7. Note this is a worst-case scenario, the maximum velocity of the AFS and the maximum force of the steering system are combined which rarely is the case.

Table 1-7: Results differential steering, Simulink model and aligning torque

Symbol	Parameter	Value	Unit
v_{diff}	Velocity motor, differential steering system	0.19	m/s
F_m	Force motor, ($F_{m,IB}$ + $F_{m,a}$)	2037	N
P_{diff}	Power motor, differential steering system	387	W

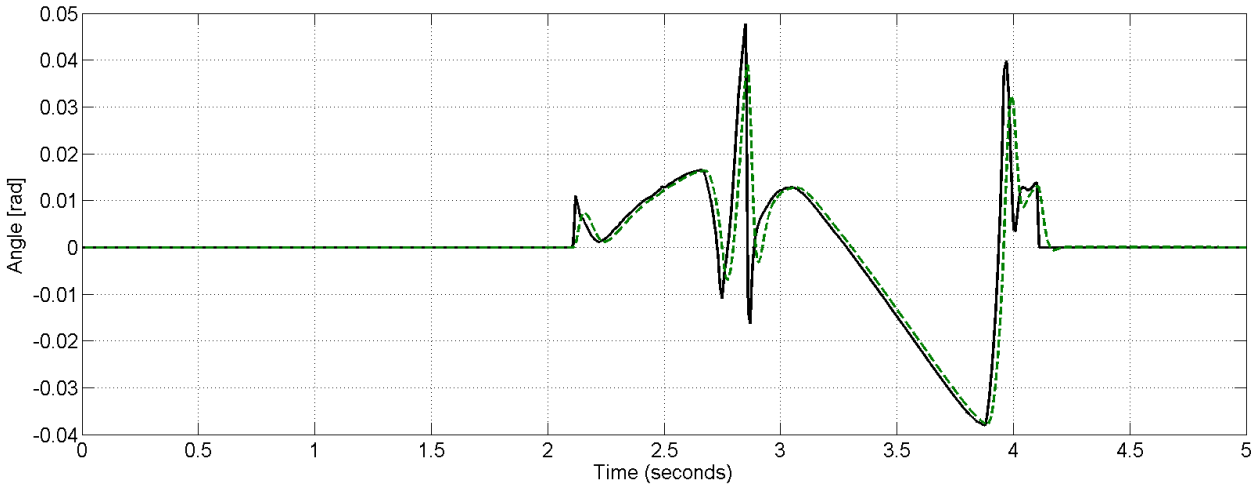

Figure 1-28: AFS angle
y-axis: line: reference, dotted line: system response

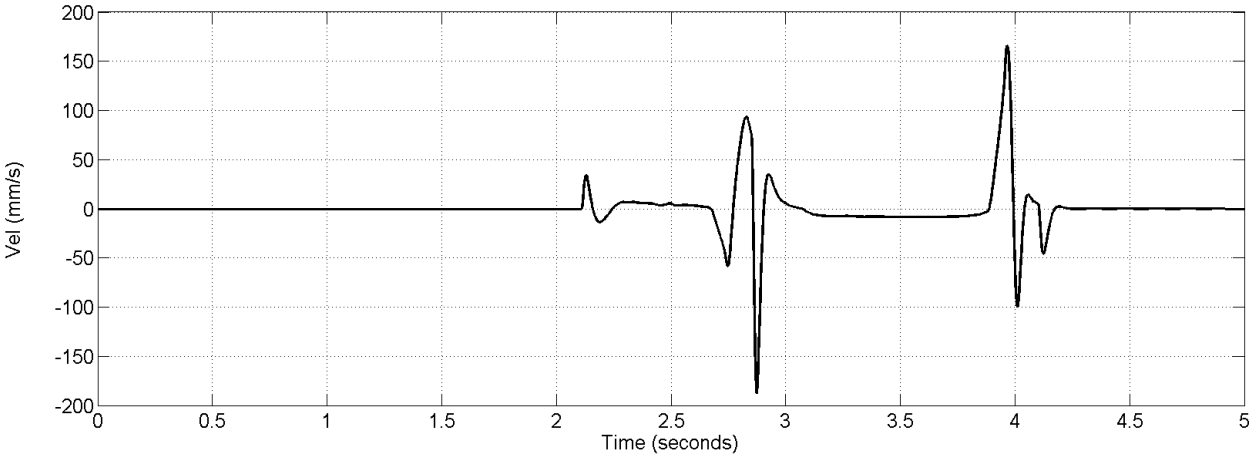

Figure 1-29: Force requirement for front wheel tracking, differential steering

1.5.2 Space

Available space in the engine compartment of the BMW 5 series e60 is very limited. Reasons are the many subsystems and an extremely efficient layout. Without making significant adjustments there is definitely no room for implementing a double AFS system.

For an independent steer-by-wire system there are opportunities. Removing the steering rack and column creates extra space, where an actuator could be placed. Figure 1-30 shows the space that would be available. At both sides there has to be room for the actuator to move the tie rod, connected to the front wheels. If the stroke length is decreased more room is available for the actuator placement.

Figure 1-30: Dimensions space steering rack [m]

1.5.3 Temperature

The environment temperature in the engine compartment is a major problem for an actuator. When the vehicle is lacking ventilation, e.g. it is standing still, the temperature could rise to 120 degrees. For electrical actuators this is a problem due to a decline in power, shown in the temperature de-rating curve, see Figure 1-31. The amount of power an actuator can deliver decreases when the environment temperature rises. Overcapacity or cooling could be a solution; both require extra space, which is already very scarce in the engine compartment of the BMW.

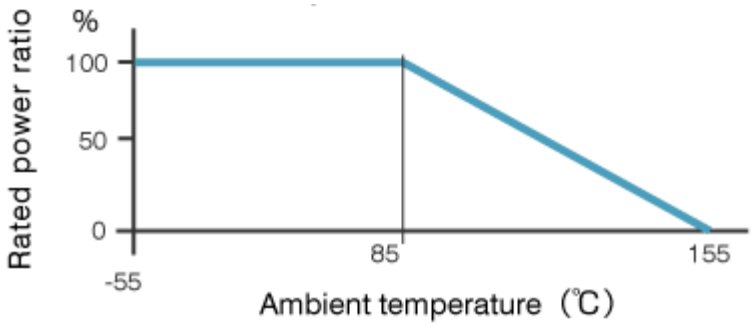

Figure 1-31: Temperature de-rating cure

1.5.4 Summary

The requirements of the proposed tyre utilization coefficient controller are clearly more demanding than the traditional steering characteristics. To actuate one front wheel in a steer-by-wire and differential steering system, combined with the TUCC, the amount of power required is 469 W and 389 W, respectively. This is considerably higher than the 188 W required in a conventional steering system.

The difference in power requirements between a differential and steer-by-wire system is small due to the equal road reaction forces acting on both systems. Displacing the AFS angle instead of the total steering angle shows a slight decrease in maximum velocity and therefore a 17% drop in power requirements for the differential steering system.

Installing an extra steering rack to build an independent differential steering system causes problems due to the space requirements. Without making significant changes to the motor compartment this is not a realistic possibility. Because there is no mechanical link required between front wheels and steering wheel, a steer-by-wire system is more flexible and realistic possibility. Environment temperatures complicate the space requirement problem. Motor power will greatly diminish at high temperatures. Overcapacity or cooling are solutions, but require scarce space.

1.6 Conclusion

This market analysis answers the next four questions.

1) How can IFWS enhance the performance of a vehicle?

2) Which current systems are used to implement independent front wheel steering into a vehicle?

3) Which control systems are used to implement IFWS and maintain driver steering feeling?

4) What are the requirements to implement IFWS?

Independent front wheel steering enables the optimization of the tyre utilization coefficients. This enhances the overall performance of a vehicle. There is a distinction between two types of active steering systems. The first system, differential steering, mechanically adds an AFS angle to the driver's steering angle. The second system, steer-by-wire, measures the driver's steering angle, electronically adds an AFS angle and powers the actuator connected to the front wheels to steer the vehicle. The mechanical link in differential steering preserves the conventional safety and haptic feedback. Steer-by-wire systems require a safety backup system.

Active steering – adding an AFS angle to the driver steering input – creates unexpected reaction forces for the driver. This steering interference makes safe driving difficult. Differential steering systems can disguise these disturbances by using a control system that combines the power steering and active steering system as shown in Figure 1-16. Steer-by-wire systems have the same problem if a direct current measurement is used as reference for the haptic feedback. Using a virtual model to calculate haptic feedback is a possible solution for implementing active steering. However, the downside is losing all road information. Using a virtual model in combination with a system that estimates the road reaction forces and controls the gain and frequencies of this feedback can result in a system without significant steering interference and loss of road information.

Power requirements from the literature are significant lower than from the tyre utilization coefficient controller, discussed in this research. For a steer-by-wire system and differential steering system the power requirements are 469 W and 389 W, respectively. The difference between differential steering and steer-by-wire is small, due to the equal road reaction forces acting on both systems. Without making significant adjustments to the engine compartment it is not possible to place a differential steering system, based on a double active steering system. Steer-by-wire systems have a space advantage, because the steering rack can be removed. High environment temperatures are a problem due to the decrease in power from an electric actuator.

Finalizing this market research three conclusions are made, which determine the direction of this thesis.

- Without making significant change to the engine compartment an independent steer by wire system is the primary solution for implementing an independent front wheel steering system
- A system combining the direct current measurement and the virtual model can give the optimal combination between road information and no steering interference.
- Using the TUCC combined with the ISBW system the power required to actuate one front wheel is 469 W.

Chapter 2

Research envelope

2.1 Background problem

An active front steering (AFS) system controls the angle of the front wheels, by adding an AFS angle to the driver's steering angle, recall section 1.2.2. *It is not possible to only adjust the angle of one front wheel, because they are mechanically linked.

A tyre utilization coefficient controller (TUCC), mentioned in section 1.1.5 optimizes the tyre utilization coefficient by adding an AFS angle, *to the drives steering angle, for each front wheel independently. To clarify, the main difference between an AFS system and the TUCC is the independent control of the front wheels. The TUCC is comparable to a separate AFS system for each front wheel.

The TUCC requires a steering system which can * independently adjust the angle of the front wheels. To implement such an independent front wheel steering (IFWS) system, it is required to understand how dynamics of the front wheel and steering motor work. Furthermore it can be challenging to provide safe haptic feedback to the driver, especially when the TUCC is constantly adjusting angle of the front wheels.

2.2 Definition of terms

The terms used throughout this thesis are shown in the table below.

Table 2-1: Definition of terms

	Term	Definition
AFS	Active Front Steering	A system which changes the angle of the front wheels to maximize performance or stability.
TUCC	Tyre utilization coefficient controller	A system which optimizes the tyre utilization coefficient by controlling the angle of both front wheels independently.
IFWS	Independent Front Wheel Steering	A system capable of steering both front wheels independently
ISBW	Independent Steer By Wire	An IFWS system where the mechanical link between steering wheel and front wheels is removed.
DCM	Direct Current Measurement	Measuring the current of the front wheel steering motor and using this a reference for the driver feedback
VM	Virtual Model	A model which calculates the forces on the front tyres based on the vehicle parameters and driver's input.
CDV	Combiner Direct current measurement & Virtual model	A system combining the DCM and the VM feedback to provide the driver with optimal feedback.
VMP	Virtual Model Presence	A number between 0 and 1 which shows the amount of VM presence in the feedback presented to the driver. 0 shows full dominance of the DCM and 1 shows full dominance of the VM.

2.3 System choice

As explained in section 1.3 there are two different IFWS systems. In one of those systems, independent differential steering, the mechanical link between steering wheel and front wheels is intact, while this connection is removed for independent steer by wire (ISBW) systems. In this thesis the choice is made to research the opportunities of an ISBW system. The main reason for this choice is the full control over the feedback provided to the driver. Main drawback of ISBW systems is the safety concern. Since this is a research project, this requirement has a lower priority compared to the implementation into commercial vehicles.

2.4 Structure and goal of thesis

This thesis is divided into three research parts, see Figure 2-1. Chapter 3 investigates the front wheel dynamics and interaction between steering motor and front wheel. The second part, chapter 4, focuses on the sources of haptic feedback provided to the driver and how this feedback is generated. Chapter 5 proposes a system design combining these feedback sources. Throughout this thesis the values of the feedback sources are given in tyre forces. The main advantage is the easy comparison with the actual tyre forces. The feedback forces are used as reference in a steering wheel system to generate the haptic feedback for the driver. This steering wheel system is outside the bounds of this thesis.

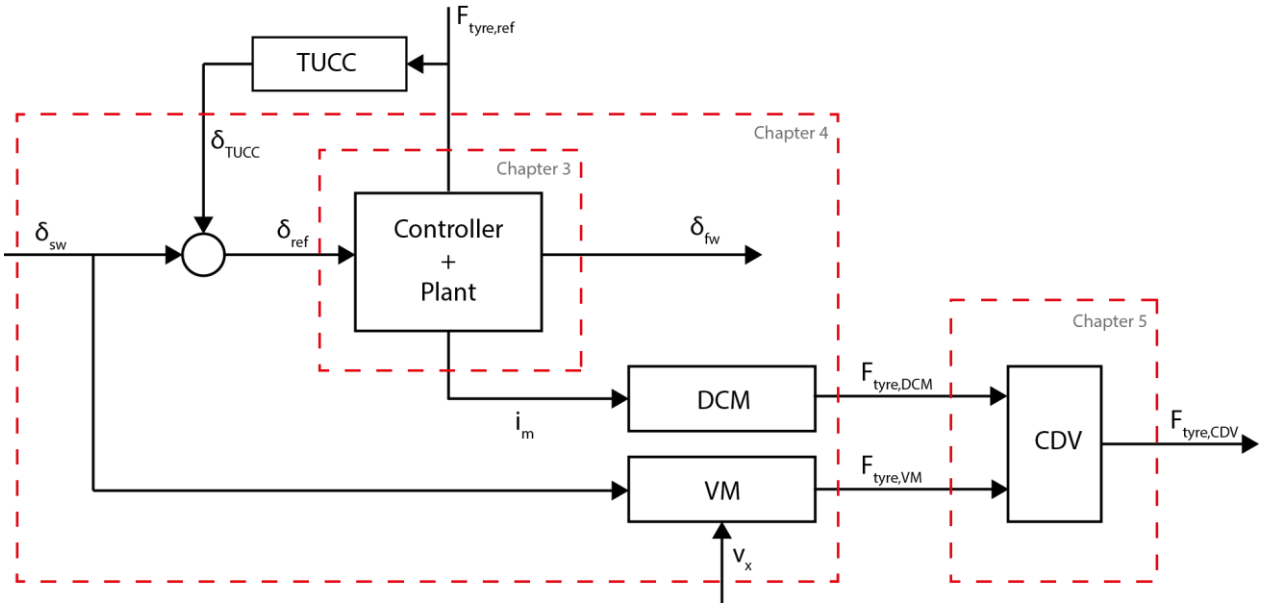

Figure 2-1: Thesis structure

δ_{sw}	= steering angle	[rad]
δ_{TUCC}	= TUCC angle	[rad]
δ_{ref}	= reference angle	[rad]
δ_{fw}	= front wheel angle	[rad]
i_m	= current steering motor	[A]
$F_{tyre,ref}$	= reference tyre force	[N]
$F_{tyre,DCM}$	= DCM tyre force	[N]
$F_{tyre,VM}$	= VM tyre force	[N]
$F_{tyre,CDV}$	= CDV tyre force	[N]

2.4.1 Front wheel dynamics

In conventional vehicles the connection between steering wheel, steering column, steering rack and front wheels, moves the front wheel in the desired direction. The power to steer the front wheels is delivered by the driver, perhaps with assistance of a power steering system. In the chosen ISBW system this connection is removed and replaced by two electric motors, each connected to a front wheel by a steering rack. These motors deliver the power required to steer the front wheels, see Figure 2-2 for a schematic overview.

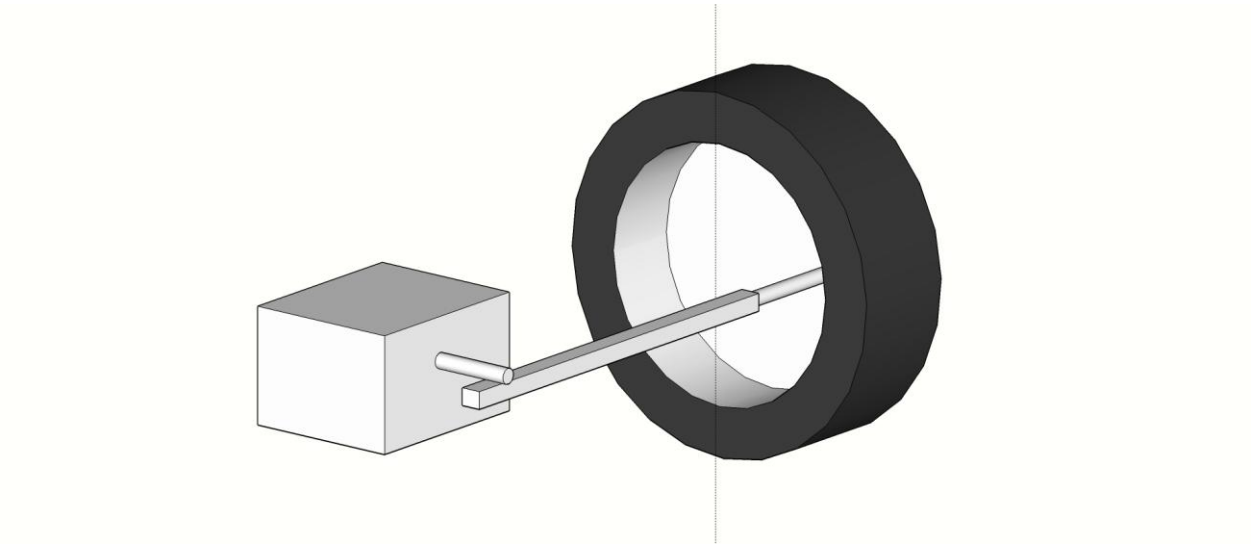

Figure 2-2: Schematic overview IFWS system

2.4.1.1 Problem statement

When the front wheel is connected to a steering motor, the motor dynamics influence the response of the total system. The amount of influence depends on the gear ratio between motor and front wheel. The gear ratio is defined as the ratio between motor turns and load turns. Increasing this ratio lowers the torque the motor has to deliver but increases its required speed. Understanding how the gear ratio also affects the inertia and damping 'felt' by both the tyre forces and by the motor torque is required for determining the response of the total system.

2.4.1.2 Research question

How will the gear ratio between steering motor and front wheel affect the dynamics of the steering mechanism?

2.4.1.3 Research design

In chapter 3 a model of the front wheel dynamics combined with tyre forces, motor and connection dynamics is proposed and used to determine how this system reacts to tyre forces and motor torque. The gear ratio between motor and front wheel is taken as a variable to see how this parameter affects the response of the system.

2.4.2 Haptic driver feedback

In conventional vehicles, the connection steering wheel, steering column, steering rack and front wheels transfers in the tyre forces to the driver. The tyre forces are felt by the driver through torque in the steering wheel. This important information for the driver is also called road information. When the mechanical connection is removed this information is lost and has to be generated by an electric motor, connected to the steering wheel. As mentioned in section 1.4.2 there are two main principles

to determine how much feedback has to be presented to the driver, direct current measurement (DCM) and virtual model (VM). These two methods are discussed in section 2.4.2.1 and 2.4.2.2.

2.4.2.1 Haptic driver feedback using DCM

It is assumed that the tyre force acting on the tyre works at a constant distant from the tyre's rotation z-axis. Therefore the road torque of the tyre is linear to the tyre force. The road torque is compensated by the steering motor, to maintain a certain steering angle. The torque the steering motor has to deliver is equal to the road torque divided by the constant gear ratio, between motor shaft and front wheel. The current drawn by an electric motor is a good and linear indication of how much torque the motor delivers. Therefore, by measuring the current drawn by the motor an approximation of the tyre forces can be made. This value can be used to provide the driver with haptic feedback.

2.4.2.1.1 Problem statement

When replacing the constant steering angle with an altering steering angle, the dynamics of the front wheel, steering rack and electric motor will also affect the required motor torque. These dynamics can disturb the linear relationship between current and tyre forces and disturb the feedback provided to the driver.

2.4.2.1.2 Research question

Can a DCM give accurate readings of the actual tyre forces?

2.4.2.1.3 Research design

A model of the front wheel, motor and steering rack dynamics is created. In different steering maneuvers the DCM is compared to get an indication how well it represents the actual tyre forces. The tyre forces in this model are simulated with the simulation package CarSim.

2.4.2.2 Haptic driver feedback using VM

As explained in section 1.4.2, using the tyre forces as reference for the driver feedback can cause problems; when the TUCC significantly alters the front wheel steering angle, the tyre forces change and thus the feedback to the driver. This is called steering interference, or in an independent front wheel steering system combined with TUCC controller, TUCC interference. If the driver is presented with this possible unexpected feedback it can provoke an unwanted steering action and destabilize the vehicle. It is desirable to have a model which can calculate the feedback for the driver onboard, purely based on the driver's steering angle and not on the actual angle of the front wheels. This model is independent of the TUCC and is not compromised by TUCC interference. The downside of using a virtual model is the absence of road information. Driving over gravel cannot be felt in the steering wheel since the feedback reference is not based on the tyre forces, but just on the steering wheel angle and other vehicle parameters.

2.4.2.2.1 Problem statement

A problem of using a virtual model is accurately calculating the tyre forces. If the calculated tyre forces do not match the tyre forces, the driver will get a wrong perception of movement and more important, when the system changes among feedback source (VM and DCM) it can suddenly create a big feedback change due to the mismatch. This is called mismatch disturbance.

2.4.2.2.2 Research question

Can a VM compute the actual tyre forces accurately?

2.4.2.2.3 Research design

In section 4.1.2 a virtual model is proposed. The tyre forces computed by this model are compared to the tyre forces to see how well this source of feedback matches to actual tyre forces. If this kind of

reference is accurate, it can be used to provide the driver with feedback when it is not possible to use the DCM, i.e. when there is too much TUCC interference.

2.4.3 Combiner DCM and VM

Combiner DCM and VM (DCV) is a system that combines both feedback sources in such a way that it can provide the driver with optimal feedback, i.e. the minimization of TUCC interference and the maximization of road information.

2.4.3.1 Problem statement

The goal is to create a system where the TUCC interference does not influence the feedback to the driver. I.e. the CDV should switch to the VM feedback when there is TUCC interference and switch to the DCM feedback when the TUCC is not active to provide the driver with road information when possible. Switching between two different feedback sources can cause sudden unwanted changes in haptic feedback. A smooth transition should be developed without making the system slow.

2.4.3.2 Research question

Is it possible to develop a system which can blend two feedback sources, providing the driver with optimal feedback?

2.4.3.3 Research design

A system combining the DCM and VM is proposed (CDV) in chapter 5. To validate the CDV, different driving maneuvers, combined with an active TUCC are simulated. In these maneuvers feedback provided to the driver is analyzed for TUCC interference and mismatch disturbance.

2.5 Summary

A tyre utilization coefficient controller optimizes the tyre utilization coefficient by using an independent front wheel steering system. This thesis covers three important aspects for implementing such a system, with the combination of optimal feedback.

Chapter 3 discusses the dynamics of the front wheel and the connection to the steering motor. It answers the first research question:

- How will the gear ratio between steering motor and front wheel affect the dynamics of the steering mechanism?

Providing haptic feedback to the driver is covered in the second part of this thesis. The accuracy of the two feedback sources are tested in chapter 4. The corresponding research questions are:

- Can a direct current measurement give accurate readings of the actual tyre forces?
- Can a virtual model compute the actual tyre forces accurately?

Combining the two feedback sources can be a solution between road information and TUCC interference. It is discussed in chapter 5, combined with the last research question:

- Is it possible to develop a system which can blend two feedback sources, providing the driver with optimal feedback?

Chapter 3

Front wheel dynamics

The goal of this chapter is to determine how the gear ratio between motor and front wheel will affect the dynamic response of the steering system. First, the power requirements are determined and a motor to steer the front wheel is selected. Upper and lower boundaries of the gear ratio are also defined. Second, a model representing the front wheel, steering rack and motor dynamics is proposed. In this model the gear ratio is used as a variable. Third, simulations are done to determine the influence of the gear ratio on the inertia and damping of the total system. A passive step response shows the systems behavior. Finally conclusions are made for implementation of an IFWS system.

3.1 Power requirements

As shown in section 1.5, tracking the reference signal of the TUCC controller requires a certain amount of power from the steering motor. Table 1-2 and Table 1-6 show the motor has to deliver a maximum force of 2037 N at an actuator distance of 0.12 m from the z-axis of the front wheel. The maximum velocity at which this force is applied is 0.23 m/s, which gives a required motor power of 469 W. The force and velocity acting at the actuation distance, result in a front wheel torque and speed, see Figure 3-1.

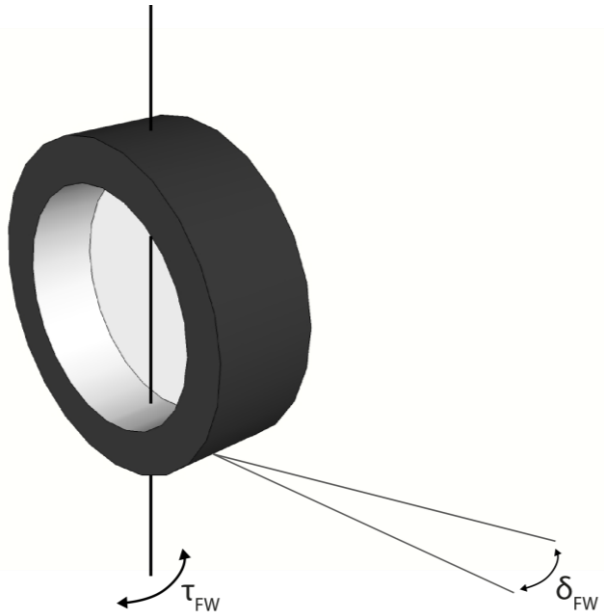

Figure 3-1: Resulting front wheel torque

Due to the uncertainties in the power requirements estimation, a safety factor is required. The high environment temperature lowers the maximum possible electric power drawn by the motor. To cope with the problems mentioned, a safety factor of 2.0 is chosen. The excess power is equally divided between torque and speed requirements, see Table 3-1. With the final requirements determined, the motor is chosen in the next section.

Table 3-1: Front wheel power requirements

Symbol	Parameter	Required	Safety factor	Required (safety)	Unit
τ_{fw}	Torque front wheel	244	√2	345	Nm
$\dot{\delta}_{fw}$	Speed front wheel	1.92	√2	2.71	rad/s
P_{fw}	Power front wheel	469	2	938	W

3.2 Motor choice

To steer the front wheel of the IFWS system, a brushless Emoteq Quantum DC QB03403 is chosen. This motor has a maximum power output of 1072 W at its optimal speed of 523 rad/s (=5000 RPM). There is a 12.5% excess motor power capacity compared to the previous determined requirements. This excess power provides the opportunity to alter the gear ratio between front wheel and motor and still meet the power requirements. When running the motor at non-optimal speeds, the motors power decreases. At the speeds where the motor power becomes equal to the power required, the upper and lower gear ratios are determined, see Table 3-2 and Figure 3-2.

Table 3-2: Gear ratio boundaries

Symbol	Parameter	Upper gear ratio	Optimal motor gear ratio	Lower gear ratio	Unit
τ_m	Torque motor	1.4	2.05	2.55	Nm
$\dot{\delta}_m$	Speed motor	670	523	370	rad/s
$N_{m/fw}$	Gear ratio motor / front wheel	247	180	136	-

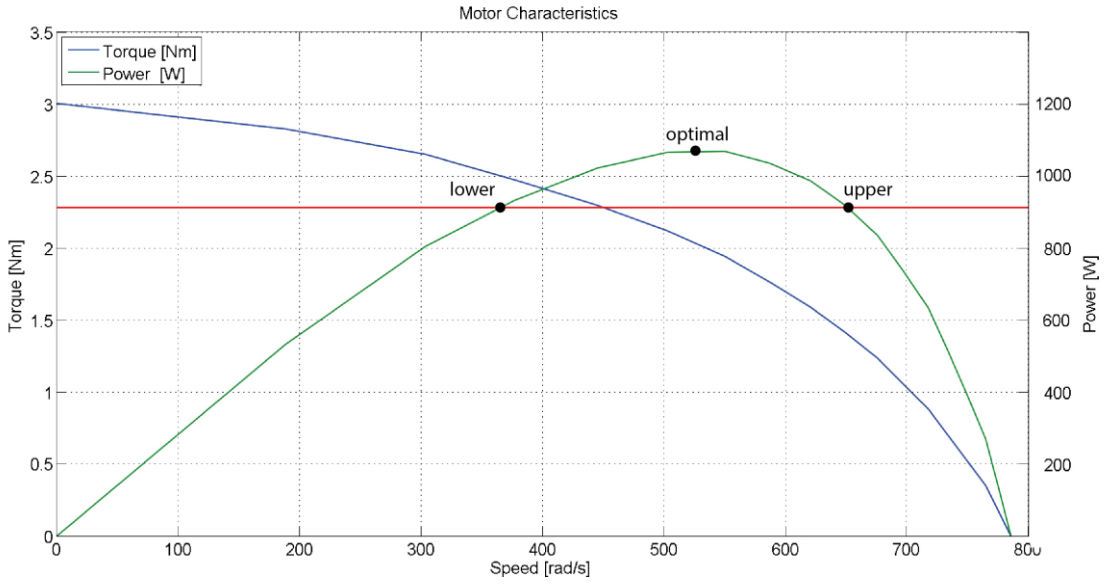

Figure 3-2: Emoteq Quantum DC QB03403 motor characteristics
Gear ratio upper, lower and optimal

3.3 Model data

The front wheel dynamics model combines the inertia and damping of the front wheel and the steering motor. Added to this model is the mass and damping of the steering rack. The connections between these components are modeled as springs, see Figure 3-3.

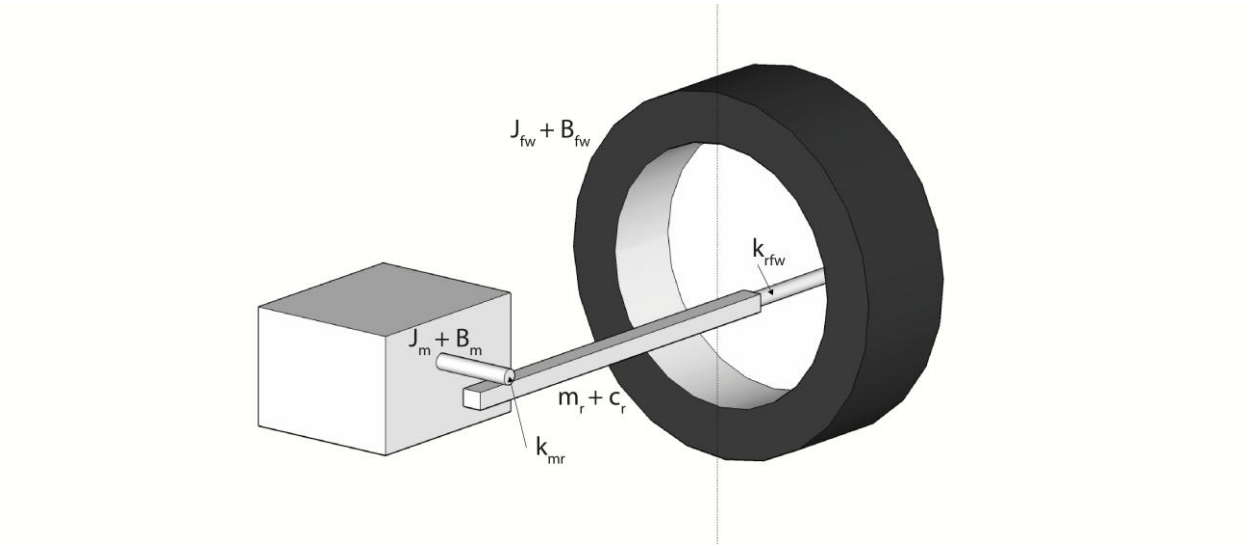

Figure 3-3: Overview front wheel steering system

3.3.1 Inertia and damping

The values for inertia and damping of the motor, steering rack and front wheel are shown in Table 3-3. The manufacturer of the motor provides the inertia and damping in their motor catalogues. The moment of inertia of the front wheel is calculated by its weight and dimensions. The value for its angular damping and the parameters of the steering rack are found in literature.

Table 3-3: Parameters front wheel steering system (a)

Symbol	Parameter	Value	Unit
J_m	Inertia motor	$2.1 \cdot 10^{-4}$	$kg \cdot m^2$
J_{fw}	Inertia front wheel	$5 \cdot 10^{-1}$	$kg \cdot m^2$
m_r	Mass rack	$1 \cdot 10^{0}$	kg
B_m	Damping motor	$2.1 \cdot 10^{-4}$	Nm·s/rad
B_{fw}	Damping front wheel	$4.4 \cdot 10^{1}$	Nm·s/rad
c_r	Damping rack	$1 \cdot 10^{0}$	N·s/m

3.3.2 Connections

Two connections combine the three bodies mentioned above. Both connections are modeled as stiff springs with defined values, see Table 3-4. The first connection, between the front wheel and the steering rack, is also known as the tie rod. The actuation distance of the tie rod, from the z axis of the front wheel, is determined as 0.12 m. Therefore the gear ratio between rack and front wheel is known, see Table 3-4. The second connection, between motor shaft and steering rack, is defined in angular stiffness. This connection includes a ball screw mechanism to transform the fast rotational movement of the motor shaft into a slower linear motion of the steering rack. The gear ratio of this connection is dependent on the total gear ratio between motor and front wheel, see the formula below.

$$N_{m/fw} = N_{m/r} \cdot N_{r/fw} \tag{3-1}$$

Table 3-4: Parameters front wheel steering system (b)

Symbol	Parameter	Value	Unit
k_{mr}	Stiffness connection motor - rack	$6 \cdot 10^5$	Nm/rad
k_{rfw}	Stiffness connection rack - front wheel	$4 \cdot 10^5$	N/m
$N_{r/fw}$	Gear ratio rack / front wheel	$1.2 \cdot 10^{-1}$	m/rad
$N_{m/r}$	Gear ratio motor / rack	$N_{m/fw}/N_{r/fw}$	rad/m

3.3.3 Tyre forces

A 225/60 R18 tyre from an E-class sedan is used in the front wheel model. The tyre parameters are extracted from the database of CarSim. Figure 3-4 shows the non-linearity of the tyre forces. The forces act on the tyre at a distance equal to the pneumatic and mechanical trail to create the tyre torque, see equation 3-2.

$$\tau_{tyre} = (t_p + t_m) F_{tyre} \tag{3-2}$$

τ_{tyre} = torque road [Nm]
t_p = trail pneumatic [m]
t_m = trail mechanical [m]

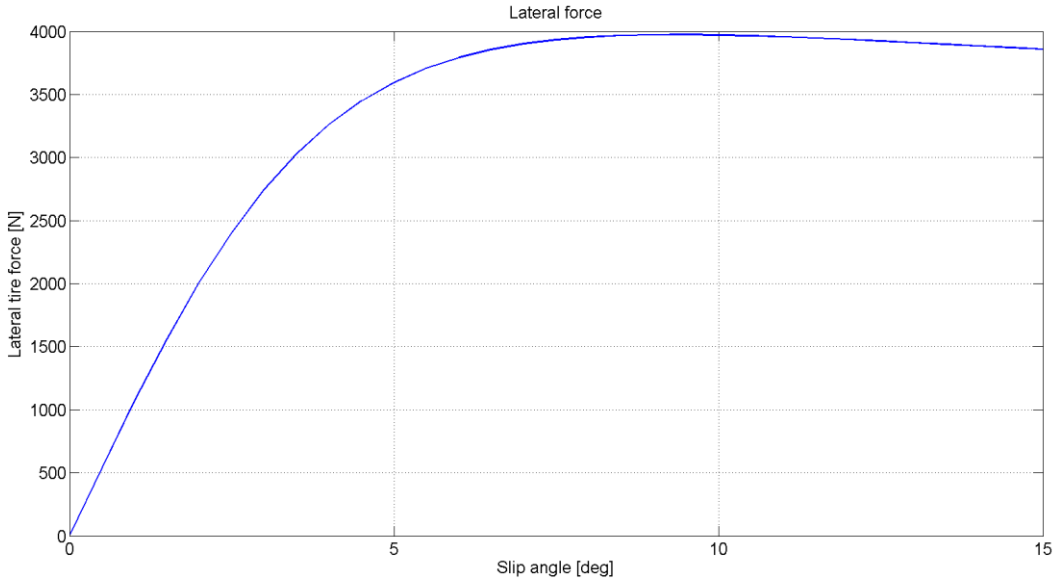

Figure 3-4: Tyre force, Front wheel dynamics

3.3.4 Equations of motion

All the steering system components are combined in the three equations below, defining the positions of motor, steering rack and front wheel, respectively. The equations are schematic also represented in Figure 3-5**.**

$$k_\tau i_m = \tau_m = J_m \ddot{\delta_m} + B_m \dot{\delta}_{\mathrm{m}} + k_{mr}(\delta_m - N_{m/r} x_r) \tag{3-3}$$

$$0 = m_r \ddot{x_r} + c_r \dot{x}_{\mathrm{r}} + k_{rfw}(x_r - N_{r/fw}\delta_{fw}) + k_{mr} N_{m/r}(N_{m/r} x_r - \delta_m) \tag{3-4}$$

$$\tau_{tyre}(\delta_{\mathrm{fw}}) = J_{fw} \ddot{\delta_{fw}} + B_{fw} \dot{\delta}_{\mathrm{fw}} + k_{rfw} N_{r/fw}(N_{r/fw}\delta_{fw} - x_r) \tag{3-5}$$

k_t	= torque constant	[Nm/A]
i_m	= current motor	[A]
x_r	= position steering rack	[m]

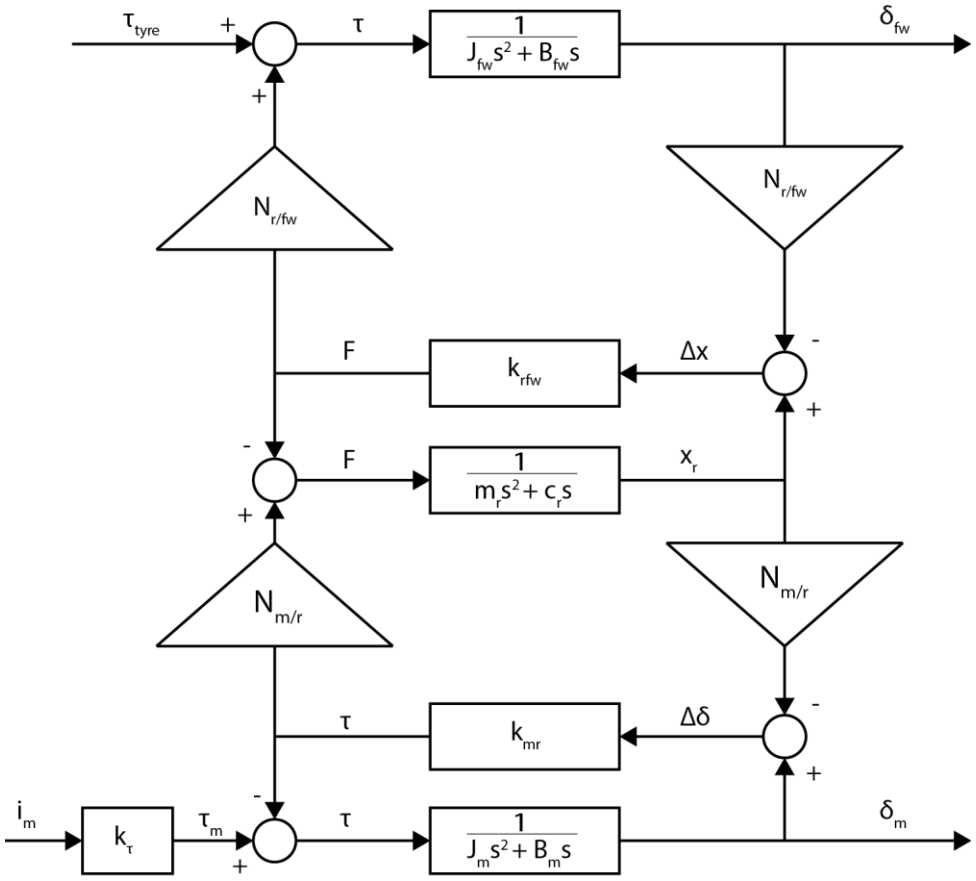

Figure 3-5: Schematic overview front wheel dynamics

3.4 Simulation method

The overcapacity of the motor provides the possibility to alter the gear ratio between motor and front wheel. Due to the decrease in motor power when running at non-optimal speeds there is an upper and lower gear ratio as shown in Figure 3-2. When implementing more extreme gear ratios the motor is not able to meet the power requirements.

3.4.1 Inertia and damping

The inertia and damping of the total system are determined by the parameters of the motor, steering rack and front wheel. The gear ratio between motor and front wheel determines how much the motor dynamics influence the total system.

Three situations are analyzed in the upcoming sections, see Table 3-5. In the first situation the inertia and damping felt by the front wheel are studied for different gear ratios. This front wheel perspective shows how much inertia and damping are present when a force is applied to the front wheel. At higher gear ratios, an increase in inertia and damping is expected since the speed of the motor shaft increases.

The second situation shows the inertia and damping felt from the motor perspective. Since a higher gear ratio lowers the amount of motor torque required to turn the motor shaft, a decrease in inertia and damping is expected at higher gear ratios.

The space available for implementing an IFWS system is very limited without making significant changes to the vehicle's motor compartment, see section 0. Lowering the required motor torque is desirable as it decreases the size of the motor.

In the final situation, the inertia and damping felt by the motor multiplied by the gear ratio are plotted. This is equal to the inertia and damping felt by the front wheel divided by the gear ratio, since the two perspectives are related by the gear ratio squared.

The final situation shows a combination of the two previous situations. Increasing the gear ratio lowers the required motor torque, described in the second situation. At high gear ratios, the motor shaft has to spin faster to provide the same front wheel response. The motor's inertia and damping become more dominant at these higher speeds and require a larger part of the motor torque. The factor of increase is equal to the gear ratio. An optimum is found where the motor has to deliver the least amount of torque to actuate the inertia and damping of the system and result in the same front wheel response.

Table 3-5: Simulation situations, inertia and damping

Situation	x-axis	y-axis
1a	$N_{m/fw}$	$J_{tot,fw}$ $B_{tot,fw}$
1b	$N_{m/fw}$	$J_{tot,m}$ $B_{tot,m}$
1c	$N_{m/fw}$	$J_{tot,m} \cdot N_{m/fw} = J_{tot,fw} / N_{m/fw}$ $J_{tot,m} \cdot N_{m/fw} = B_{tot,fw} / N_{m/fw}$

$J_{tot,(fw/m)}$ = inertia total, felt by (front wheel / motor) [kg·m^2]
$B_{tot,(fw/m)}$= damping total, felt by (front wheel / motor) [Nm·s/rad]

3.4.2 Passive step response

A passive step response shows how the front wheel steering system will behave if, at a certain steering angle, there is no motor input, but only the tyre forces acting on front wheel. The front wheel will move from the step angle towards the neutral position. In this transition some overshoot can present. How the gear ratio influences this response is analyzed in this section. For the accuracy of the DCM, this response is very important. In chapter 4 the DCM is further discussed. A quick summary of how this system works is given below.

Tyre forces act on the front wheel and cause it to move. A position sensor detects this displacements and a controller powers the steering motor to counter this. The current drawn by this motor is used as approximation of the road torque and thus used for determining the feedback provided to the driver.

If the front wheel reacts quickly to the tyre forces, there is a quick displacement and quick response of the motor. The phase shift between the tyre force and the driver feedback will be small. On the other hand, if the tyre forces are not able to displace the front wheel significantly, there will be no current in the motor and also no accurate representation of the tyre force in the DCM.

In this simulation the upper, lower and optimal motor gear ratios, together with the optimal inertia and damping gear ratios, found in section 3.5.1, are analyzed. Two different situations are proposed, see Table 3-6. The first situation introduces a step at the front wheel angle, within the linear region of the tyre forces. The second situation analyses the same behavior with the step input reaching beyond this linear region, into the nonlinear tyre forces.

Table 3-6: Simulation situations, passive step response

Situation	x-axis	y-axis	Step δ_{fw}	$N_{m/fw}$
2a	time	δ_{fw} F_{tyre}	3 deg	N_{opJ} N_{low} N_{opm} N_{up} N_{opB}
2b	time	δ_{fw} F_{tyre}	12 deg	N_{opJ} N_{low} N_{opm} N_{up} N_{opB}

N_{opJ} = gear ratio optimal inertia [-]
N_{low} = gear ratio lower [-]
N_{opm} = gear ratio optimal motor [-]
N_{up} = gear ratio upper [-]
N_{opB} = gear ratio optimal damping [-]

3.5 Results and discussion

3.5.1 Inertia & damping

Situation 1a

Figure 3-6 shows the representation of the coupled inertia and damping of the motor, steering rack and front wheel. At the low gear ratios, the dynamics of the motor are too small to affect the system. After a gear ratio of 10 and 100 the motor inertia and damping, respectively, become significant. The motors damping is significant at a higher gear ratio, because the inertia / damping ratio of the motor is higher than the inertia / damping ratio of the front wheel - steering rack coupling.

Choosing a high gear ratio results in a system with high inertia and damping. The tyre forces will not be able to rapidly push the front wheel back to its neutral steering position. Also at higher gear ratios the inertia increases while the damping stays almost constant, which results in a more oscillating system.

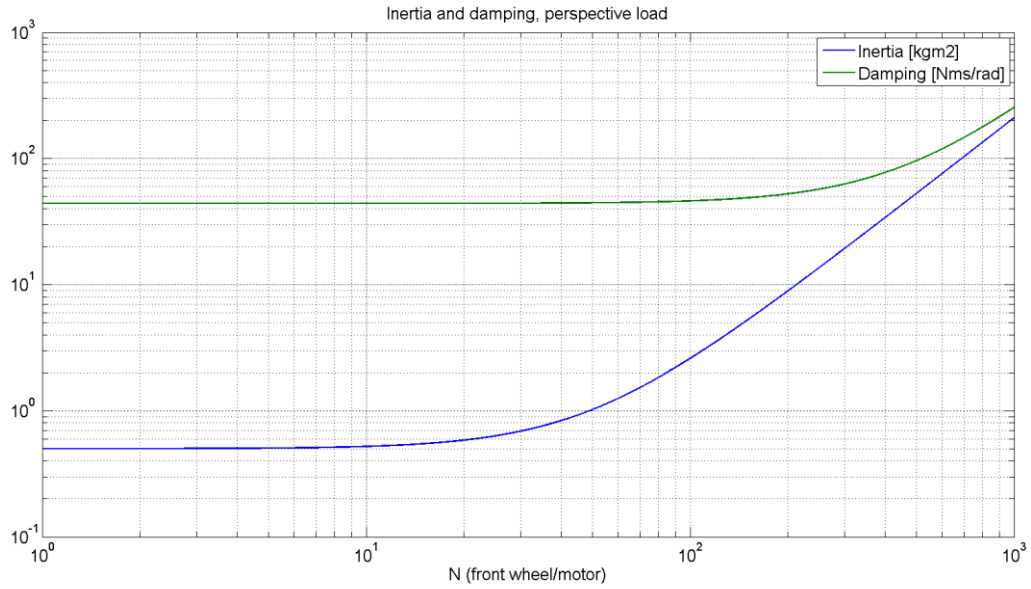

Figure 3-6: Inertia and damping, perspective load

Situation 1b

The inertia and damping from the motor's perspective are shown in Figure 3-7. After a gear ratio of 200 and 1000, the values for inertia and damping saturate as they become purely based on the motor's own values. A low gear ratio results in a high inertia and damping value, felt by the motor. Therefore a too low gear ratio is not desirable, since it will increase the motor torque requirements, which requires a bigger motor.

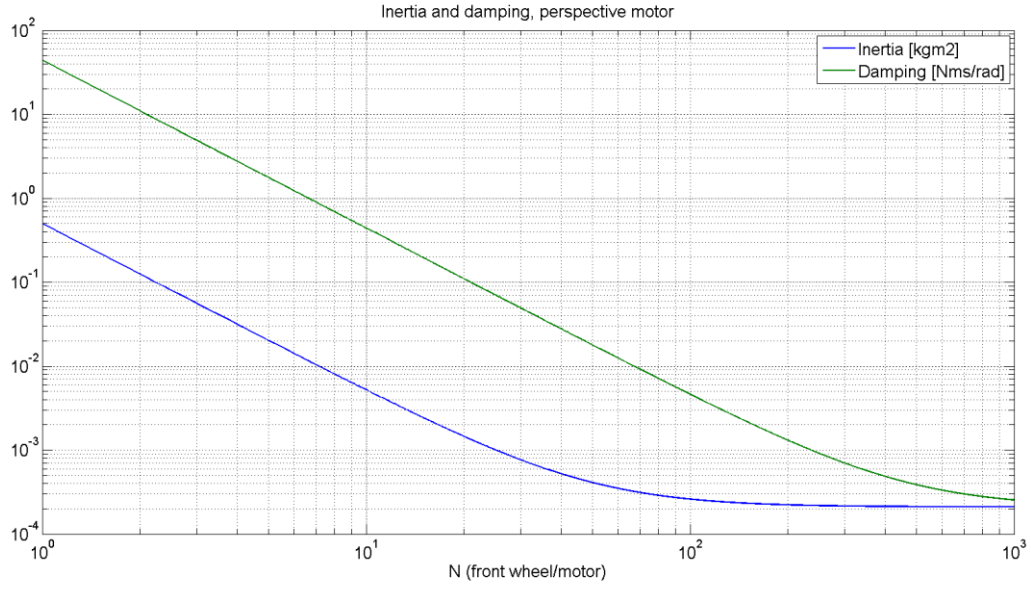

Figure 3-7: Inertia and damping, perspective motor (a)

Situation 1c

From the previous two situations it is clear a gear ratio too low or too high is not desirable. Figure 3-8 shows the inertia and damping of the total system times the gear ratio, from the perspective of the motor. This situation shows an optimum, at which the lowest amount of torque is required from the motor, to let the inertia of the system follow a certain front wheel angle.

Increasing the gear ratio lowers the required motor torque, see situation 1b, until the motor itself has to accelerate and spin so fast that its own dynamics slow down the system and the required torque rises, see situation 1a. An optimal inertia gear ratio is found at N_{opJ} = 49. This same optimum is found for the damping, at N_{opB} = 457. The combined optimum of the inertia and damping is between these two gear ratios and could ultimately be determined by the frequency and amplitude of the front wheel angle.

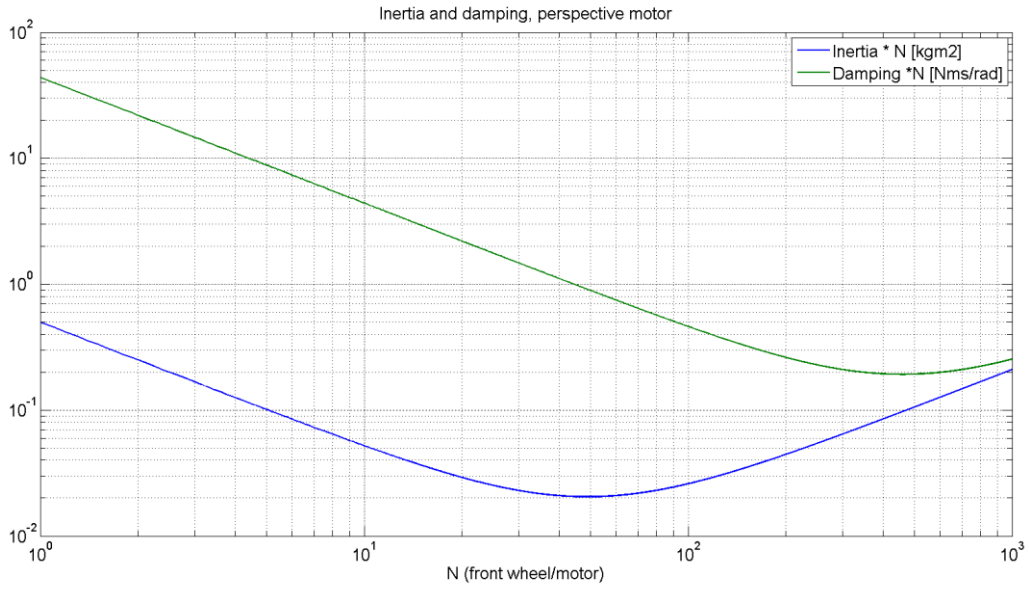

Figure 3-8: Inertia and damping, perspective motor (b)

3.5.2 Passive step response

Table 3-7 shows the different gear ratios analyzed in this study. The response of front wheel is a direct result of the inertia and damping felt by the front wheel, see situation 1a.

Table 3-7: Gear ratios step response

$N_{m/fw}$	Parameter	Value
N_{opJ}	Gear ratio optimal inertia	49
N_{low}	Gear ratio lower	136
N_{opm}	Gear ratio optimal motor	180
N_{up}	Gear ratio upper	247
N_{opB}	Gear ratio optimal damping	457

Situation 2a

Figure 3-9 shows the angular position of the front wheel. A lower gear ratio results in a faster system. In Figure 3-10 the tyre force acting on the front wheel is shown. The front wheel moves from the step angle towards its neutral position. The tyre force is linear and this system behaves as a conventional mass damper spring system. Table 3-8 shows the natural frequency and damping ratio for different gear ratios. It is clear that the response of the upper and optimal damping gear ratio with a frequency of 1.5 and 0.85 Hz respectively is too slow. The response at higher gear ratios is also more oscillating which is not desirable.

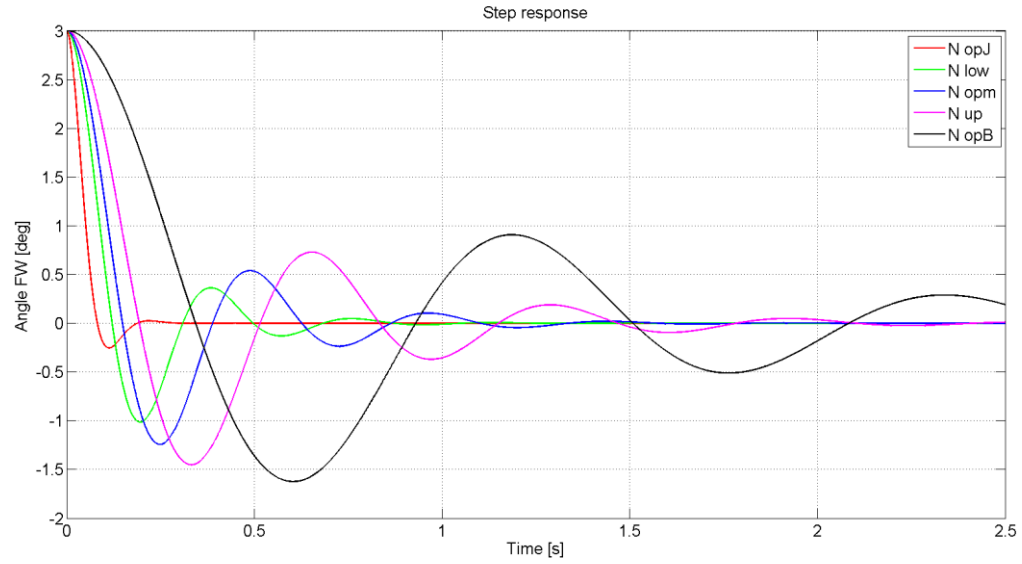

Figure 3-9: Step response 3 deg, front wheel angle

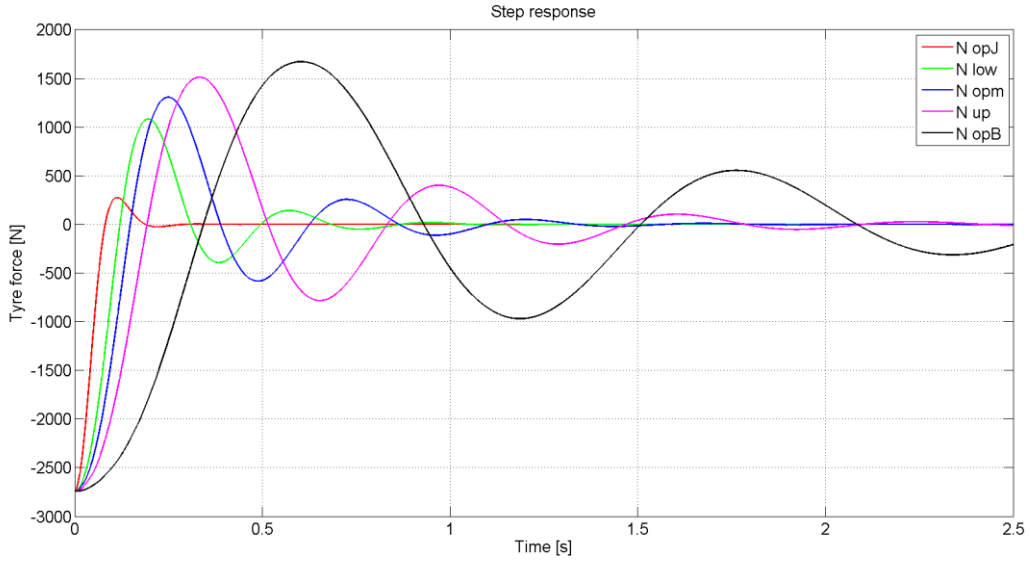

Figure 3-10: Step response 3 deg, tyre force

Table 3-8: Natural frequency and damping ratio, linear tyre force

$N_{m/fw}$	Parameter	Natural frequency	Unit	Damping ratio
N_{opJ}	Gear ratio optimal inertia	5.0	Hz	0.70
N_{low}	Gear ratio lower	2.7	Hz	0.30
N_{opm}	Gear ratio optimal motor	2.1	Hz	0.26
N_{up}	Gear ratio upper	1.5	Hz	0.22
N_{opB}	Gear ratio optimal damping	0.85	Hz	0.18

Situation 2b

Figure 3-11 shows the response of the front wheel when the tyre force partly operates in its nonlinear region. The response of the system is much slower compared to situation 2a. The nonlinear tyre forces saturate and cannot provide enough force to quickly accelerate the tyre to its neutral position, see

Figure 3-12 and Table 3-9. Values for the damping ratio could not be estimated in this non-linear system.

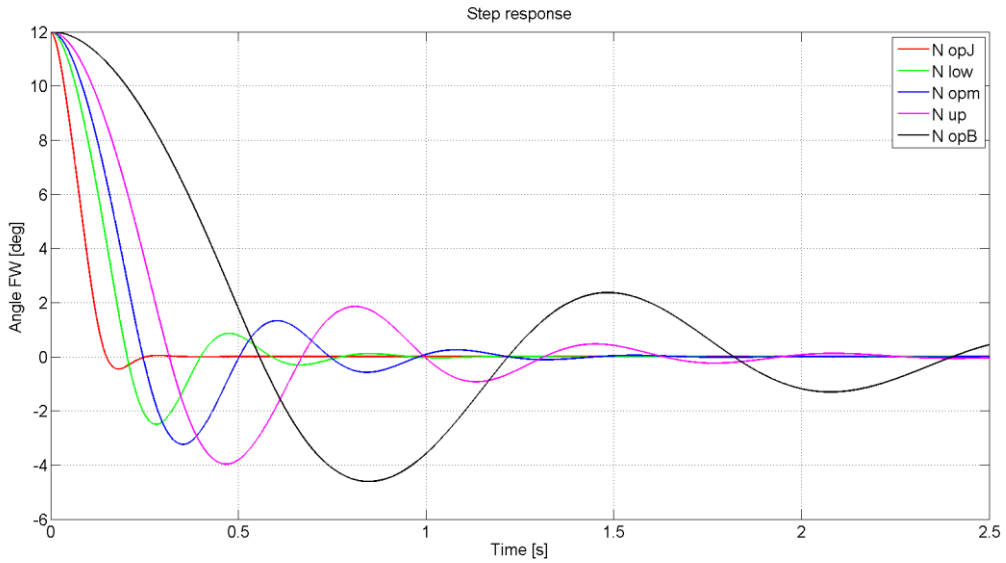

Figure 3-11: Step response 12 deg, front wheel angle

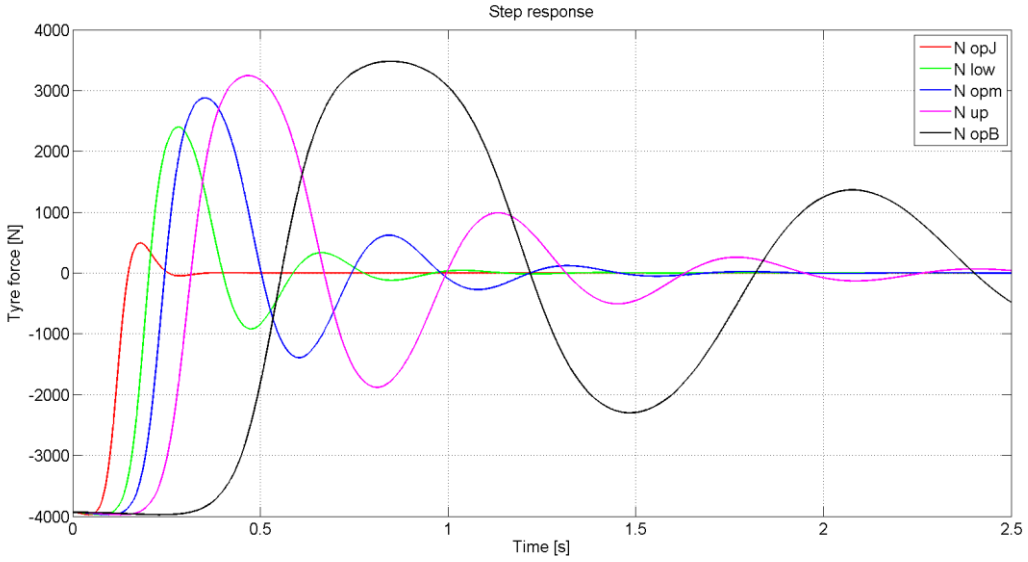

Figure 3-12: Step response 12 deg, tyre force

Table 3-9: Natural frequency and damping ratio, non-linear tyre force

$N_{m/fw}$	Parameter	Natural frequency	Unit	Damping ratio
N_{opJ}	Gear ratio optimal inertia	≈ 4.0	Hz	-
N_{low}	Gear ratio lower	≈ 2.5	Hz	-
N_{opm}	Gear ratio optimal motor	≈ 1.8	Hz	-
N_{up}	Gear ratio upper	≈ 1.4	Hz	-
N_{opB}	Gear ratio optimal damping	≈ 0.69	Hz	-

3.7 Summary

The gear ratio between motor and front wheel is very important for determining the response of the steering system. A model of a front wheel steering system, combined with a variable gear ratio is constructed to determine how the gear ratio affects the dynamics.

A high gear ratio increases the inertia and damping felt by the tyre forces and slows down the response of the system. A low motor torque means a smaller motor can be installed. A smaller motor decreases the inertia and damping of the total system. A motor too small provides problems since the motor may not be able to spin at the extreme high speeds and deliver the required power.

A low gear ratio results in a lower inertia and damping of the system and therefore a quicker responding system. A high natural frequency of the steering system and the tyre forces is desirable since it provides advantages for the DCM. These advantages are discussed in chapter 5. The simulation also shows less oscillations in the passive response of the steering system.

The Emoteq Quantum DC QB03403 motor has a 12.5 % overcapacity. This overcapacity provides the opportunity to alter the gear ratio and still meet the power requirements. To maximize the passive response, within the motor's power range, a lower boundary gear ratio is desirable (N_{low}), see Figure 3-13. The steering system with a gear ratio of 136, has an eigenfrequency in the linear tyre region of 2.7 Hz and a damping ratio of 0.30.

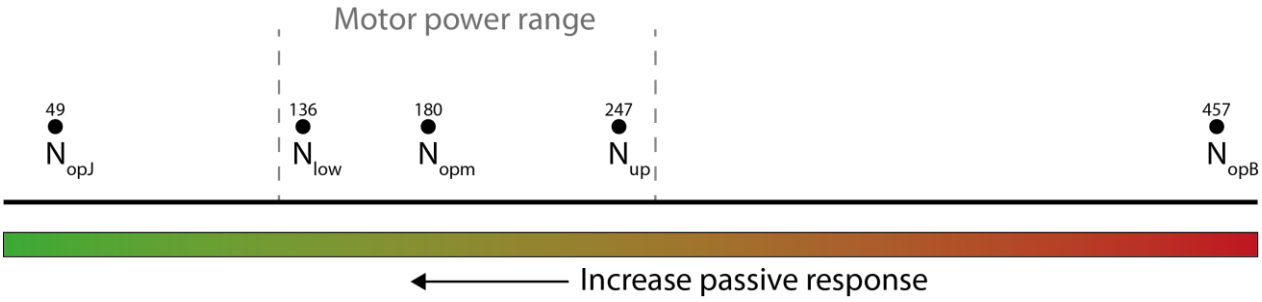

Figure 3-13: Range gear ratios

Chapter 4

Haptic driver feedback

Combining the advantages of the DCM and VM can give the driver an optimal combination of road information provided by the DCM and minimal TUCC interference provided by the VM. The TUCC discussed before determines how much TUCC angle is added to the driver's input and thus how much TUCC interference is present. When there is a constant change in TUCC activity, there will be a lot of changes in the presences of the two feedback sources. Therefore it is important to have two feedback sources that match well and can accurately determine the lateral tyre forces. If the two sources do not match well a change in feedback source can create big shocks in the driver feedback, called mismatch disturbance.

4.1 Model data

4.1.1 Direct current measurement

The goal of this section is to show that by measuring the current required by the steering motor, an accurate estimation of tyre forces can be formed. In the previous chapter the dynamics of the front wheel steering system are discussed. The same model is used to get an indication of the accuracy of a DCM. Values for inertia and damping are the same and shown in Table 4-1.

Table 4-1: Parameters front wheel steering system

Symbol	Parameter	Value	Unit
J_m	Inertia motor	$2.1 \cdot 10^{-4}$	$kg \cdot m^2$
J_{fw}	Inertia front wheel	$5 \cdot 10^{-1}$	$kg \cdot m^2$
m_r	Mass rack	$1 \cdot 10^{0}$	kg
B_m	Damping motor	$2.1 \cdot 10^{-4}$	Nm·s/rad
B_{fw}	Damping front wheel	$4.4 \cdot 10^{1}$	Nm·s/rad
c_r	Damping rack	$1 \cdot 10^{0}$	N·s/m
k_{mr}	Stiffness connection motor - rack	$6 \cdot 10^{5}$	Nm/rad
k_{rfw}	Stiffness connection rack - front wheel	$4 \cdot 10^{5}$	N/m
$N_{m/fw}$	Gear ratio motor / front wheel	$1.36 \cdot 10^{2}$	rad/m
$N_{r/fw}$	Gear ratio rack / front wheel	$1.2 \cdot 10^{-1}$	m/rad
k_τ	Torque constant motor	$2.08 \cdot 10^{-1}$	Nm/A

Besides the inertia and damping, the tyre force pushing against the front wheel determines how much torque the steering motor has to deliver. The simulation package CarSim, further discussed in section 4.1.3, simulates the tyre force by using the same reference steering angle, see Figure 4-1. This new way of calculating the tyre forces replaces the lookup table described in section 3.3.3.

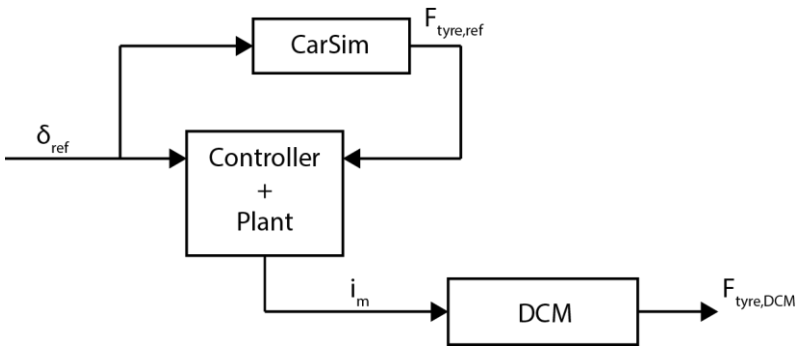

Figure 4-1: DCM setup

To make sure the actual front wheel angle follows the reference angle, a controller is installed. This controller consists of two parts as shown in Figure 4-2. The feed forward part anticipates the inertia and damping of the system and controls accordingly. The feedback part, using a position sensor to measure the actual front wheel angle, covers mismatches of the feed forward controller and rejects external disturbances, like the tyre force.

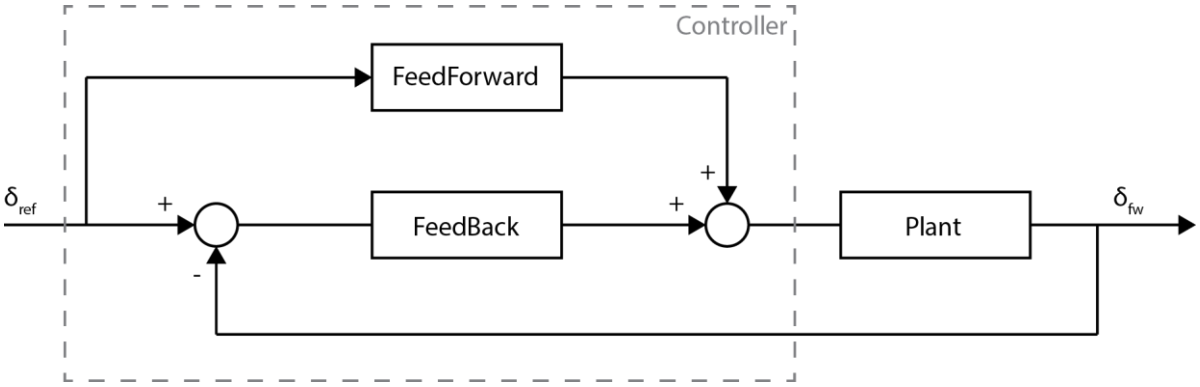

Figure 4-2: Front wheel position controller

4.1.2 Virtual model data

Creating a virtual model, which can accurately approximate the forces acting on the front wheels can be a solution for the problem of TUCC interference. The goal of this model is to determine the forces acting on the front tyre. These forces are used to determine the feedback provided to the driver. The decision is made to use a bicycle model combined with non-linear tyre forces. The accuracy between a two track model and the bicycle model is almost negligible. Research showed that implementation of non-linear tyre forces improves the performance of a model [28]. Figure 4-3 schematically shows how the total virtual model works.

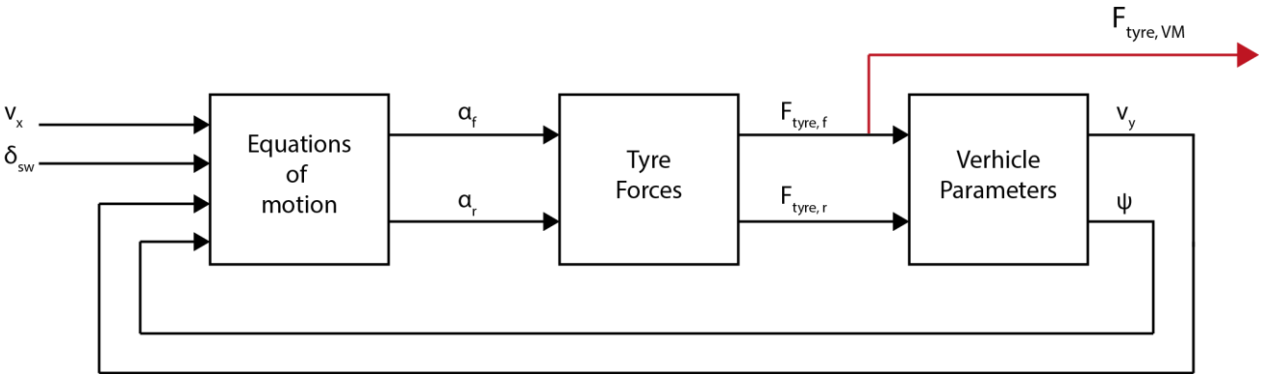

Figure 4-3: Overview virtual model

v_x	= longitudinal velocity	[m/s]
v_y	= lateral velocity	[m/s]
δ_{sw}	= steering angle	[rad]
α_f	= slip angle front axle	[rad]
α_r	= slip angle rear axle	[rad]
$F_{tyre,f}$	= tyre force front wheel	[N]
$F_{tyre,r}$	= tyre force rear wheel	[N]
ψ	= yaw angle	[rad]

4.1.2.1 Theory

The VM has two degrees of freedom, the steering angle and the longitudinal velocity of the vehicle. The basic bicycle model consists of two equations of motion as stated in the equations below. The first one determines the lateral acceleration of the vehicle, while the second one shows the yaw acceleration around its center of gravity. The important parameter in these formulas are the front tyre forces as they determine how much feedback has to be presented to the driver.

$$m\,\dot{v}_{\mathrm{y}} + \mathrm{m}\,\dot{v}_{\mathrm{x}}\dot{\psi} = 2 \cdot F_{tyre,\mathrm{f}} + 2 \cdot F_{tyre,\mathrm{r}} \tag{4-1}$$

$$I_z\ddot{\psi} = 2 \cdot F_{tyre,\mathrm{f}}\, l_f - 2 \cdot F_{tyre,\mathrm{r}}\, l_r \tag{4-2}$$

m	= total mass of the vehicle	[kg]
I_z	= moment of inertia about the z-axis	[kg m^2]
l_f	= distance from the COG to front axis	[m]
l_r	= distance from the COG to rear axis	[m]

The slip angles of front and rear tyres are given in the equation below. They are functions of the steering angle, yaw rate and lateral and longitudinal velocity.

$$\alpha_f = \delta_{sw} - \frac{v_y + l_f\dot{\psi}}{v_x}, \quad \alpha_r = -\frac{v_y - l_r\dot{\psi}}{v_x} \tag{4-3}$$

The slip angles, combined with the road friction coefficient are used in the non-linear tyres force function to determine the lateral forces working on front and rear axle. These lateral forces are used again in the first two equations to achieve an equilibrium. The tyre force calculation will be further discussed in section 4.1.2.3.

4.1.2.2 Vehicle parameters

For the vehicle parameters, a standardized E-class sedan is chosen. This vehicle is comparable to the BMW e60, which is analyzed in section 1.5. Table 4-2 shows the parameters used in the virtual model.

Table 4-2: Vehicle parameters virtual model

Symbol	Parameter	Value	Unit
m	Total vehicle mass	1.83 $\cdot 10^3$	kg
I_z	Moment of inertia about z-axis	3.234 $\cdot 10^3$	kg·m^2
l_f	Distance CG to front axle	1.40 $\cdot 10^0$	m
l_r	Distance CG to rear axle	1.65 $\cdot 10^0$	m

4.1.2.3 Tyre parameters

The tyres used on the E-class sedan are 225/60 R18. Parameters such as the road friction coefficient, slip angle and vertical load are used to find the tyre force. The lookup table is exported from CarSim and used in this model. Figure 4-4 shows the lateral tyre force as a function of the slip angle.

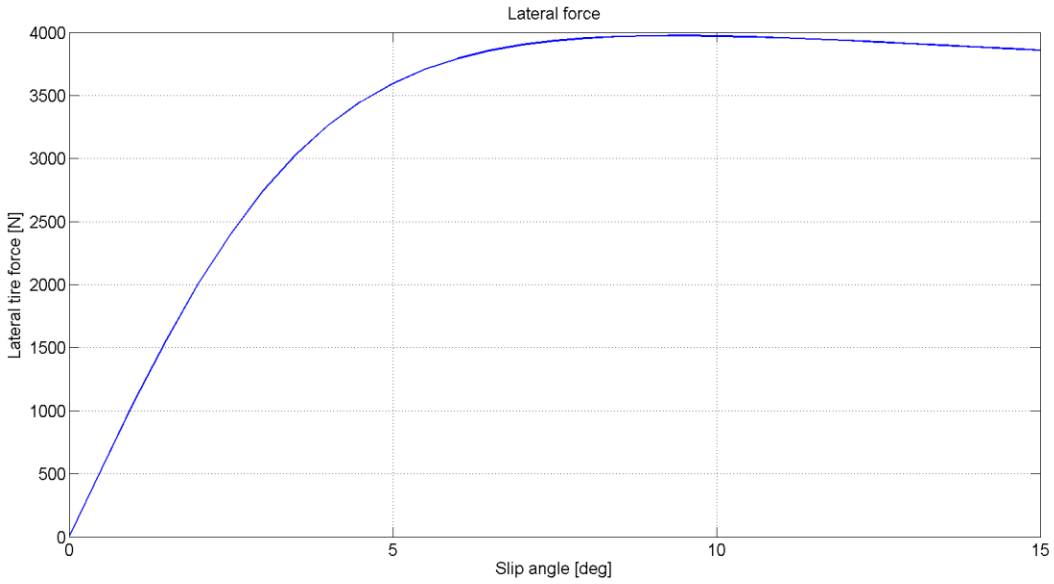

Figure 4-4: Lateral tyre force, VM
Vertical load = 4000 N, Road friction coefficient = 0.7

4.1.3 CarSim

CarSim is a simulation package that provides accurate prediction concerning the states of the vehicle. It is a 15-DOF multi-body model incorporating different dynamics like suspension, aerodynamics, brakes, powertrain and steering. Instead of the much simpler virtual model, it is too complicated to run onboard the vehicle. The same E-class sedan, as is described in chapter 3, is used in CarSim.

4.2 Simulation method

Different driving maneuvers are simulated to determine the accuracy of the DCM and the VM. Since there is no TUCC activity present in these simulations the steering angle of the VM is the same as the steering angle for the CarSim program and the DCM model, see Figure 4-5. Comparing the DCM and the VM to the front tyre forces computed by CarSim gives insight in the accuracy of the two feedback sources.

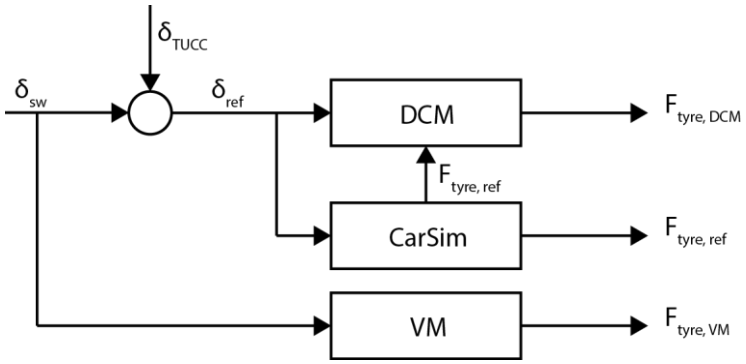

Figure 4-5: Simulation setup

4.2.1 Definition of validity

Using graphical and numerical methods, the DCM and VM are compared in the different driving maneuvers. The front wheel tyre forces are plotted versus time. The numerical approach is done by calculating the RMS error (%), see the equation below. The RMS error is a positive number and is a solution for an error fluctuating between positive and negative.

$$RMS\ error\ (\%) = \frac{\int RMS(F_{tyre,(DCM/VM)} - F_{tyre,ref})}{\int RMS(F_{tyre,ref})} \quad (4\text{-}4)$$

$F_{tyre,(DCM/VM)}$ = Tyre force (DCM / VM) [N]
$F_{tyre,(ref)}$ = Tyre force ref [N]

4.2.2 Modified double lane change

The double lane change is the first maneuver tested. The vehicle moves from one lane to another and back to the original lane. There are different ISO standards for velocities and lateral displacements. Since the TUCC controller would be primarily active in extreme maneuvers, the accuracy of the feedback sources is important especially in these extreme regions. Therefore the steering angle of the double lane change is maximized at the different simulation velocities. Figure 4-6 and Figure 4-7 show the relative position and front wheel angle of the vehicle. Three different vehicle velocities, 60, 90 and 120 km/h, are simulated at which the DCM and the VM are compared to the tyre forces computed by the CarSim package. The tyre forces computed by the CarSim are defined as reference tyre force, see Table 4-3.

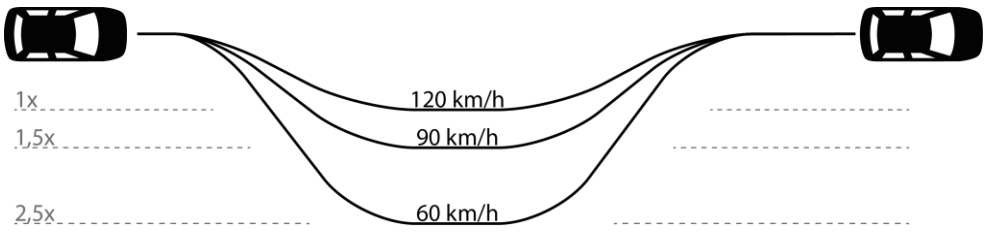

Figure 4-6: Modified double lane change, relative position at different speeds

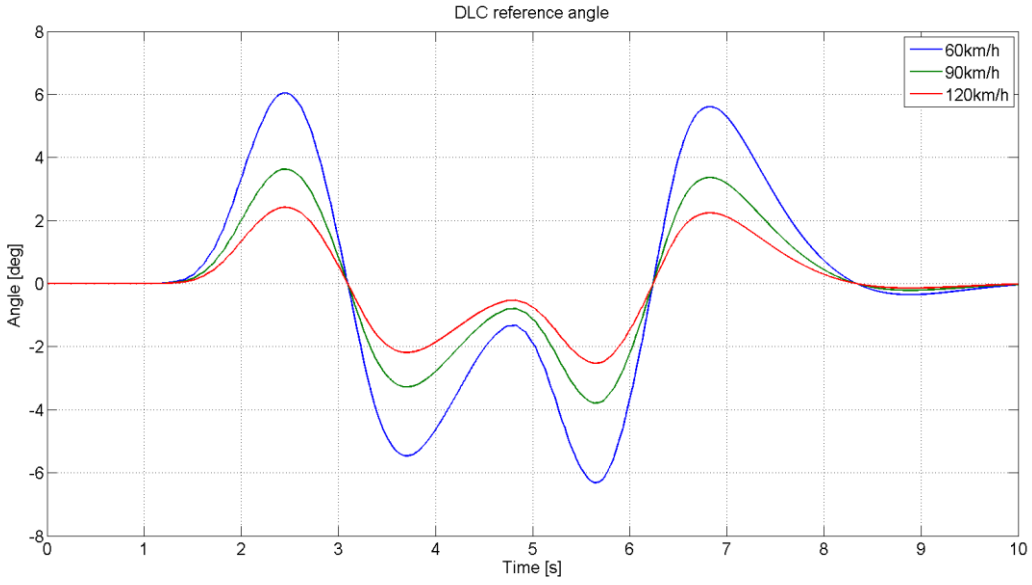

Figure 4-7: Modified double lane change, reference angle front wheels

Table 4-3: Simulation situation, modified double lane change

Situation	x-axis	y-axis	Velocity
1a	time	$F_{tyre,VM}$ $F_{tyre,DCM}$ $F_{tyre,ref}$	60 km/h
1b	time	$F_{tyre,VM}$ $F_{tyre,DCM}$ $F_{tyre,ref}$	90 km/h
1c	time	$F_{tyre,VM}$ $F_{tyre,DCM}$ $F_{tyre,ref}$	120 km/h

4.2.3 Steady state cornering

The second driving maneuver is a steady state corner. The front wheels start turning after 1 s and reach the desired constant front wheel angle in 0.5 s. Three different front wheel angles are chosen in such a way that the tyre forces do not saturate, see Figure 4-8.

The error between the VM and the reference is predominantly the mismatch in tyre force at steady state. Therefore the steady state tyre force of the VM and the reference is plotted for four different vehicle velocities, see Table 4-4. Since the DCM is based on the reference tyre forces, it is expected that there are mainly errors in the transient phase of the simulation. These errors could be fluctuating, therefore the RMS error of the DCM is plotted for four different vehicle velocities.

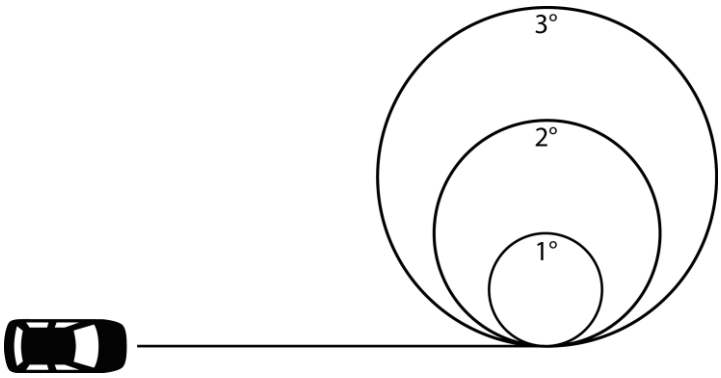

Figure 4-8: Steady state cornering, different front wheel angle

Table 4-4: Simulation situation, steady state cornering

Situation	x-axis	y-axis	Front wheel angle
2a	60 km/h 75 km/h 90 km/h 105 km/h	$F_{tyre,VM}$ $F_{tyre,ref}$	1 deg 2 deg 3 deg
2b	60 km/h 75 km/h 90 km/h 105 km/h	DCM RMS error (%)	1 deg 2 deg 3 deg

4.3 Results and discussion

4.3.1 Modified double lane change

Situation 1a

Figure 4-9 shows the tyre forces of the double lane change at 60 km/h. The DCM shows a good match with the reference tyre forces. Some fluctuations are present, which are a response of the front wheel dynamics. By implementing a filter these fluctuations can easily be removed. The VM lacks some accuracy at the high tyre forces. At the point, t = 3.5 s, the mismatch error is around 20 %. There is almost no phase lag present between the VM and the reference tyre force.

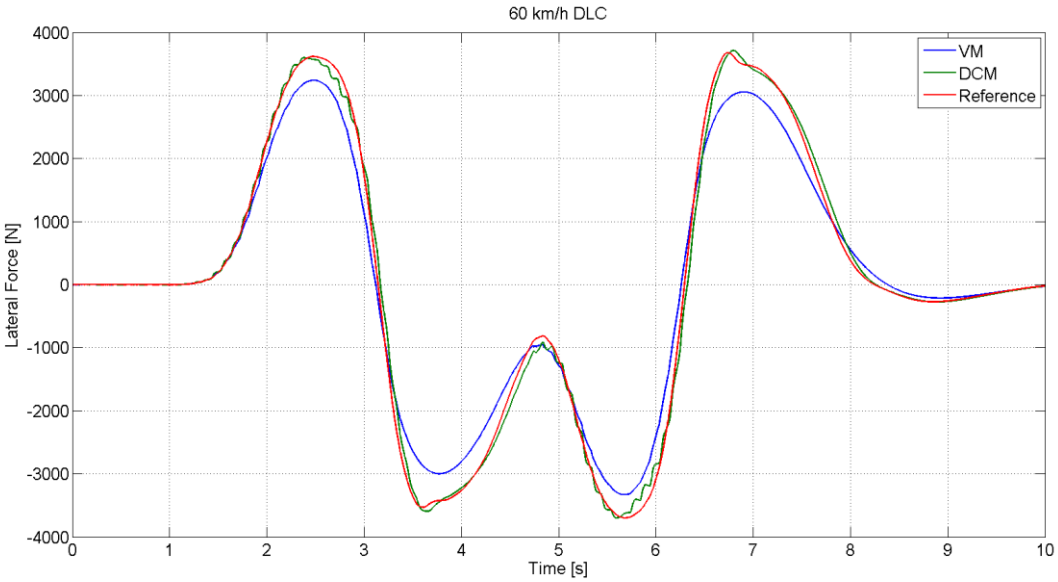

Figure 4-9: Double lane change, 60 km/h

Situation 1b

Figure 4-10 shows the tyre forces of the double lane change at 90 km/h. The accuracy of the DCM is comparable with situation 1a, although there is some phase lag introduced. The accuracy of the VM has improved significantly. At t = 3.5 s the mismatch error is reduced to 13 %. There is some error in the VM tyre forces at t = 5.0 and t = 8.3 s. There is still no phase shift present between the VM and the reference tyre force.

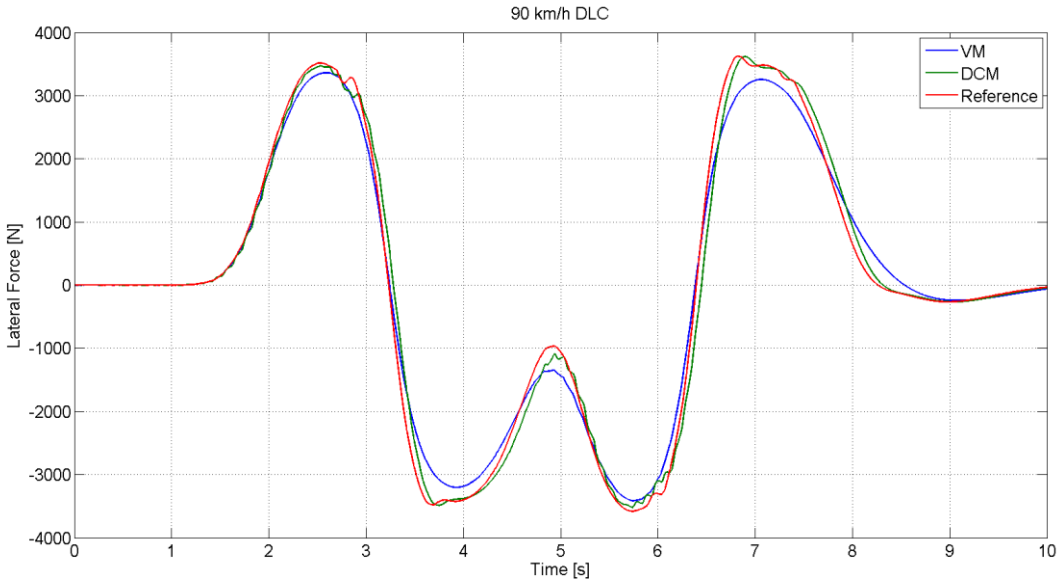

Figure 4-10: Double lane change, 90 km/h

Situation 1c

Figure 4-11 shows the tyre forces of the double lane change at 120 km/h. The accuracy and phase shift of the DCM is comparable with situation 1b. The peak tyre forces of the VM shows almost a perfect match with the reference. The phase shift of the virtual model has increased. The trend noticed in situation 1b continued. At t = 5 and 8.3 s the error of the VM tyre forces has increased even more compared to the reference forces. The mismatch at t = 5 s is around 50 %.

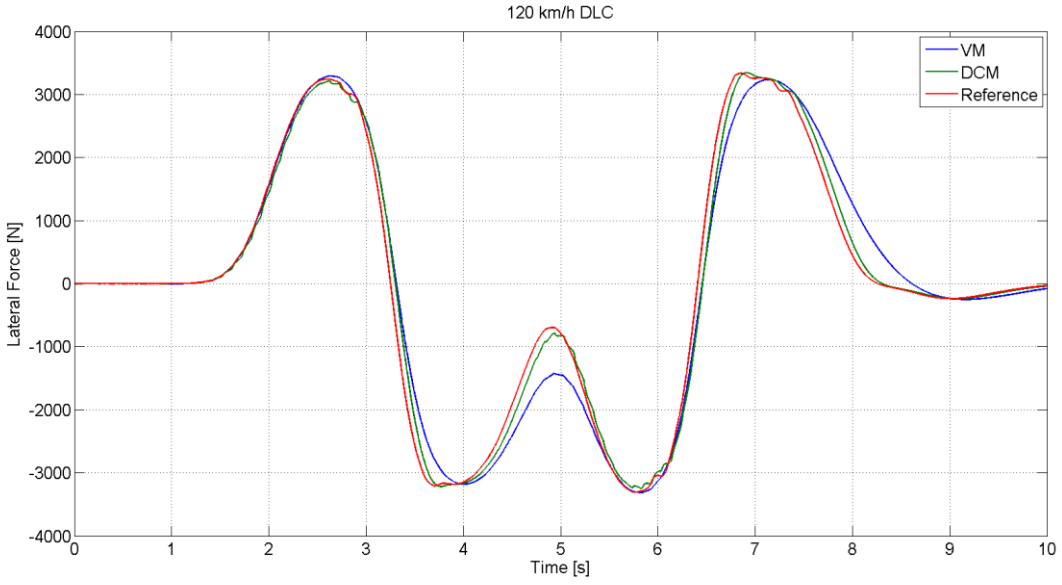

Figure 4-11: Double lane change, 120 km/h

Table 4-5 shows the RMS error of the double lane change. The accuracy of the DCM slightly decreases at the higher velocities. Reason is the previously observed phase shift at higher velocities. The optimal velocity for the VM is 90 km/h. As shown in the figures above, at low vehicle velocities the VM is less accurate in reproducing the high tyre forces. The low and medium tyre forces show almost a perfect match between VM and reference forces. At high vehicle velocities the VM is accurate in reproducing the high tyre forces, while the medium and low tyre forces are estimated too high.

Table 4-5: RMS error double lane change

RMS error (%)	60 km/h	90 km/h	120 km/h
DCM vs. ref	5.168	7.781	9.215
VM vs. ref	15.56	10.78	15.59
DCM vs. VM	15.93	10.5	10.4

4.3.2 Steady state cornering

Situation 2a

Figure 4-12 shows the tyre force when driving in a steady state corner. Four different steady state vehicle velocities are studied. The front wheel angle is 1, 2 and 3 degrees. The same observations are made as in the double lane change maneuver: at low velocities the small tyre forces are represented more accurate than the high tyre forces. For high velocities it is reversed. The high forces are generated almost without error, while the low forces are estimated too high by the VM. The VM has a sweet spot around 90 km/h. The medium tyre forces show a perfect match and the higher and lower tyre forces show good resemblances as well.

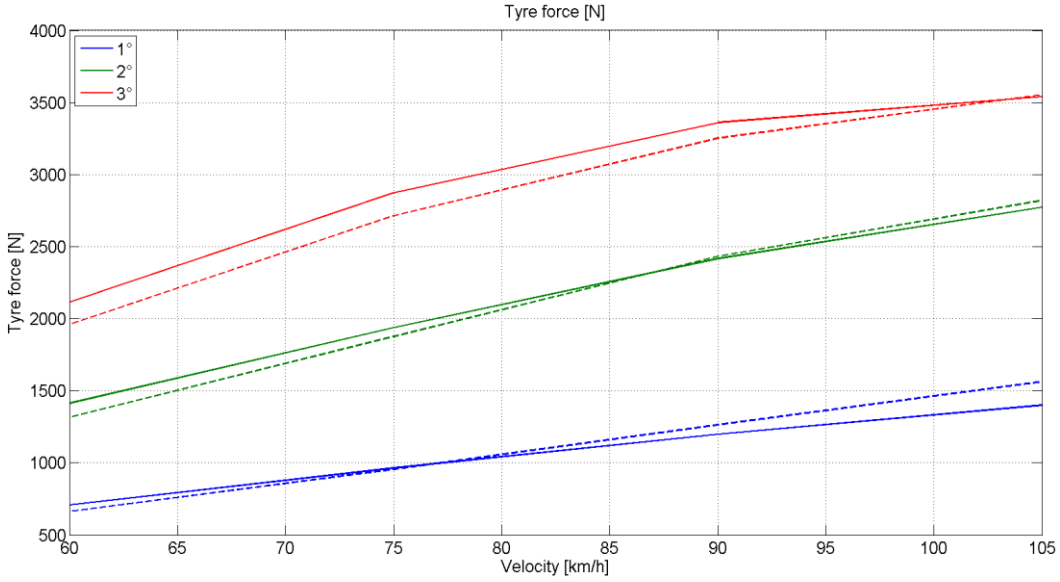

Figure 4-12: Steady state cornering, VM and ref, 60 / 75 / 90 / 105 km/h
Line: reference tyre force, dotted line: VM tyre force

Situation 2b

Figure 4-13 shows the RMS error of the DCM versus the reference tyre forces. Since this is a maneuver where the front wheels only move in the beginning of the tests, the front wheel dynamics do not influence the simulation much. As expected the resemblance of the DCM and the reference forces is almost perfect. At higher velocities there is a greater mismatch. Nevertheless the error is within 1% and can be neglected.

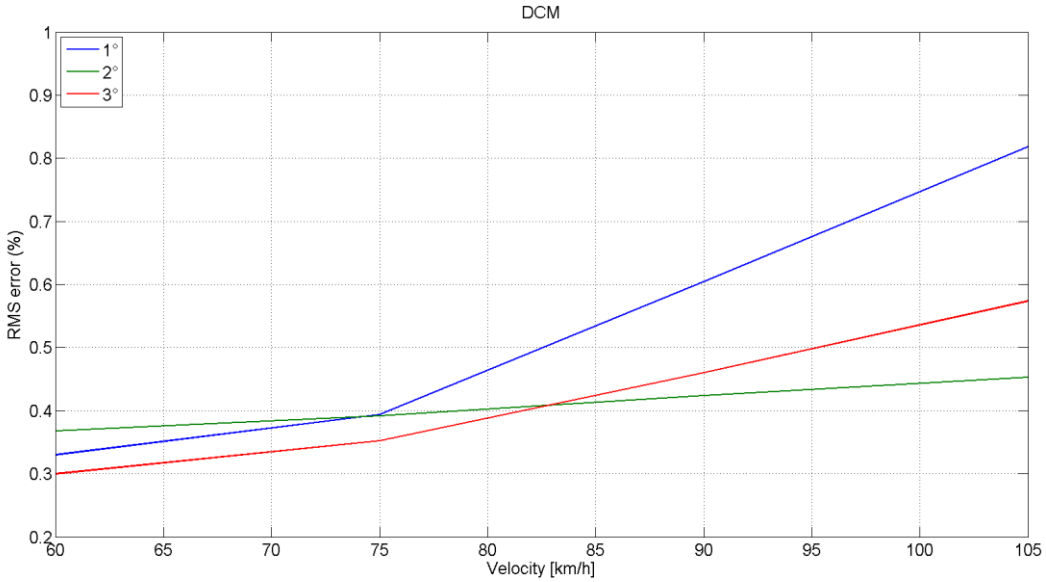

Figure 4-13: Steady state cornering, DCM, 60 / 75 / 90 / 105 km/h

4.4 Summary

There are two main principles to determine the amount of haptic feedback presented to the driver. The DCM uses the current drawn by the electric motor, while the VM computes the tyre forces by using the input parameters: steering angle and vehicle velocity. The feedback sources are tested in this chapter for accuracy and phase shift. Two driving maneuvers are used. The first one is a modified double lane change and second one is a steady state corner.

The simulations show that the DCM is mainly affected by the front wheel dynamics. There is some phase shift in the modified double lane change, especially at higher velocities. The RMS errors of the modified double lane change are 5.2, 7.8, and 9.2 % for the velocities 60, 90 and 120 km/h, respectively. These errors are a result of the constant change in front wheel angle. When there is a constant front wheel angle, the DCM perfectly represents the reference tyre forces.

In the steady state corner the VM shows a sweet spot around 90 km/h, where it can optimally calculate the reference tyre forces. At lower velocities there is a perfect match of the low tyre forces, while the high tyre forces are computed too low. High velocities show a good match of the high tyre forces, while the VM calculates the low tyre forces too high.

The mismatch in low and high velocities is confirmed by the RMS error at the modified double lane change. For 60 and 120 km/h the error is 16%, while this error is reduced to 11% for 90 km/h. In the next chapter a system is designed to combine the DCM and VM. This system should give an optimal combination between road information and minimal TUCC interference.

Chapter 5

Combiner DCM and VM

Providing the driver with haptic feedback, optimizing road information and minimizing TUCC interference requires a system which can blend the two feedback sources. TUCC interference is defined as the increment in tyre force created by the addition of a TUCC angle to the front wheel angle. This chapter first defines the problems that occur. A combiner of the DCM and the VM (CDV) is proposed using a Virtual Model Presence (VMP) map and two filters. An error estimation of the TUCC interference and the mismatch disturbance is made. Different simulations show the performance of the system.

5.1 Problem definition

5.1.1 Transitions

When the TUCC applies an angle to the front wheel angle, a fast transition should be made from the DCM to the VM feedback. The fast transition is required since the DCM can confuse the driver due to the TUCC interference. On the other hand, the constant switching problem, explained in the next section, requires a slow transition from the VM to the DCM. The properties of both feedback sources and the related transitions are shown in Figure 5-1.

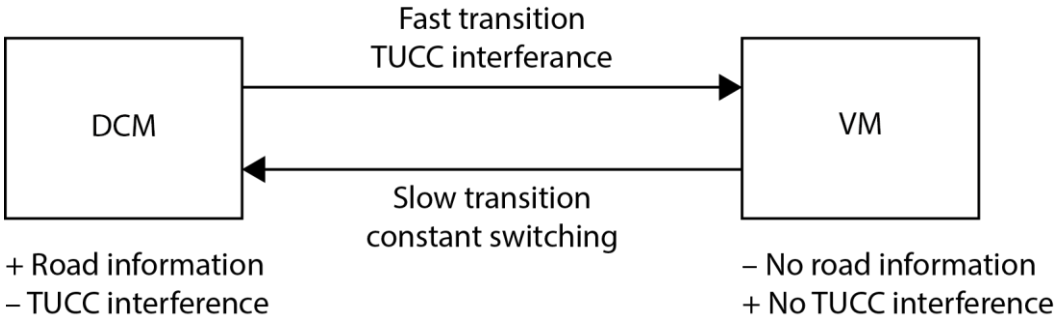

Figure 5-1: DCM and VM properties and required transitions

5.1.2 Constant switching

The constant switching problem occurs when the TUCC adjusts the angle of the front wheels, for example, with a sin wave. A sin wave switches between positive and negative and has the value zero for a short period of time. When the TUCC angle is zero there is no TUCC interference and the source of feedback should switch from VM to DCM. Because the TUCC angle is zero only for a short time, the feedback will quickly switch back to the VM source. If the mismatch between VM and DCM is significant, this constant switching will generate sudden shocks in the driver feedback, as shown in Figure 5-2.

An obvious solution for this problem would be to use the derivative of the TUCC angle to determine whether the TUCC angle is approaching zero or the angle is just crossing the zero line. Since the TUCC angle is based on the steering wheel angle, which is a measured value, taking a derivative is not a desirable solution due to measurement noise.

Implementing a low pass filter to determine the feedback source delays the transition to another feedback source. This will smoothen out the constant switching problem. The downside of this solution

is the included slower transition from the DCM to the VM. Therefore the driver will be subjected to the TUCC interference, when the TUCC is suddenly activated.

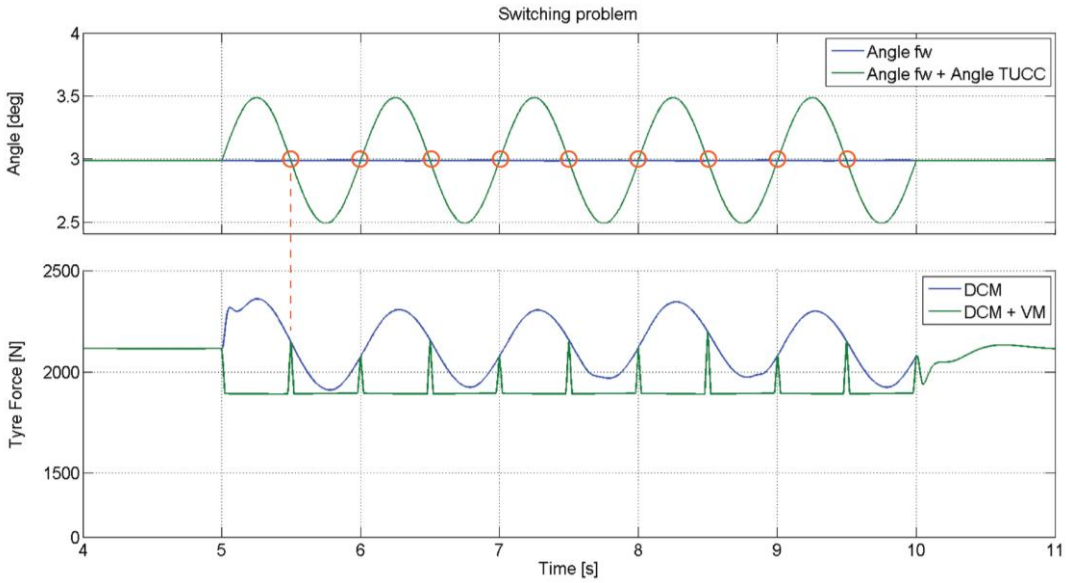

Figure 5-2: Switching problem
Steady state cornering, 60 km/h, 3deg front wheel angle. TUCC angle: 1 Hz, 0.5 deg

5.2 CDV design

Combining the two different feedback sources requires a controller, called CDV. A transition phase from one feedback source to another has to minimize sudden shocks in the haptic feedback presented to the driver. Figure 5-3 shows the design of the controller. It contains a VM presence map, two first order filters and a controller to ultimately blend the feedback sources.

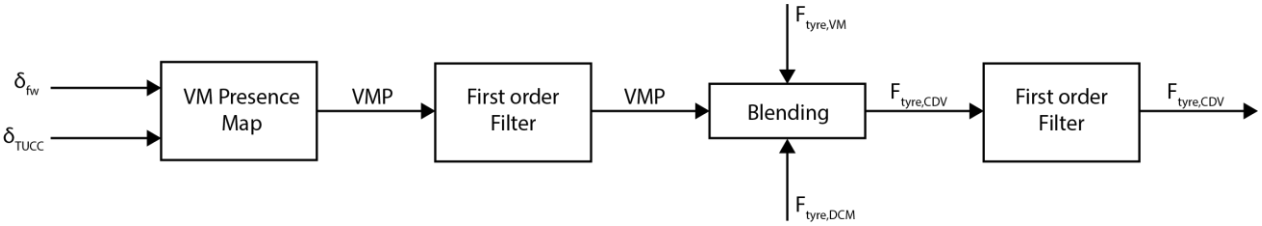

Figure 5-3: Combiner DCM and VM

5.2.1 VM Presence map

The VMP value shows how much VM feedback is presented to the driver. It is a number between 0 and 1. A VMP of 1 shows that the driver feedback is exclusively generated by the VM and thus independent of the actual tyre force. If the VMP is 0 the feedback only consists of the DCM. The tyre force that also includes road information is transferred to the driver. A number within these values shows a blend between the DCM and the VM.

The equations below show how the VMP is determined. At low steering angles (< 1 deg) the VMP is an exclusive function of the TUCC angle. This is called the steady state phase. p_1 determines the TUCC angle in which the transition is made between DCM and VM. At higher steering angles the VMP is a function of both the TUCC and the steering angle. This is called the proportional phase. p_2 shows the roll off of the VMP at higher steering angles (> 1 deg)**.** The VMP map is plotted in Figure 5-4.

$$a_1(\delta_{\mathrm{TUCC}}) = \begin{cases} \frac{|\delta_{\mathrm{TUCC}}|}{p_1} & ,if\ \frac{|\delta_{\mathrm{TUCC}}|}{p_1} < 1 \\ 1 & ,if\ \frac{|\delta_{\mathrm{TUCC}}|}{p_1} \geq 1 \end{cases} \quad (5\text{-}1)$$

$$a_2(\delta_{\mathrm{TUCC}}, \delta_{sw}) = \begin{cases} \frac{|\delta_{\mathrm{TUCC}}|}{p_2 \cdot |\delta_{sw}|} & ,if\ \frac{|\delta_{\mathrm{TUCC}}|}{p_2 \cdot |\delta_{sw}|} < 1 \\ 1 & ,if\ \frac{|\delta_{\mathrm{TUCC}}|}{p_2 \cdot |\delta_{sw}|} \geq 1 \end{cases} \quad (5\text{-}2)$$

$$VMP = \min(a_1, a_2) \quad (5\text{-}3)$$

VMP	= virtual model presence	[-]
a_1	= VMP steady state phase	[-]
a_2	= VMP proportional phase	[-]
p_1	= TUCC steady state constant	[deg]
p_2	= TUCC proportional constant	[-]
δ_{TUCC}	= TUCC angle	[deg]
δ_{sw}	= steering angle	[deg]

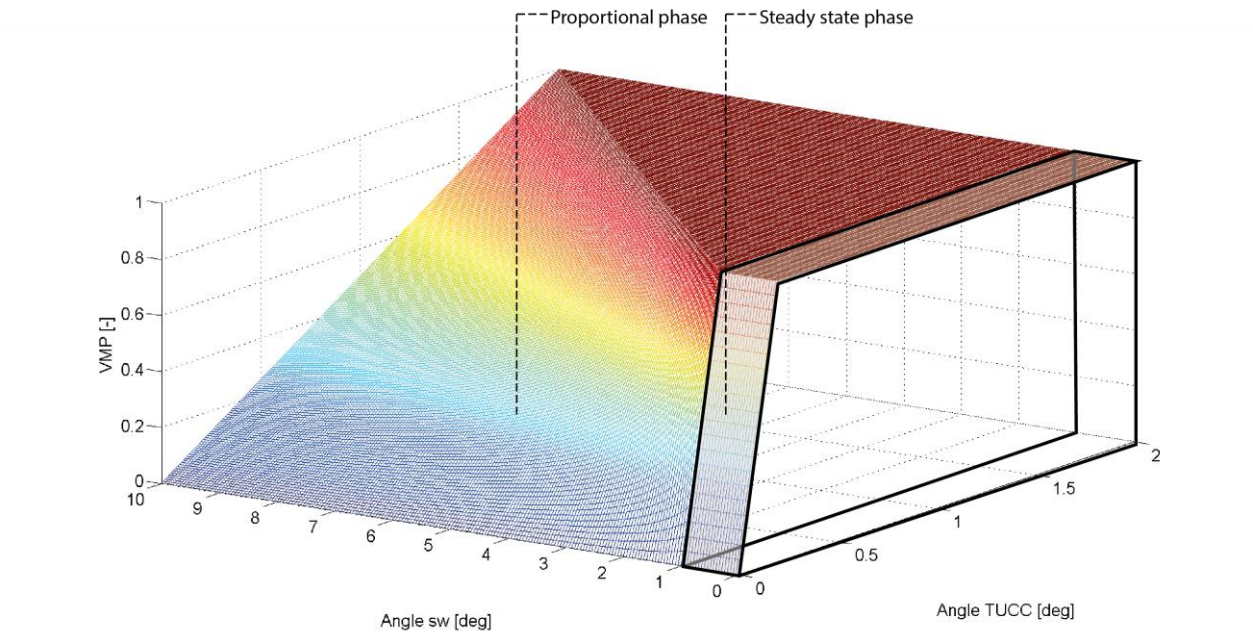

Figure 5-4: VM presence map
p_1 = 0.2 deg, p_2 = 0.2

5.2.1.1 TUCC interference and mismatch disturbance estimation

The two main contributors causing sudden shocks in the steering wheel are the TUCC interference and the mismatch disturbance. Figure 5-5 helps to schematically show how the TUCC interference and the mismatch disturbance are defined. The DCM* is the DCM reading, without the TUCC interference. In the real system this parameter is nonexistent and is only defined in the figure to clarify both errors. The mismatch disturbance is the difference between $F_{tyre,VM}$ and $F_{tyre,DCM*}$. The TUCC interference is the difference between the $F_{tyre,DCM}$ and $F_{tyre,DCM*}$.

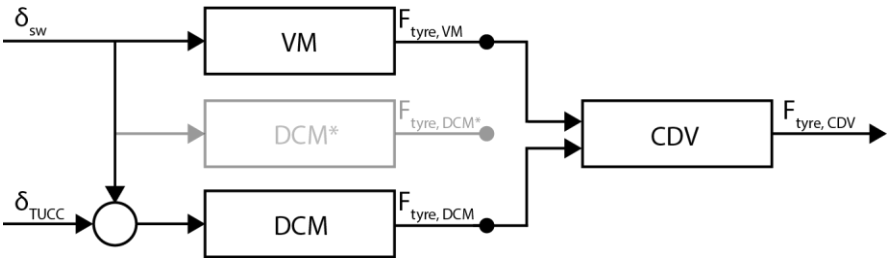

Figure 5-5: Combining TUCC interference and mismatch disturbance
DCM is the direct current measurement at the corresponding steering angle, without the addition of a TUCC angle.*

TUCC interference
TUCC interference is defined as the change in tyre force created by the addition of a TUCC angle to the steering angle. How much TUCC interference is transferred to the driver depends on the VMP map. Only at small TUCC angles, the TUCC interference is transferred to the driver. Due to the small TUCC angle increments it is possible to linearize the tyre forces. In the linear tyre region, a value of 1000 N/deg is found as a value for tyre stiffness.

Maximum TUCC interference of proportional phase
The TUCC interference ratio shows how much TUCC interference is presented to the driver compared to the total tyre forces, see the equation below. A higher steering angle results in a higher tyre force. Due to the higher tyre forces, the TUCC transition angle can be increased without increasing the TUCC interference ratio. The TUCC transition angle increases proportional to the steering angle. The advantage of a larger TUCC transition angle is the increase of road information.

Figure 5-6 shows the TUCC interference ratio in a transition from the DCM to the VM. The maximum TUCC interference ratio is in the middle of the TUCC transition angle, with a value of 5 % of the tyre forces. As the TUCC transition angle is proportional to the steering angle, the maximum TUCC interference ratio remains constant for all steering angles in the proportional phase of the VMP map.

$$I_{TUCC} = \frac{\delta_{\mathrm{TUCC}}}{\delta_{\mathrm{fw}}} (1 - a_2) \cdot 100 \qquad (5\text{-}4)$$

I_{TUCC} = TUCC interference ratio [%]

Maximum TUCC interference of steady state phase
In the steady state phase the maximum TUCC interference is not a ratio of the tyre forces. It is an error independent of the steering angle and thus the tyre forces. The steady state phase of the VMP map shows a TUCC transition angle of 0.2 deg. The maximum TUCC interference is in the middle of the transition, at a TUCC angle of 0.1 deg. In the middle of the transition the VMP value is 0.5. Multiplying the 1000 N/deg tyre stiffness with the previous two numbers results in a 50 N maximum steering interference in the steady state of the VMP map.

Maximum TUCC interference
Figure 5-7 shows the maximum TUCC interference transferred to the driver, determined by the steady state and the proportional phase of the VMP map. At low steering angles the VMP is exclusively determined by the TUCC angle. When the VMP would also be dependent of the steering angle there is a very fast transition at small steering angles. This results in the absence of road information at minimal TUCC angles. The independency of the steering angle facilitates a larger TUCC transition angle. The cost of maintaining road information is the non-proportional TUCC interference, displayed in Figure 5-7 as 50 N of tyre force.

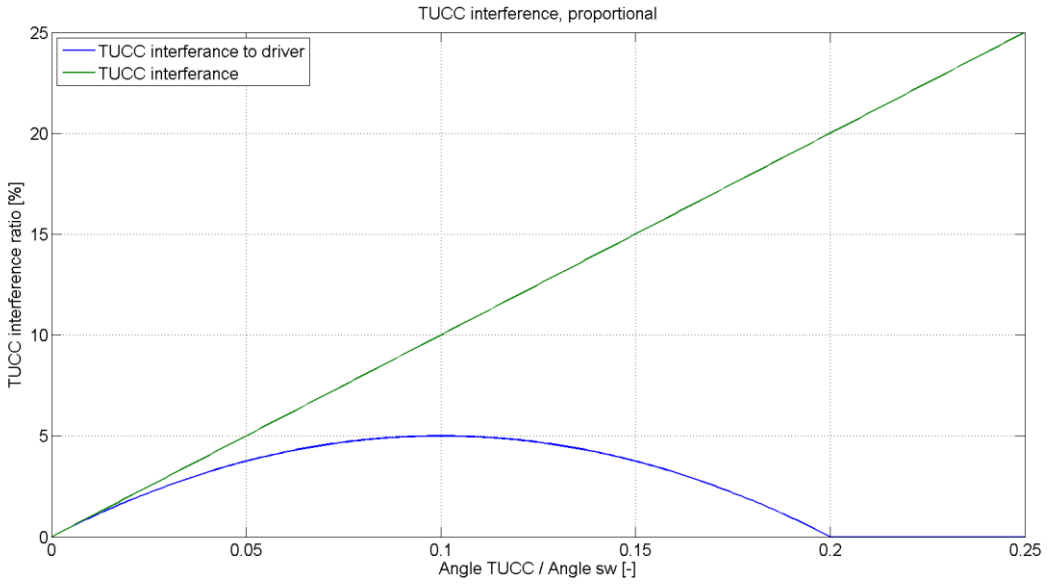

Figure 5-6: TUCC interference, in the proportional phase of the VMP map

The increase in tyre forces at higher steering angles allow an increase in TUCC interference transferred to the driver. The green line shows the TUCC interference created by the increasing TUCC angle. The blue line shows how much of this TUCC interference is transferred to the driver. On the x-axis, the TUCC angle divided by the steering angle is plotted. A maximum TUCC interference ratio to the driver of 5 % is shown in the figure. The maximum TUCC interference ratio remains constant for all steering angles in the linear tyre region.

The crossover point from steady state to proportional phase is at a steering angle of 1 deg. At higher steering angles the VMP is not only a function of the TUCC angle, but also of the steering angle. Figure 5-7 shows the increasing TUCC interference transferred to the driver. In Figure 5-8 the steering interference ratio of both the steady state and proportional phase are shown. At higher steering angle the maximum steering interference is limited to 5 % of the tyre forces.

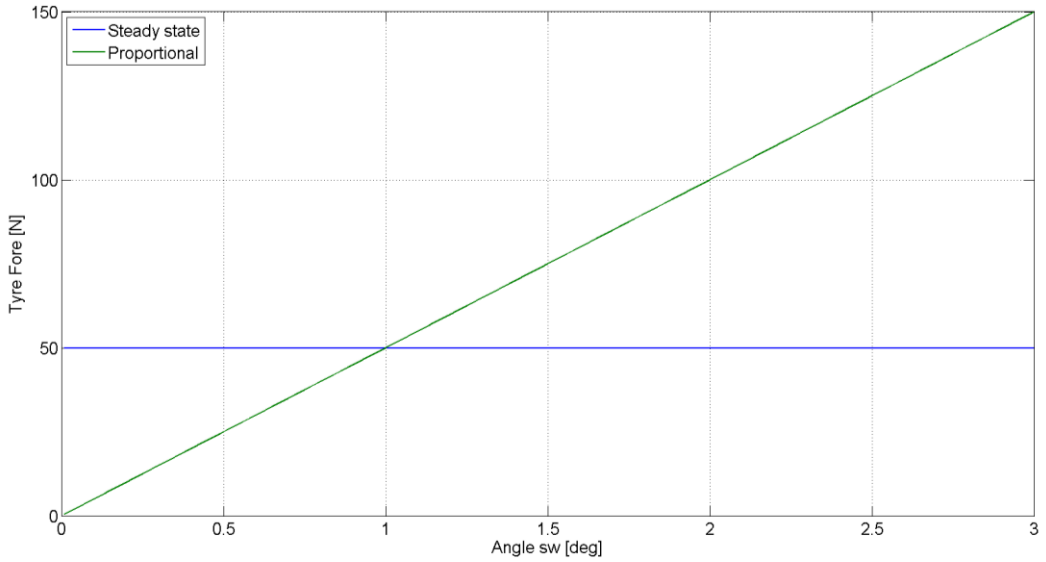

Figure 5-7: Maximum TUCC interference *as function of the steering angle*

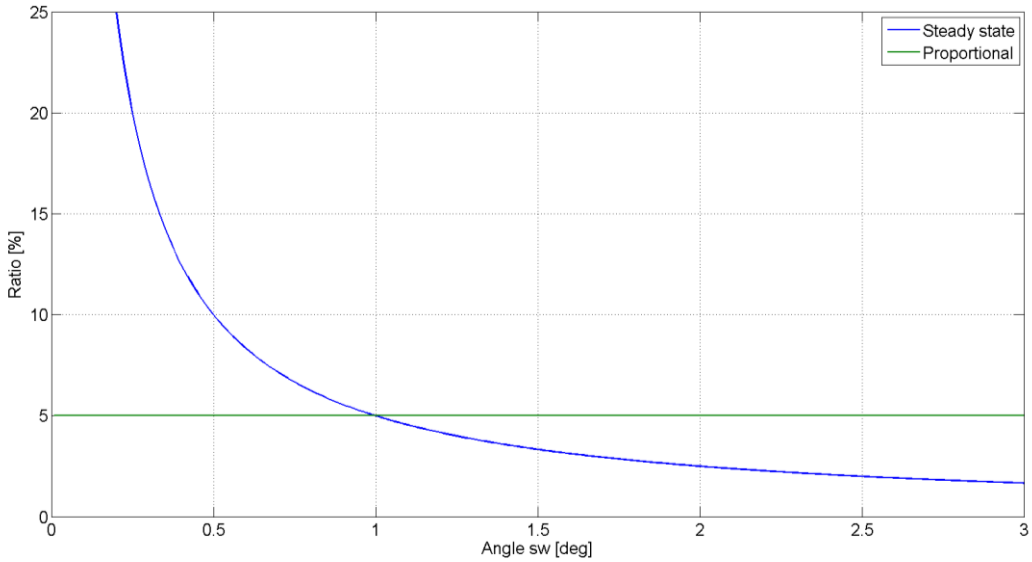

Figure 5-8: Maximum TUCC interference ratio as function of the steering angle

Mismatch disturbance

The mismatch between DCM and VM can cause shocks in the feedback provided to the driver when a transition is made from one feedback source to another. It is important to have an accurate DCM and VM to minimalize this disturbance. Chapter 4 shows a worse case error of 16 % between the VM and DCM in a steady state corner simulation.

Combining TUCC interference and mismatch disturbance

In the CDV, the combination of TUCC interference and mismatch disturbance can be co- or counteracting. In the co-acting combination of TUCC interference and mismatch disturbance the angle of the front wheel moves in a direction which changes the DCM value towards the VM value. In Figure 5-9 the VM value is 16% lower compared to the DCM value, called mismatch disturbance. The TUCC decreases the angle of the front wheel and lowers the DCM value. Since TUCC interference is only presented to the driver in the transition phase from DCM to VM the result is a CDV value that converges faster to the final VM value.

The counter-acting combination of TUCC interference and mismatch disturbance shows the opposite result, see Figure 5-10. The front wheel moves in a direction where the TUCC interference increases the gap between the DCM and VM. This combination shows a slower transition to the VM value.

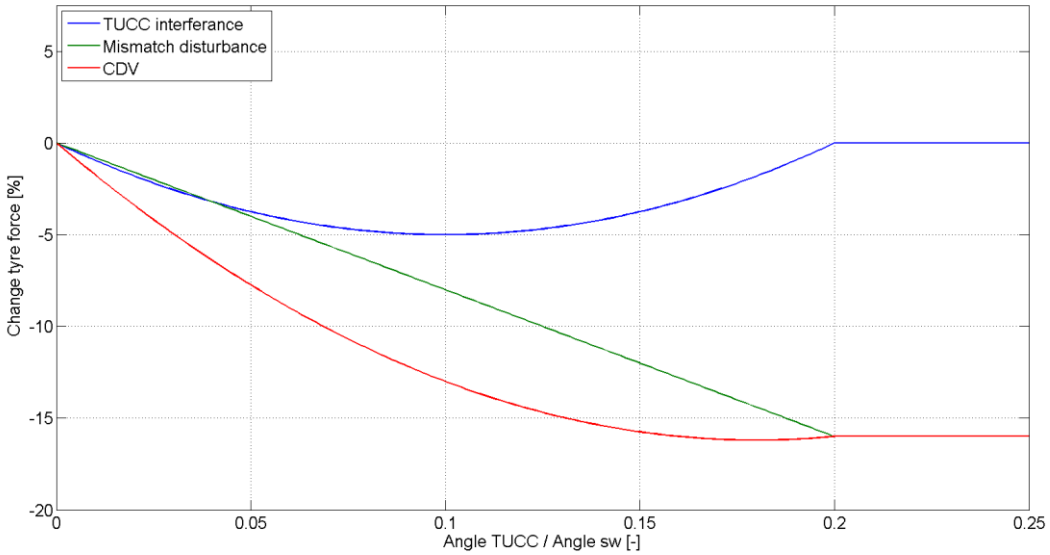

Figure 5-9: Mismatch disturbance and TUCC interference, co-acting

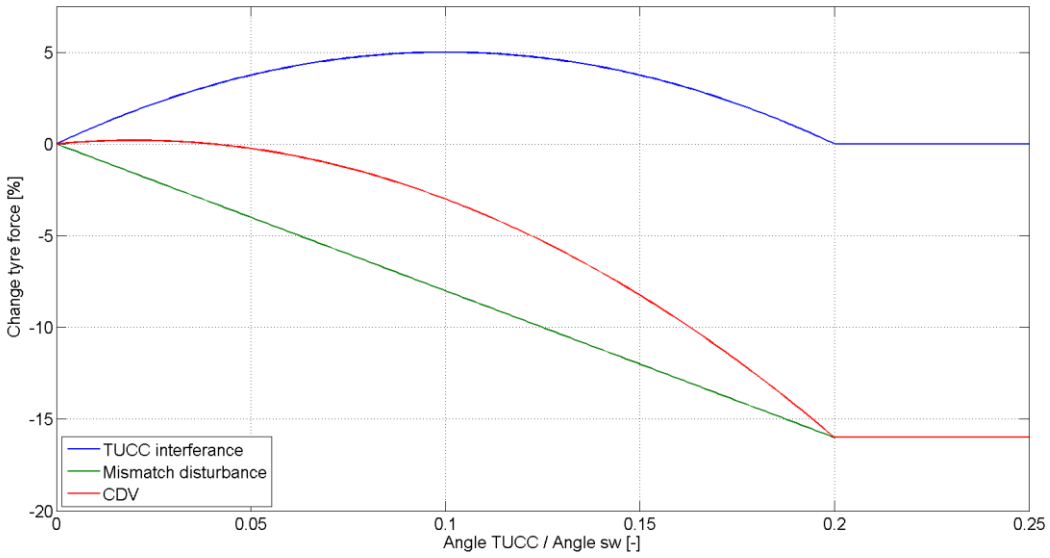

Figure 5-10: Mismatch disturbance and TUCC interference, counter-acting

5.2.2 First order filter

Two first order filters are installed to solve the constant switching problem. Peaks in the feedback presented to the driver are filtered without compromising the road information.

The first filter filters sudden drops in the VMP, caused by the constant switching problem. To cope with this problem a low bandwidth filter is desirable. On the other hand a high bandwidth guarantees the fast transition from the DCM to the VM, which is required to minimize sudden TUCC interference. This first filter has a cut off frequency of 8 Hz.

The second filter smoothens out sudden changes in the feedback presented to the driver. These peaks are caused by mismatch disturbance and the TUCC interference. The bandwidth of this filter cannot

be too low, otherwise the road information is filtered out as well. A cut off frequency of 6 Hz is chosen for this filter.

5.2.3 Blending

With the VMP determined the two feedback sources are blend to achieve an optimal combination between road information (DCM) and minimal TUCC interference (VM), see the equation below. The CDV tyre force is used as the reference value for the feedback to the driver.

$$F_{tyre,CVD} = F_{tyre,VM} \cdot VMP + F_{tyre,CDV} \cdot (1 - VMP) \quad (5\text{-}5)$$

5.3 Simulation method

Section 4.3.2 shows the largest mismatch between VM and DCM at a low vehicle velocity combined with high tyre forces. A steady state corner, discussed in section 4.2.3 is used as simulation maneuver. The vehicle velocity is 60 km/h combined with a steering angle of 3 deg. This worst case scenario is chosen to test the accuracy of the CDV.

5.3.1 TUCC interference

At the steady state corner a TUCC angle is added to the steering angle of the front wheels. Three different amplitudes are chosen, see Table 5-1. The first amplitude, 0.6 deg, remains completely within the VMP map. The second and third amplitudes go outside this map and cause the feedback to the driver, to be completely based on the VM for a period of time. Three different frequencies of the TUCC are used. 1 and 2 Hz are chosen as the TUCC is predominantly active in this region, see Figure 1-21. A frequency of 2.7 Hz is simulated as it is the natural frequency of the steering system, shown in Table 3-8. This section only discusses the extreme simulations, marked in yellow in the table below. The other simulations are shown in Appendix A.

Table 5-1: Simulation situation, TUCC interference

Situation	x-axis	y-axis	δ_{TUCC}	
			Amplitude	Frequency
1a	time	$F_{tyre,VM}$	0.6 deg	1.0 Hz
1b		$F_{tyre,DCM}$	1.2 deg	1.0 Hz
1c		$F_{tyre,CDV}$	1.8 deg	1.0 Hz
2a		VMP	0.6 deg	2.0 Hz
2b		δ_{TUCC}	1.2 deg	2.0 Hz
2c			1.8 deg	2.0 Hz
3a			0.6 deg	2.7 Hz
3b			1.2 deg	2.7 Hz
3c			1.8 deg	2.7 Hz

5.3.2 Simulation objectives

The simulations mentioned above have 3 objectives. The first one is to analyze the VMP range at different frequencies and TUCC amplitudes. Two filters are implemented into the CDV controller. It is therefore important to analyze how these filters will affect the behavior of the VMP value and the feedback presented to the driver.

The second objective is the phase shift between the DCM and the TUCC angle. Phase shift is caused by inertia of the steering systems and it affects the DCM reading. If a significant part of the current drawn by the motor is necessary to accelerate the system's inertia, the DCM is not an accurate estimation of the tyre force.

The last goal is to determine the heights of the CDV peaks when the TUCC is active. This will show how much mismatch disturbance and TUCC interference is presented to the driver and how well the designed controller works.

5.4 Results and discussion

Simulations situations 1a, 1c, 3a and 3c are discussed in this chapter. The TUCC imposes an earlier defined TUCC angle to the steering angle of the front wheel. At t = 3.5 s the TUCC is active for approximately 2 seconds, completing a number of cycles. The figures below show the tyre forces measured by the DCM and calculated by the VM. The CDV combines both inputs to provide the driver with road information while not making the vehicle unstable by transferring too much steering information.

5.4.1 Low TUCC frequency

Situation 1a

Figure 5-11 shows that the TUCC angle remains within the VMP map, shown by the unsaturated VMP. At maximum TUCC amplitudes the VMP approaches 1. This means the CDV is almost completely based on the VM, for example at t = 3.8 s.

The DCM shows little phase lag compared to the TUCC angle. This means the tyre forces are accurately measured at this TUCC frequency, with little interference of the inertia of the steering system.

The amplitude of the CDV remains within the bounds of the mismatch between VM and DCM. The time span t = 4.1 - 4.3 s shows the co-acting combination of mismatch disturbance and TUCC interference. The transition to the VM value is fast compared to the counter-acting combination, for example at the time span 4.6 - 4.8 s.

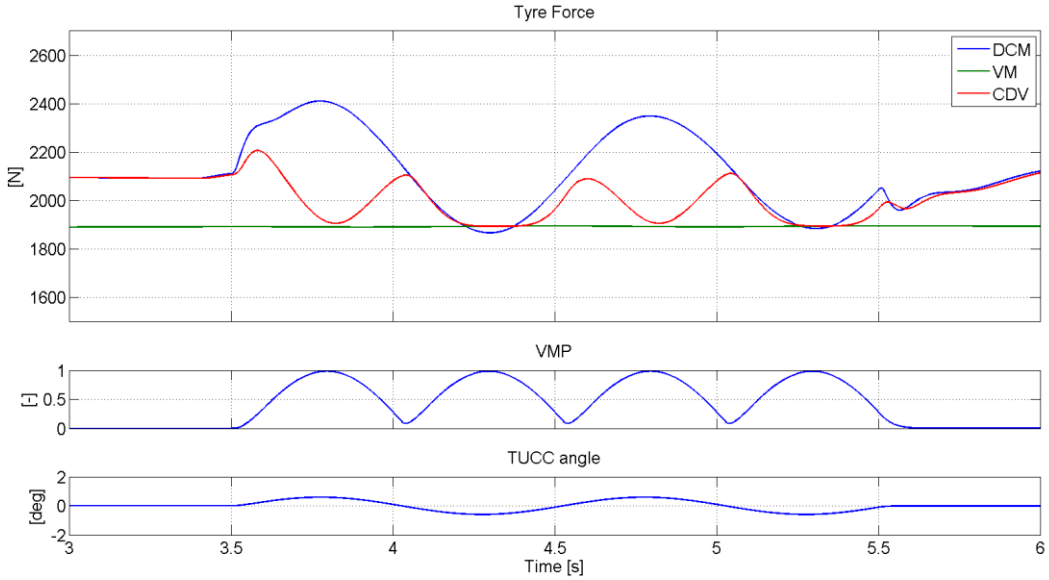

Figure 5-11: Steady state corner 3 deg, 60 km/h, TUCC amplitude 0.6 deg, frequency 1 Hz

Situation 1c

In this situation, the VMP saturates as shown in Figure 5-12. The TUCC angle is for a large part outside the transition phase of the VMP map. When the TUCC is active the CDV is almost completely determined by the VM. At the crossing points, the VMP drops to 0.26 - causing minor peaks in the CDV. The second filter of the CDV lowers these peaks to around 2/3 (instead of 0.74) of the mismatch disturbance. The phase lag of the DCM is consistent with the pervious situation. The co- and counter-

acting combination between mismatch disturbance and TUCC interference is less recognizable due to the dominance of the VM.

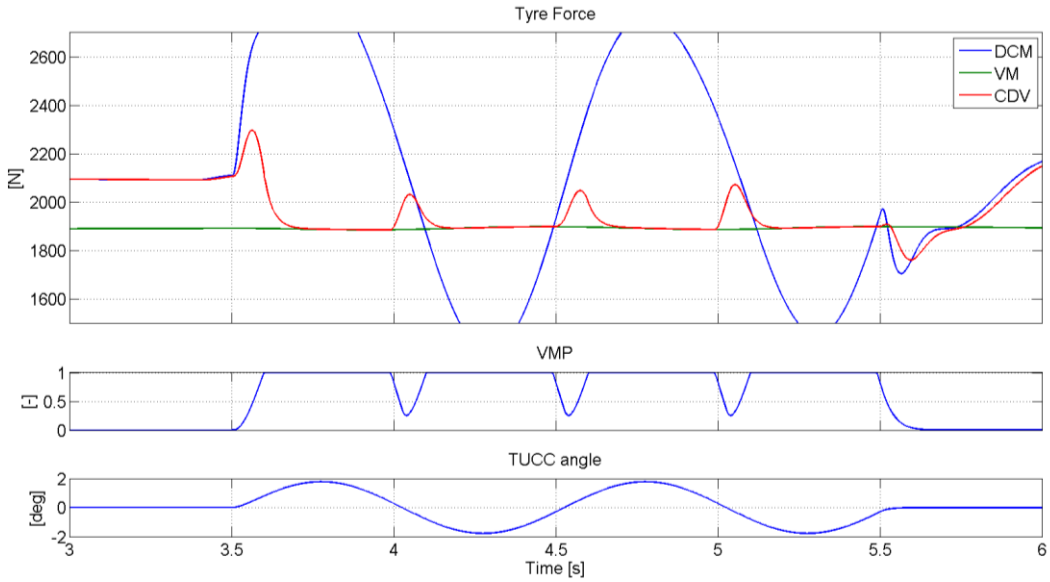

Figure 5-12: Steady state corner 3 deg, 60 km/h, TUCC amplitude 1.8 deg, frequency 1 Hz

5.4.2 High TUCC frequency

Situation 3a

Increasing the frequency of the TUCC angle shows two important phenomena. The amplitude of the VMP is smaller. The first filter, which is designed to smoothen out the constant switching problem, also decreases the amplitude of the VMP at higher frequencies. A more damped VMP is not a big issue. It removes some road information by not approaching zero and transfers a little TUCC interference when the TUCC angle is outside the transition phase of the VMP map.

The second phenomenon of actuating the front wheel steering system at the higher frequency is the dominance of the inertia and damping in the power consumption of the motor. This causes two problems. The first problem is the inaccurate representation of the tyre forces by the DCM. The current drawn by the motor not only handles the tyre forces, but also has to accelerate the inertia of the steering system. At higher frequencies this part becomes more dominant.

The second problem is the phase lead in the DCM compared to the TUCC angle. Since inertia shows a 180 deg phase lag to achieve the desired front wheel angle, the controller has to implement phase lead to the current of the motor. At a frequency of 2.7 Hz the phase lead of the DCM is 71 deg. This phase lead creates significant peaks in the CDV value, clearly seen at t = 3.9 s. If there is no TUCC angle (and the VMP is zero), there is little TUCC interference in the DCM. The phase lead causes the maximum TUCC interference to shift to the lower VMP values. The result is a large TUCC interference presence in the CDV value.

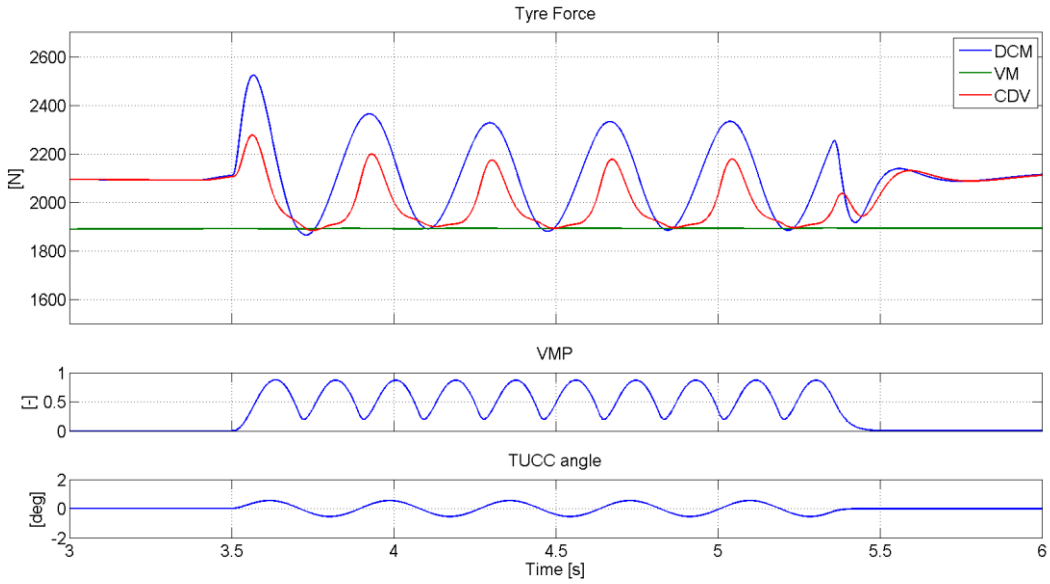

Figure 5-13: Steady state corner 3 deg, 60 km/h, TUCC amplitude 0.6 deg, frequency 2.7 Hz

Situation 3c

Obviously the same phase lead problem occurs at a higher TUCC amplitude. At this high TUCC frequency and amplitude, the peaks of the VMP should be much steeper. Due to the first filter of the CDV the VMP peaks are damped and thus less deep. The higher VMP minima lowers the TUCC interference in the CDV. The amplitude of the CDV is comparable to the mismatch disturbance. The filters of the CDV reduce the mismatch disturbance to 58 % (= VMP).

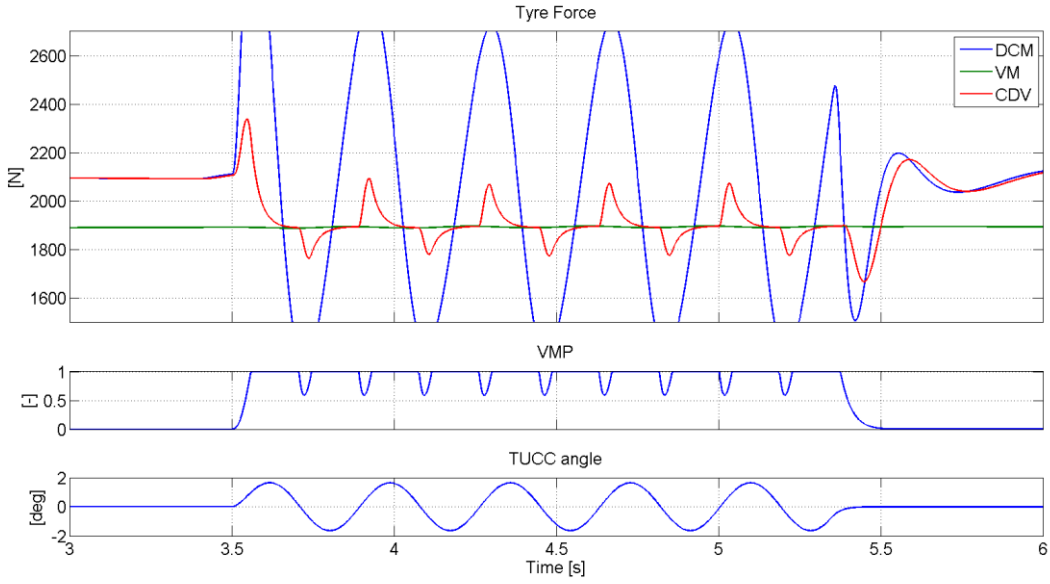

Figure 5-14: Steady state corner 3 deg, 60 km/h, TUCC amplitude 1.8 deg, frequency 2.7 Hz

5.4.3 Validity of CDV

Table 5-2 shows the phase lead of the DCM and the VMP range at the different simulation situations. The CDV works accurate at low TUCC frequencies. Acceptable amounts of TUCC interference are transferred to the driver at different TUCC amplitudes.

At higher TUCC frequencies the presence of the inertia and damping become more dominant in the required motor power and cause phase lead in the DCM. The phase lead shifts the high TUCC interference towards the low VMP values which results in high TUCC interference peaks in the CDV values. At high TUCC amplitudes these disturbances are less significant since the CDV is more based on the VM and sudden peaks, caused by the constantly switching problem, are filtered by the two implemented filters.

Table 5-2: TUCC interference, steady state corner 3 deg, 60 km/h

Situation	δ_{TUCC} Parameters		Phase lead DCM	VMP	
				Lower value	Upper value
1a	0.6 deg	1.0 Hz	7 deg	0.09	1.0
1b	1.2 deg			0.17	1.0
1c	1.8 deg			0.26	1.0
2a	0.6 deg	2.0 Hz	22 deg	0.17	0.92
2b	1.2 deg			0.31	1.0
2c	1.8 deg			0.49	1.0
3a	0.6 deg	2.7 Hz	71 deg	0.20	0.88
3b	1.2 deg			0.39	1.0
3c	1.8 deg			0.58	1.0

5.4.4 Phase shift DCM

As noted before, the phase lead in the DCM is caused by the inertia and damping of the front wheel steering system. Figure 5-15 shows the magnitude and phase shift at increasing TUCC frequencies. Due to the resonance, the motor current required for the front wheel to follow a certain angle decreases towards the natural frequency. Beyond this point the magnitude, defined as $F_{tyre,DCM}$ / $F_{tyre,ref}$ shows an increase. This results in an overestimation by the DCM of the tyre forces. Together with the increasing phase lead the DCM gives at higher TUCC frequencies an inaccurate representation of the tyre forces.

By lowering the gear ratio between motor and front wheel, the passive response and thus the eigenfrequency of the steering system increases. A higher eigenfrequency improves the bandwidth of the DCM. The motor power requirements limit the minimal gear ratio. In Figure 5-16 the magnitude and phase lead of the DCM are plotted for the two lowest gear ratios analyzed in chapter 3. Installing a motor with a lower operation speed and higher constant torque value can be the solution for lowering the gear ratio and therefore increasing the bandwidth of the DCM. The disadvantage of this solution is higher motor torque, which means a larger motor and bigger space requirements.

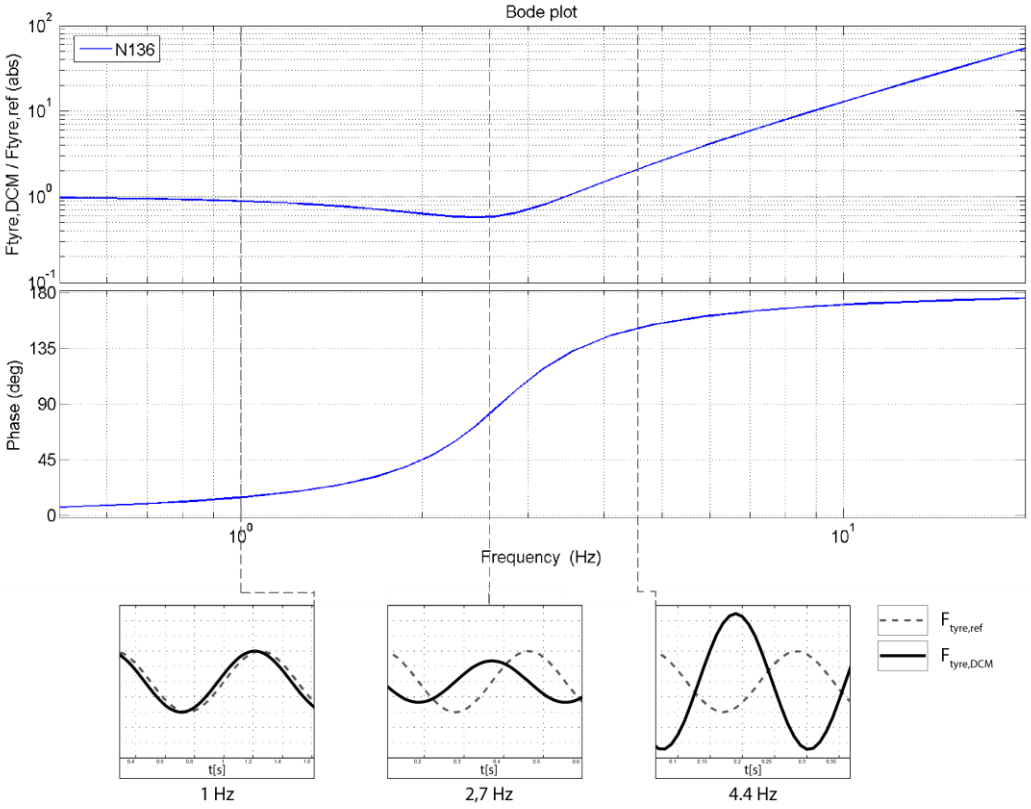

Figure 5-15: Phase shift DCM at different TUCC frequencies.

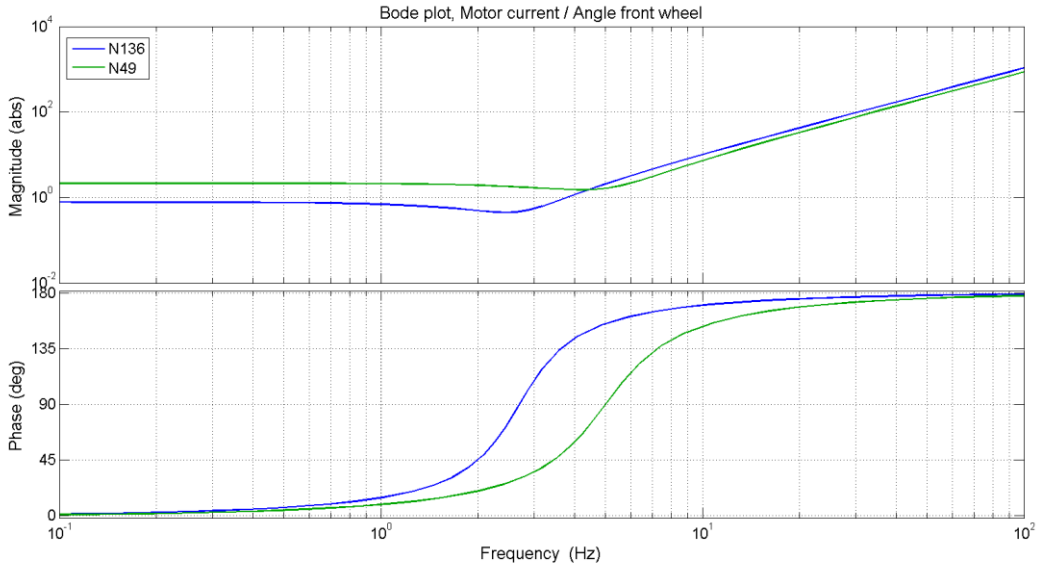

Figure 5-16: Bode plot, performance DCM at different TUCC frequencies.
Blue line: lower gear ratio (N_{low} = 136), Green line: optimal inertia gear ratio (N_{opl} = 49)

5.5 Summary

Providing the driver with haptic feedback, optimizing road information and minimizing TUCC interference, requires a system which can blend two feedback sources, called CDV. It consists of a VM presence map, two first order filters and a controller to ultimately blend the feedback sources. A low pass filter delays the transition to another feedback source. This will smoothen out the constant switching problem.

The VMP value shows how much DCM and VM feedback is presented to the driver. At low steering angles the VMP is exclusively determined by the TUCC angle. At higher steering angles the VMP is also a function of the steering angle. This is feasible as at higher steering angles the tyre forces increase and therefore more TUCC interference can be transferred to the driver. The mismatch disturbance and TUCC interference cause shocks in the feedback when a transition is made between feedback sources. TUCC interference is limited to 5 % of the total tyre forces by the design of the VMP map.

A steady state corner is used as driving maneuver in the simulations. The vehicle velocity is 60 km/h combined with a steering angle of 3 deg. The high tyre forces at a low vehicle speed give a large mismatch disturbance and test the CDV in a worst case scenario. Different TUCC amplitudes and frequencies are added to the front wheel angle to test the validity of the CDV.

At low TUCC frequencies the DCM shows little phase lag compared to the TUCC angle. The amplitude of the CDV remains within the bounds of the mismatch between VM and DCM. At higher amplitudes the TUCC angle is for a large part outside the transition phase of the VMP map. The feedback to the driver is more based on the VM and the filters decrease the constant switching problem to 2/3 of the mismatch of the feedback sources.

At high TUCC frequencies the amplitude of the VMP value is decreased by the first filter. This removes some road information and transfers a little TUCC interference. The presence of the inertia and damping become more dominant compared to the tyre forces and cause a phase shift. At a frequency of 2.7 Hz the phase lead of the DCM is 71 deg. This phase causes the maximum TUCC interference to shift to the lower VMP values. The result is a large TUCC interference presence in the CDV value. At higher TUCC amplitudes these disturbances are less significant since the CDV is more based on the VM and sudden peaks, caused by the constant switching problem, are filtered.

Due to the system resonance, the motor current required for the front wheel to follow a certain angle decreases towards the natural frequency. Together with the increasing phase lead, the DCM gives an inaccurate representation of the tyre forces at higher TUCC frequencies. Installing a motor with a lower operation speed and higher constant torque value can be the solution for lowering the gear ratio and therefore increasing the bandwidth of the DCM. However, the space requirements of a bigger motor can cause problems in terms of implementation.

Chapter 6

Conclusions and recommendations

This thesis covers three important aspects for implementing an independent front wheel steering system, with the combination of optimal driver feedback.

6.1 Conclusions

6.1.1 Front wheel dynamics

A model of the front wheel steering system with a variable gear ratio is studied to answer the first research question: how will the gear ratio between steering motor and front wheel affect the dynamics of the steering mechanism?

A low gear ratio between motor and front wheel shows a fast responding steering system to the tyre forces. The lowest gear ratio within the bounds of the motor range is 136. This gear ratio results in an eigenfrequency of 2.7 Hz of the steering system and the tyre force. The damping ratio is 0.30.

A high gear ratio lowers the required motor torque to cope with the tyre forces. A smaller motor has advantages in terms of space requirements. A too high gear ratio provides problems, since the motor has to spin at very high speeds and may not be able to provide enough power.

A low gear ratio increases the response of the steering system to the tyre force. An increase in response is desirable for the accuracy of the direct current measurement (DCM). The disadvantage of a low gear ratio is the high required motor torque to cope with tyre forces. This results in a large motor.

A compromise should be chosen between the motor size on the one hand and a low gear ratio – to maximize the passive response of the steering system – on the other hand.

6.1.2 Haptic driver feedback

The front wheel dynamics model is used to answer the next research question: can a direct current measurement give accurate readings of the actual tyre forces? Further, a virtual model (VM) based on the bicycle model is created to answer the research question: can a virtual model compute the tyre forces accurately? Both feedback sources are compared to the reference tyre forces in a modified double lane change and a steady state corner. The reference tyre forces are simulated using CarSim.

In a steady state corner the DCM approaches the reference tyre forces within a 0.9 % error. At a vehicle velocity of 60, 90 and 120 km/h, the RMS error of the double lane change is 5.2, 7.8, and 9.2 % respectively. At a steady state corner the motor torque only has to compensate for the tyre force. No power is required to move the front wheel, therefore the DCM accuracy is very high. In a double lane change extra motor torque is required to change the angle of the front wheel. This interferes with the measurement of the tyre forces. The dominance of this interference depends on the frequency of the steering angle. Therefore the DCM accuracy decreases for a dynamic maneuver.

In the steady state corner the VM underestimates the higher tyre forces at a vehicle velocity of 60 km/h. At 120 km/h the lower tyre forces are overestimated. A vehicle speed of 90 km/h provides the best VM accuracy. This is confirmed by the double lane change. At 60 and 120 km/h the RMS error is 16 %, while this error is reduced to 11% at 90 km/h. The error in the VM is caused by the approximation

of nonlinear vehicle dynamics. Improving the model increases the accuracy and lowers the mismatch between the DCM and the VM. However it is not desirable to create a too complex model as an onboard computer has to run the model real-time.

6.1.3 Combiner DCM and VM

A Combiner DCM and the VM (CDV) is tested in a steady state corner, combined with an active TUCC to answer to last research question: Is it possible to develop a system which can blend two feedback sources, providing the driver with optimal feedback?

At low TUCC frequencies (< 1 Hz) the CDV blends the VM and the DCM well. A low TUCC angle results in a low VMP value which shows that the CDV value is mainly based on the DCM. For higher TUCC angles, the VMP value increases to and saturates at 1. The phase lead of the DCM, compared to the TUCC angle is small (< 11 deg). The filters implemented in the CDV reduce the constant switching problem. A TUCC angle three times the bounds of VMP map results in a switching problem and 66 % of the mismatch disturbance is passed to the driver.

At a TUCC frequency of 2.7 Hz, the phase lead of the DCM increases to 71 deg. The amplitude of the CDV reaches beyond the mismatch disturbance as more TUCC interference is transferred. At a TUCC angle three times the bounds of VMP map, these peaks in the CDV value decrease as they are filtered by the two first order filters.

At higher TUCC frequencies the presence of inertia and damping of the steering system become more dominant compared to the tyre forces. Toward the natural frequency of the steering system the magnitude of the required motor current decreases. To overcome the phase lag of the inertia and damping, phase lead in the motor's torque is required and introduced by the controller. Due to the changing magnitude and the increasing phase lead at higher TUCC frequencies, the DCM gives an inaccurate representation of the tyre forces.

The phase lead in the DCM shifts the maximum TUCC interference towards incorrect and lower VMP values. The result is a large TUCC interference in the CDV feedback. At TUCC amplitudes outside the VMP map these interferences are less significant since the CDV is more based on the VM and sudden peaks are filtered.

6.2 Recommendations

At high TUCC frequencies, the accuracy of the CDV is poor. This is caused by the phase lead in the DCM and results in too much TUCC interference. The mismatch disturbance can be reduced by improving the VM. To improve the performance of the CDV, the following recommendations are made.

6.2.1 TUCC interference

Decrease the inertia and damping of the steering system

Installing a motor with a high constant torque value coupled to the front wheel with a low gear ratio will lower the inertia and damping of the steering system. This increases the eigenfrequency and improves the bandwidth of the DCM.

Replace the DCM with load sensing bearings for a more accurate reading of the tyre forces

The inertia and damping of the motor disturbs the reading of the DCM. Installing load sensing bearings in the front wheels can solve this disturbance problem and may provide a better estimation of the tyre forces.

6.2.2 Mismatch disturbance

Improve the accuracy of the Virtual model

Including neglected vehicle dynamics into the VM increases its accuracy. And an improved VM lowers the mismatch disturbance and decrease the shocks in the CDV when the TUCC is active.

Introduce a steady state VMP value

The range of the VMP is from 0 to 1. This means the CDV can be determined by the DCM or by the VM completely. By adding a steady state VMP value, for example 0.5, this VMP range is decreased. In the new situation the CDV cannot be fully determined by the DCM anymore and only by a 50/50 blend of the two feedback sources. Therefore the mismatch disturbance is also reduced by 50 %. The cost of this reduction is the decrease in road information when no TUCC interference is present as the CDV is determined by the DCM for only 50 percent.

Chapter 7

Appendix

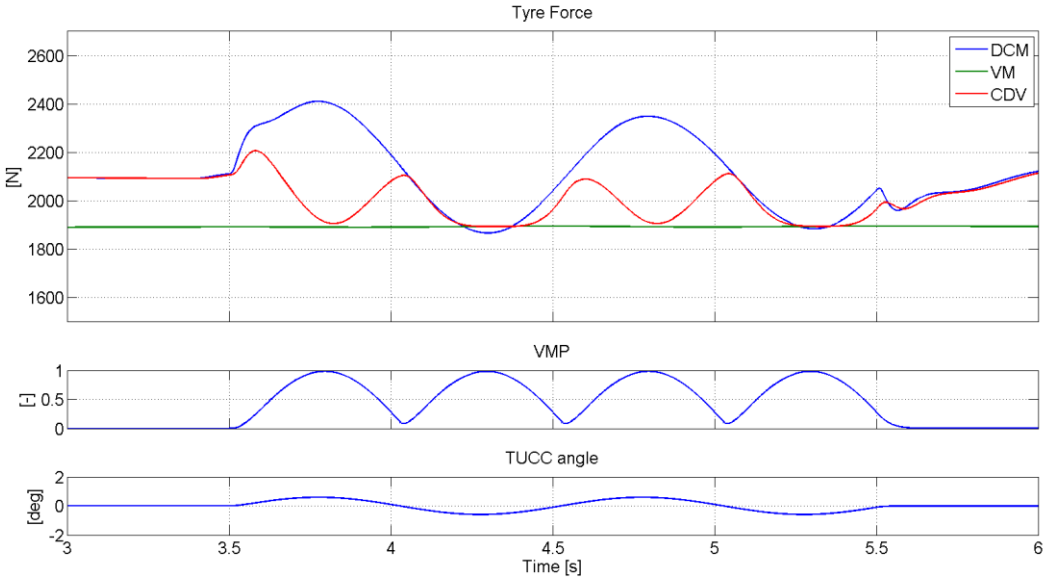

Figure 7-1: Steady state corner 3 deg, 60 km/h, TUCC amplitude 0.6 deg, frequency 1 Hz

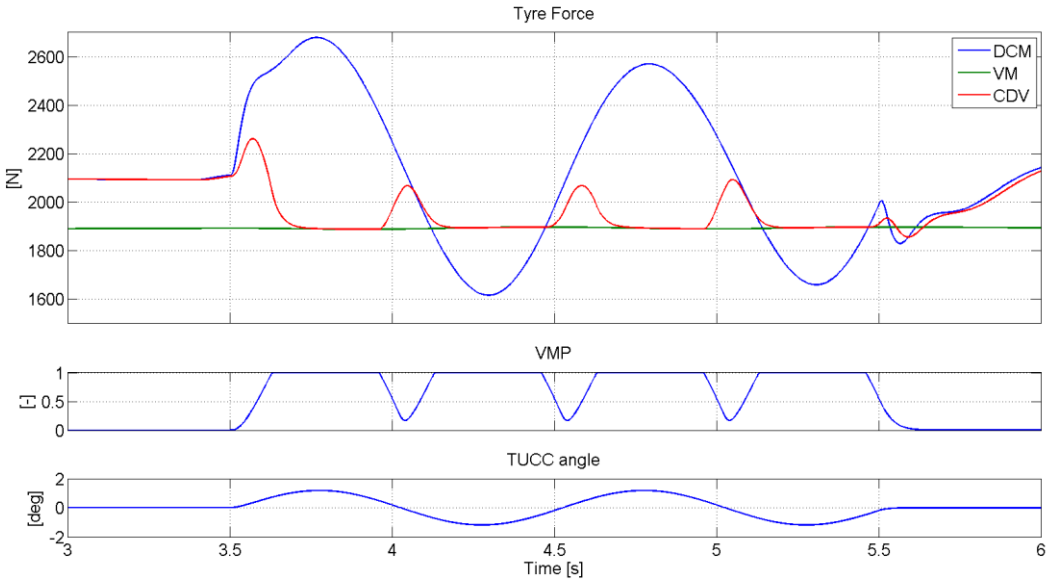

Figure 7-2: Steady state corner 3 deg, 60 km/h, TUCC amplitude 1.2 deg, frequency 1 Hz

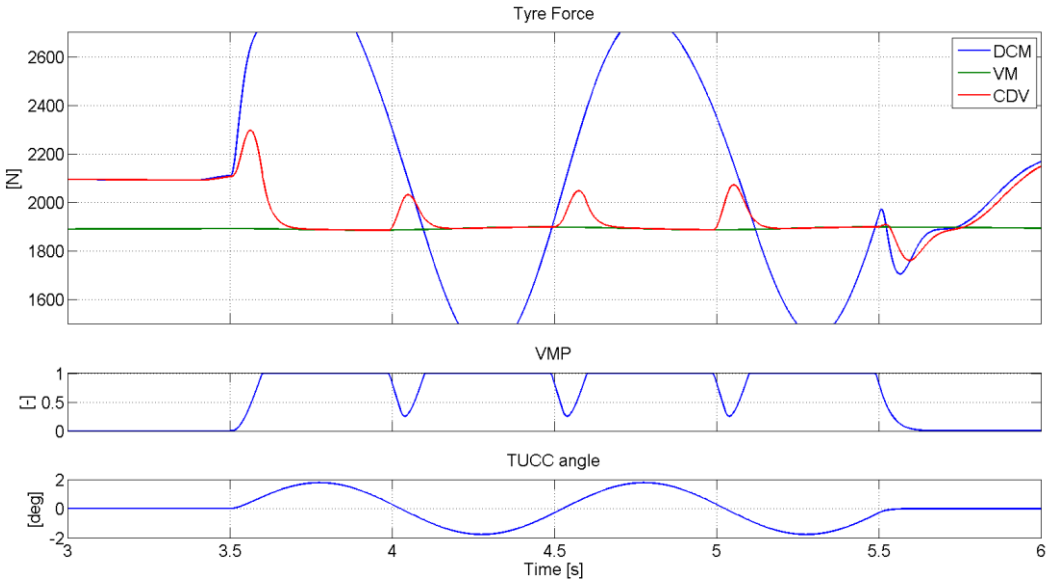

Figure 7-3: Steady state corner 3 deg, 60 km/h, TUCC amplitude 1.8 deg, frequency 1 Hz

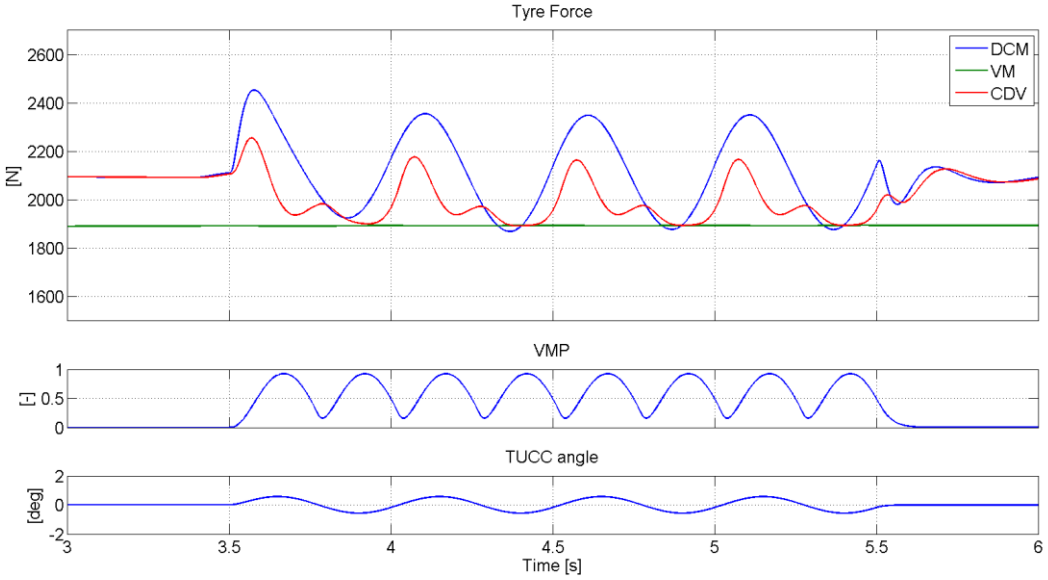

Figure 7-4: Steady state corner 3 deg, 60 km/h, TUCC amplitude 0.6 deg, frequency 2 Hz

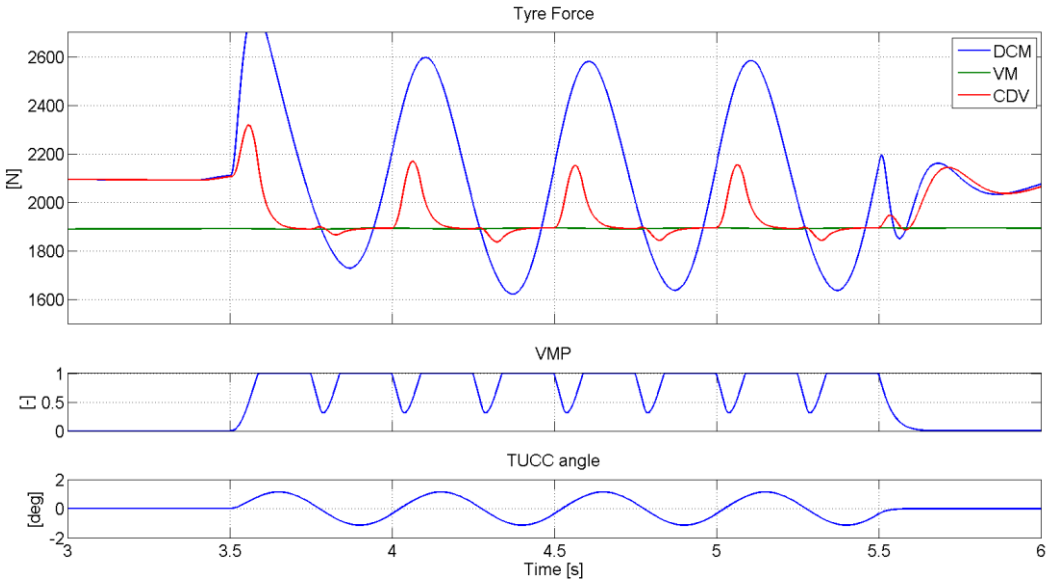

Figure 7-5: Steady state corner 3 deg, 60 km/h, TUCC amplitude 1.2 deg, frequency 2 Hz

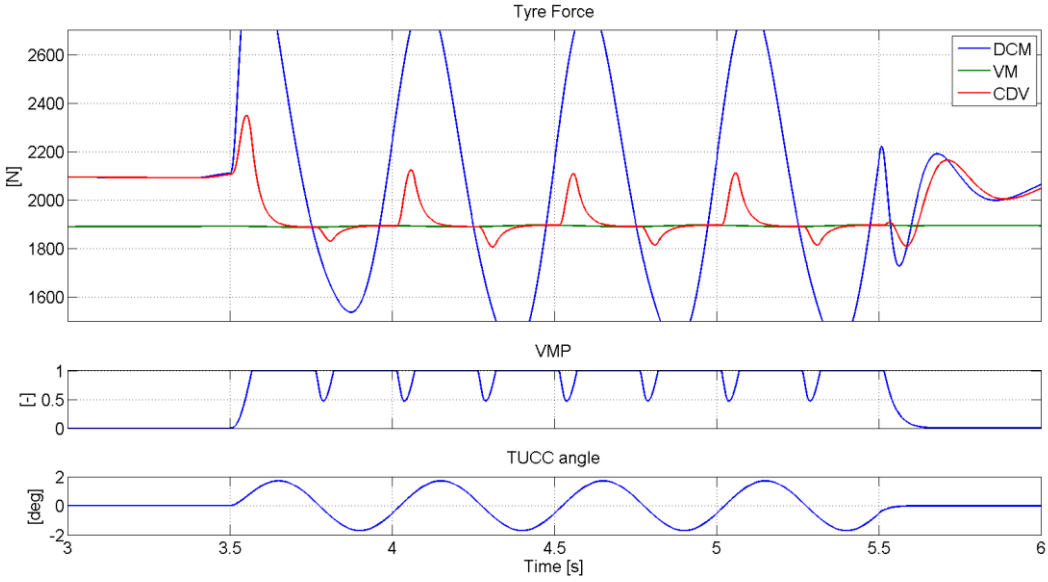

Figure 7-6: Steady state corner 3 deg, 60 km/h, TUCC amplitude 1.8 deg, frequency 2 Hz

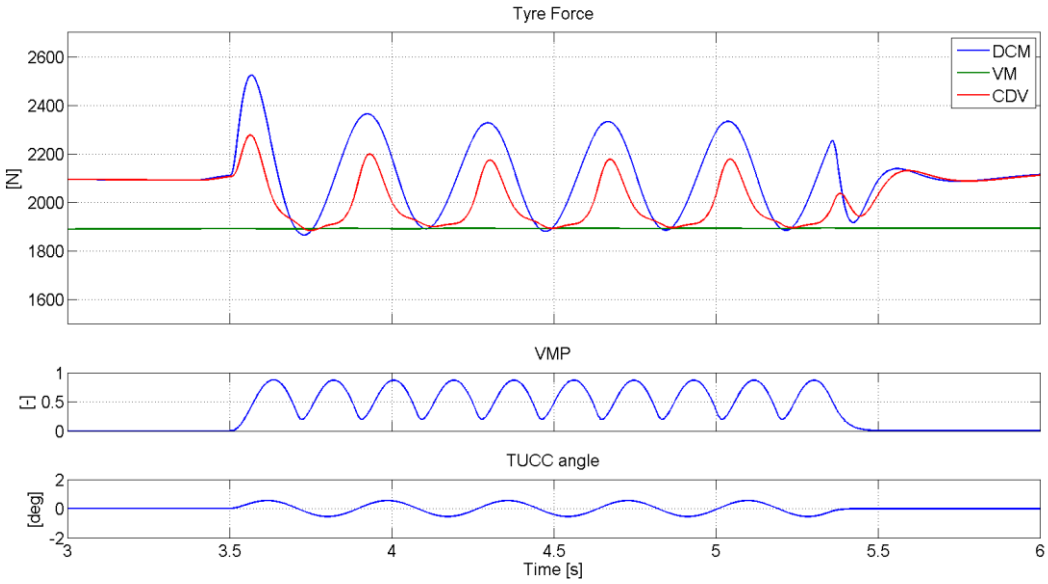

Figure 7-7: Steady state corner 3 deg, 60 km/h, TUCC amplitude 0.6 deg, frequency 2.7 Hz

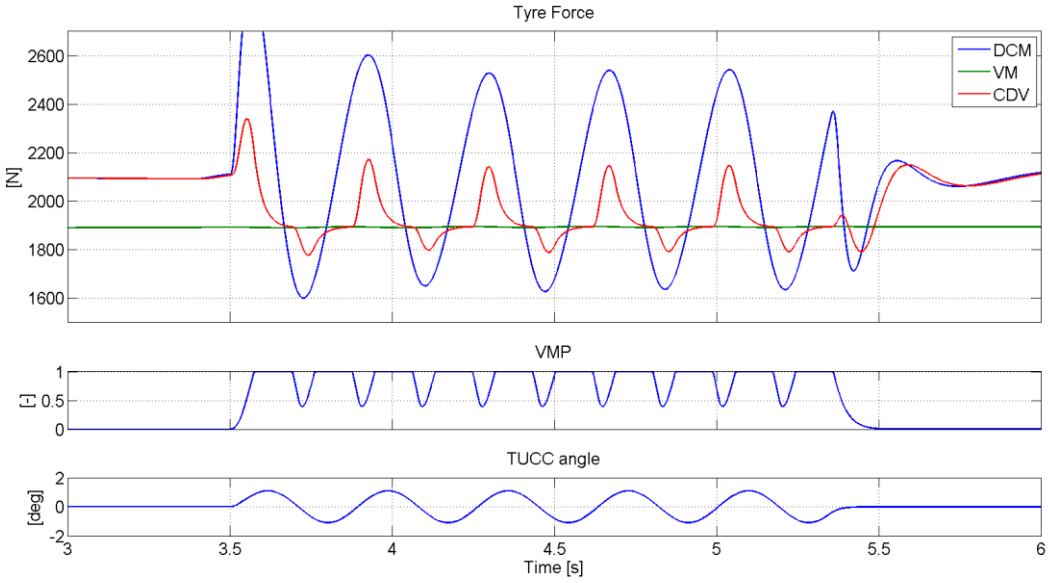

Figure 7-8: Steady state corner 3 deg, 60 km/h, TUCC amplitude 1.2 deg, frequency 2.7 Hz

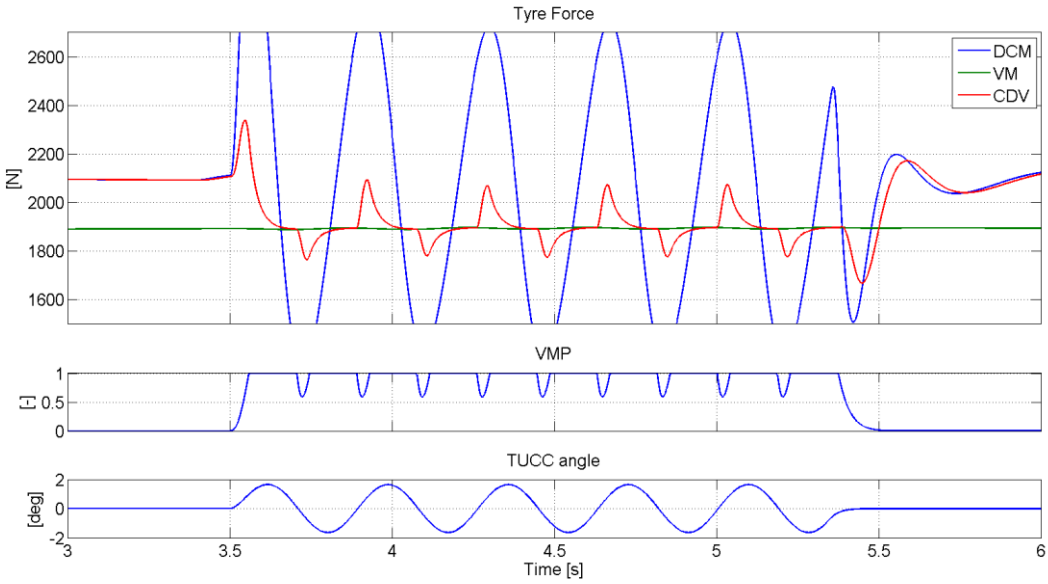

Figure 7-9: Steady state corner 3 deg, 60 km/h, TUCC amplitude 1.8 deg, frequency 2.7 Hz

Chapter 8

Bibliography

[1] H. B. Pacejka, "Tyre and vehicle dynamics (2nd ed.)," *SAE International,* 2006.

[2] A. Kunnappillil Madhusudhanan, M. Corno, and E. Holweg, "Lateral Vehicle Dynamics Control Based On Tyre Utilization Coefficients and Tyre Force Measurements," 52nd IEEE Conference on Decision and Control, 2013.

[3] A.K.W. Ahmed, V. Rawat, and R.B. Bhat, "Active Front Independent Steering System and its Control for Road Vehicle with Understeer Characteristics," International Conference on Advances in Electrical and Mechanical Engineering, Phuket, 2012.

[4] E. F. Gaffney III, and A.R. Salinas, "Introduction to Formula SAE Suspension and Frame Design," SAE paper no. 971584, 1997.

[5] V. Rawat, "Active Independent Front Steering for Yaw-Rate Control and Tire Work-Load Equalization in Road Vehicles," Concordia University, Montreal, 2007.

[6] Y. Shibahata, "Progress and future direction of Chassis control technology," Honda R&D Co. Ltd., Tochigi R&D Cente, Haga-gun, 2005.

[7] B. Heissing and M. Ersoy, "Chassis Handbook," Wiesbaden: Springer Fachmedien, 2011.

[8] C. L. Seacord and D. K. Vaughn, " Preliminary system design for a digital flyby-wire flight control system for an F-8C aircraft," NASA Center for AerospaceInformation, 1976.

[9] E. Mehdizadeh, M. Kabganian, and R. Kazemi , "A New Force Feedback for Steer-by-Wire Vehicles via Virtual," 2011 50th IEEE Conference on Decision and Control and, Orlando, 2011.

[10] D. Heitzer, & A. Seewald, "Development of a fault tolerant steer-by-wire steering system," 2004.

[11] D. Gordon, "Experimental Isolation of Drivers' Visual Input," Public Roads, 1966.

[12] A.K.W. Ahmed, V. Rawat, and R.B. Bhat, "Vehicle Steering Mechanism for Active Independent Front Steering System," 3rd International Conference on Mechanical, Production and Automobile Engineering, Bali, 2013.

[13] W. Ahmed, "Steering System and Method for Independent Steering of Wheels". US Patent 8 126 612, 2012.

[14] W. Evers, A. van der Knaap, I. Besselink, and H. Nijmeijer, "Analysis of a variable geometry active suspension," International Symposium on Advanced Vehicle Control, Kobe.

[15] B. Németh and P. Gáspár, "Variable-Geometry Suspension Design in Driver Assistance Systems," 2013 European Control Conference, Zürich, 2013.

[16] "Michelin Active Wheel," in *Motor Show*, Paris, 2008.

[17] Mogi, Sugai, Sakurai, Suzuki, "Development of a New Steer-by-wire System," NTN TECHNICAL REVIEW No.79, 2011.

[18] S. Zetterström, "Electromechanical Steering, Suspension, Drive and Brake Modules," Volvo Car Corporation, Göteborg, Sweden, 2002.

[19] R. Minaki and Y. Hori, "Experimental Verification of Reaction Torque Control Based on Driver Sensitivity to Active Front Steering," The University of Tokyo, Tokyo, 2011.

[20] B.H. Nguyen and J.H. Ryu, "Direct Current Measurement Based Steer-By-Wire," IEEE International Symposium on Industrial Electronics (ISIE 2009), Seoul, 2009.

[21] "http://forums.5series.net/e60-discussion-2/e60-steering-ratio-none-active-steering-15958/," [Online]. [Accessed 13 11 2013].

[22] A. Liu and S. Chang, "Force feedback in a stationary driving simulator," Nissan Cambridge Basic Research, Cambridge, 1995.

[23] R. S. Sharp and R. Granger, "On car steering torques at parking speeds," IMechE Journal of Automobile Engineering, 2003.

[24] F. H. Heacock and Harold Jeffery, "The Application of Power Assistance to the Steering of Wheeled Vehicles," Proceedings of the Institution of Mechanical Engineers: Automobile Division, 1953.

[25] P. Yih, "STEER-BY-WIRE: IMPLICATIONS FOR VEHICLE HANDLING AND SAFETY," Stanford university, 2005.

[26] D. Pang, "Steering Wheel Torque Control of Electric Power Steering by PD-Control," Kintex, Gyeonggi-Do, 2005.

[27] S.-C. Chang, "Synchronization in a steer-by-wire vehicle dynamic system," International Journal of Engineering Science 45, Changhua, 2006.

[28] J. A. s. L. N. Kristoffer Lundahl, "INVESTIGATING VEHICLE MODEL DETAIL FOR CLOSE TO LIMIT MANEUVERS AIMING AT OPTIMAL CONTROL," Department of Electrical Engineering, Link¨oping University, Linkoping, Sweden.